STUDY OF SWIRLING JETS ON AN IMPINGEMENT SURFACE

by

Ryan Stoner

A Thesis Submitted to the Faculty of the

DEPARTMENT OF MECHANICAL ENGINEERING

In Partial Fulfillment of the Requirements

For the Degree of

MASTER OF SCIENCE

In the Graduate College

THE UNIVERSITY OF ARIZONA

2020

THE UNIVERSITY OF ARIZONA
GRADUATE COLLEGE

As members of the Master's Committee, we certify that we have read the thesis prepared by: Ryan Stoner
titled: The Study of Jet Streams on an Impingement Surface

and recommend that it be accepted as fulfilling the thesis requirement for the Master's Degree.

Sergey V Shkarayev
Sergey V Shkarayev Date: May 26, 2020

Yitshak Zohar Date: May 26, 2020

Jekan Thanga Date: May 26, 2020

Final approval and acceptance of this thesis is contingent upon the candidate's submission of the final copies of the thesis to the Graduate College.

I hereby certify that I have read this thesis prepared under my direction and recommend that it be accepted as fulfilling the Master's requirement.

Sergey V Shkarayev
Sergey V Shkarayev Date: May 26, 2020
Thesis Committee Chair
Aerospace and Mechanical Engineering

Acknowledgements

I would like to give my sincere appreciation to many people who have helped me throughout my research. Firstly, I would like to thank Professor Sergey Shkaravey, my advisor, for his continued guidance and advice during my research. His motivation helped me to continual make progress on the thesis. I would also like to thank Adrien Bouskela for helping me with visualization and instrumentation guidance.

I would like to thank Teri Elwood for her support and encouragement while I worked on my thesis. Finally, I wish to thank Raytheon Missile Systems and Eddie Calloway for providing funding for my master's degree.

Table of Contents

List of Figures

Nomenclature

ϕ = Azimuthal Direction

ρ = Mean Density

v = Mean Kinematic Viscosity

θ = Impingement Angle from Vertical

A = Seeding Chamber

B = Blower

C = Plenum Chamber

D = Exit Diameter

d = Impingement Wall Distance

E = Radiator

F = Diffuser

G = Parabolic Mirror

H = Impingement Wall

I = Razor Blade

J = High Speed Camera

K = Jet Stream Flow

L = Point Light Source

M_ϕ = Angular Momentum

M_x = Momentum Integral Expression

N = Nozzle

O = Nozzle Coordinate System Origin

O_S = Impingement Coordinate System Origin

P = Mean Pressure

R = Orifice Radius

Re = Reynolds Number

r = Radial Direction

S = Swirl Number

$S_{\phi x}$ = Swirl Intensity

U = Axial Mean Velocity

Ue = Mean Exit Velocity

Us = Impingement Axial Mean Velocity

u = Axial Fluctuating Velocity

V = Azimuthal Mean Velocity

Vs = Impingement Azimuthal Mean Velocity

v = Azimuthal Fluctuating Velocity

W = Radial Mean Velocity

w = Radial Fluctuating Velocity

X = Axial Direction

X_S = Impingement Axial Direction

Y = Lateral Direction

Y_S = Impingement Lateral Direction

Z = Vertical Direction

Z_S = Impingement Vertical Direction

Acronyms

ADC: Analog to Digital Converter

CAD: Computer Aided Design

CTA: Constant Temperature Anemometry

DAQ: Data Acquisition System

PLA: Polylactic Acid

NI: National Instruments

Abstract

There has been extensive research performed on the turbulent jet stream flow including unimpeded and impinged flow. Vortex jet streams however has not been studied in as great of detail. Some researchers have focused on the development of vortex flow as well as axial and azimuthal velocity profiles generated from these jet streams. The need for better control over aircraft carries and decrease the wait time between landing aircraft at airports has driven a need for further research into these vortex flows. If an impingement surface is introduced into these example environments at which angle should it be positioned to quickly dissipate the flow?

This research will validate a blower jet stream system, develop vortex nozzles, validate the tripped nozzle and characterize the vortex flow on an impingement surface. To start, an existing converging/diverging blower motor system was utilized for all the experiments performed. A tripped nozzle configuration was used to confirm that the results generated matched those of pervious experiment published. This confirmed not only the physical setup but also the data acquisition methods. Next varying nozzle configuration were designed, printed and tested to determine their functionality. The results confirmed that the nozzles generated increasing levels of vortex flow ranging from low, medium and high azimuthal axis components.

After all the nozzles were characterized in the unimpeded configuration the impingement wall was introduced. The tripped nozzle was used as a baseline for this setup since the results for this configuration are well defined. Next each of the vortex nozzles went through the same series of tests. This involved varying speeds of the jet flow as well as three different impingement wall angles. The results showed that at low swirl numbers the jet stream profile match the tripped nozzle setup closely. As the swirl number increase the flow became harder to dissipate. This resulted in the wall needing to be positioned at a steeper angle. Another interesting observation was at the higher vortex flows there was as axial vortex generated that was not seen in any of the other setups. Overall, it was determine that vortex flow required a near vertical wall to effectively impede the flow.

1. Introduction

1.1 Background and Motivation

Exhaustive research has been completed on jet stream flow both in the free form environment as well as in an impingement and confinement configurations. Thus far however there has yet to be a study of swirling jets on an impingement surface. Swirling jets interacting with surfaces have been seen in multiple engineering problems. One such case involves an aircraft carrier and the effect they have on incoming aircraft known as the "burble" affect [1]. It was found that the air flow that was interacting with the aft end of the carrier, as well as the superstructure, was causing a low-pressure zone being generated by a vortex [1]. This burble area in the airflow increased the decent rates of the aircraft as they were attempting to land, increased the likelihood of missing the arresting cable. The turbulent environment of an aircraft carrier was model by the Navy, see Fig. 1.1.1 [13]. The leading edge of the bow generates turbulence, as this airflow moves downstream the burble affect is created. Turbulence is also created from the edges of the landing surface as well as the superstructure. These features create edge and standing vortices along the forward edge of the deck and behind the super structure, respectively. A solution to these problems was purposed, columnar-vortex generators that would attempt to control the direction and strength of the vortices that are being generated [4].

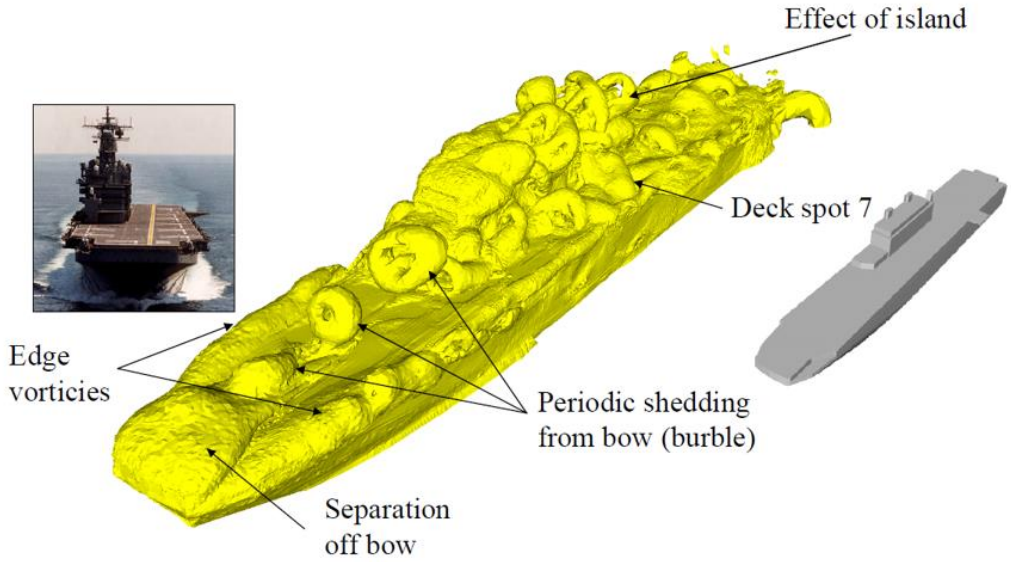

Fig 1.1.1: Airflow Simulation of Aircraft Carrier [13].

But it has yet to be determined if these columnar-vortex generators would be functional in practice. Another important case study involving swirling jet impingement is the wake vortex generated from aircraft during takeoff and landing at airports. The vortices created by the aircraft is the limiting factor for aircraft spacing and ultimately airport capacity [3]. If the swirling jet impingement case can be studied more closely than a solution to these problems may be feasible.

1.2 Physics of Jets and Swirl Flow

To better understand the mechanics behind the jet stream environment it is worthwhile to step back and look at the fundamental equations of fluid flow for streams and vortices. The most important of these governing equations is the cylindrical frame of reference of the incompressible Reynolds-averaged Naiver-Stokes equations [12]:

$$\frac{1}{r}\frac{\partial}{\partial r}(rW) + \frac{\partial U}{\partial x} = 0, \tag{1}$$

$$W\frac{\partial W}{\partial r} + U\frac{\partial W}{\partial x} + \frac{\partial \overline{w^2}}{\partial r} + \frac{\partial \overline{uw}}{\partial x} - \frac{1}{r}\left(V^2 + \overline{v^2} - \overline{w^2}\right) = -\frac{1}{\rho}\frac{\partial P}{\partial r} + \frac{1}{r^2}\left[\nu r^3 \frac{\partial}{\partial r}\left(\frac{W}{r}\right)\right], \tag{2}$$

$$W\frac{\partial V}{\partial r} + U\frac{\partial V}{\partial x} + \frac{VW}{r} + \frac{\partial \overline{uv}}{\partial x} + \frac{1}{r^2}\frac{\partial}{\partial r}\left(r^2\overline{vw}\right) = \frac{1}{r^2}\frac{\partial}{\partial r}\left[\nu r^3 \frac{\partial}{\partial r}\left(\frac{V}{r}\right)\right], \tag{3}$$

$$W\frac{\partial U}{\partial r} + U\frac{\partial U}{\partial x} + \frac{\partial \overline{u^2}}{\partial x} + \frac{1}{r}\frac{\partial(r\overline{uw})}{\partial r} = -\frac{1}{\rho}\frac{\partial P}{\partial x} + \frac{1}{r}\frac{\partial}{\partial r}\left[\nu r \frac{\partial U}{\partial r}\right]. \tag{4}$$

Where the radial, azimuthal and axial directions are denoted as (r, ϕ, x) and the velocity components as (W+w, V+v, U+u) respectively where capital letters are the mean components and

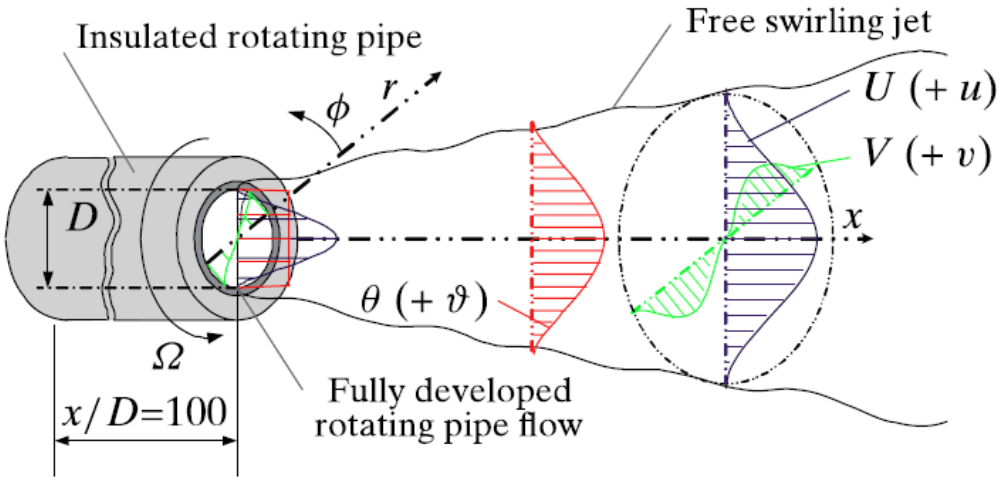

Fig 1.2.1: Free Flow Developing Swirling Jet [12].

lower-case letters are the fluctuating components, seen in Fig. 1.2.1. P, ρ and v are mean pressure, density and kinematic viscosity, while the overbar indicates time average.

The above equations can be further simplified [7, 12]. This simplification takes advantage of a thin shear layer approximation and assumes a high Reynolds number flow as well as assuming all viscous terms can be neglected based on an order of magnitude estimate. In this way (2) simplifies to

$$\frac{1}{\rho}\frac{\partial P}{\partial r} = -\frac{\partial \overline{w^2}}{\partial r} + \frac{1}{r}\left(V^2 + \overline{v^2} - \overline{w^2}\right). \tag{5}$$

By neglecting the first term on the right-hand side, the azimuthal and radial turbulence intensities are comparable, a simple radial equilibrium relation can be derived,

$$\frac{\partial P}{\partial r} \approx \rho\frac{V^2}{r}. \tag{6}$$

Equation (6) verifies the existence of a radial pressure gradient induced by the swirling motion of the stream [8]. Next equation (5) can be multiplied with r and then integrated it across the jet, i.e. from the centerline (r = 0) to a radial position where the presence of the jet is not detectable ($r \rightarrow \infty$). Then the boundary conditions corresponding to a free axisymmetric jet issuing into a quiescent environment at r = 0 can be applied, [12].

$$W = V = 0; \quad \frac{\partial U}{\partial r} = 0; \quad \frac{\partial \overline{uw}}{\partial r} = \frac{\partial \overline{vw}}{\partial r} = 0, \tag{7}$$

And at ($r \rightarrow \infty$),

$$V = U = 0; \quad \overline{uw} = \overline{vw} = 0; \quad \frac{\partial U}{\partial r} = \frac{\partial V}{\partial r} = 0; \quad \frac{\partial \overline{uw}}{\partial r} = \frac{\partial \overline{vw}}{\partial r} = 0, \tag{8}$$

The following relation is obtained.

$$\int_0^\infty r(P - P_\infty)\, dr = -\frac{1}{2}\rho \int_0^\infty r\left(V^2 + \overline{v^2} + \overline{w^2}\right) dr. \qquad (9)$$

By substituting (9) into (4) the following momentum integral relation can be formulated [12].

$$\frac{d}{dx}M_x = \frac{d}{dx} 2\pi\rho \int_0^\infty r\left[U^2 - \frac{V^2}{2} + \overline{u^2} - \frac{\overline{v^2} + \overline{w^2}}{2}\right] dr = 0. \qquad (10)$$

Multiplying (3) with $r\, dA$, where $dA = 2\pi\, r\, dr$, derives an integral expression for the conservation of the axial flux of angular momentum [12]. This was integrated under the same conditions as the previous derivation.

$$\frac{d}{dx}M_\phi = \frac{d}{dx} 2\pi\rho \int_0^\infty r^2 (UV + \overline{uv})\, dr = 0. \qquad (11)$$

The swirl intensity is commonly defined as the ratio of the angular momentum, M_ϕ, divided by the momentum integral expression, M_x, times the radius of the orifice, R [9].

$$S_{\phi x} = \frac{M_\phi}{R M_x}. \qquad (12)$$

However, the above equation can be simplified further to only the contributions from the stream wise and azimuthal mean velocities if the other components are negligible. The swirl intensity reduces to an expression identical to the one in laminar flow,

$$S_{\phi x} = \left[\int_0^\infty r^2 UV\, dr\right]\left[R \int_0^\infty r\left(U^2 - \frac{1}{2}V^2\right) dr\right]^{-1}. \qquad (13)$$

To characterize free swirling jets it is common to use (13) in conjunction with the Reynolds number, defined as

$$Re = \frac{U*D}{\upsilon} \qquad (14)$$

However, these are not enough to define the flow alone, the initial conditions such as the near-field region are also important classifications that need to be defined [10]. The ratio between the azimuthal velocity, V, and the normal velocity U, can be utilized to form a swirl number.

$$S = \frac{V}{U}, \qquad (15)$$

Which along with Reynolds number, Re, fully defines the flow field. The swirl intensity, $S\phi x$, is primarily used to compare different studies which makes measuring it vital [12]. While the swirl intensity for the nozzles used in this experiment will be measured and presented, the swirl number will be used primarily throughout this paper.

1.3 Literature Survey

A literature survey of jet stream work was performed to develop test methods as well as understand the progress made in the field. The first work that was investigated was the turbulent jet stream characterization that S. C. Crow & F. H. Champagne (1971) performed [6]. With the use of a diverging/ converging blower system they were able to study a jet stream that ranged from Reynolds numbers of 6.2×10^4 to 1.24×10^5 [6]. Both smoke generation as well as Schlieren photography were used as visualization techniques on the jet stream [6]. To maintain a consist centerline velocity for the range of Reynolds number, a trip ring was installed into the jet nozzle exit. This trip ring disturbed the boundary layer of the stream breaking up any boundary layer structure that had formed and ensuring truly turbulent flow. Finally, to enhance the results measured from the jet stream a speaker was installed to excite the blower system. The natural frequency of the puffs generated by the jet was measured using high speed cameras. This data was then used to determine which frequencies the speaker should be set to. The variables that were changed during the experiment include velocity, forcing frequency, and Reynolds numbers. The primary focus was to observe how the jet stream changed with different Strouhal numbers, a factor of both forcing frequency and velocity. The amplitude of the forcing frequency was varied to understand the role this played on the jet stream. Centerline velocity profiles were taken constantly to show the affects that each setup change had compared to the original profile. The resulting conclusion from this experiment was that the jet stream could be manipulated in multiple different ways to better control and isolate certain aspects of the flow.

The next study researched was the work done on turbulent impinging jet streams by C. D. Donaldson and R. S. Snedeker (1970) [2]. They focused on three different jet flows: subsonic jets, moderately under-expanded jets, and highly under-expanded jets. Rather than characterizing the environments by the Reynolds number for the jet stream, exit pressure differentials was chosen [2]. These differentials for each type of flow were 0.8, 0.372 and 0.148, respectively. Both spark and continuous Schlieren photography was utilized to visualize the jet stream flow [2]. For their experiments Pitot tubes and static pressure probes were used as pressure was of main concern. Not only did they studied the impingement on a flat plate, but also experimented with convex and concave hemispheres as well as a cylindrical cup [2]. The experiment was performed at multiple distances away from the jet nozzle as well as varying impingement angles to fully define the characteristics of the flow [2]. One of the major focus points of the experiment was the flow field

at the impingement point. These characteristics included stagnation point, recirculation, and expansion rates of the exiting flow. To better understand the recirculation that was accruing on the impingement surface, a viscous grease mixture was applied to the surface and short controlled bursts were performed. This aided in the discovery of a recirculation pockets just outside of the stagnation point.

The third study that was examined during this literary survey was the work performed by M. A. Mendez, J. M. Buchlin (2015) involving a jet stream impingement in confinement [5]. To characterize the confined environment flow, visualization as well as Particle Image Velocimetry was used. An environment, where one of the impingement walls was oscillatory, was chosen as the focus of this study [5]. In this experiment they varied the speed of oscillation, the distance from the jet nozzle, and the centerline height of the oscillation wall. From the two flow visualization techniques, along with the use of post processing software, they were able to measure jet stream direction and speed for each case study. It was shown that the areas where the oscillation wall were the closest to the nozzle, generated a vortex, which in turn pulled the main jet stream towards the vortex. When the oscillation wall was furthest away from the nozzle, i.e.. a flat plate, the jet straightened out and had mirroring vortices on either side of the jet. It was also observed that as the entire wall was set further away from the jet nozzle the vortexes created were of lesser magnitude.

The fourth study was numerical method work by Z. Rusak, Y. Zhang, H. Lee, and S. Wang (2017) on swirling flow inside of contracting and diverging pipes [15]. This group studied a great deal of previous works to baseline the progress made in the field and to identify experimental setups to replicate in the model. They used the experimental setups to define boundary conditions for the simulation. Their study was focused on swirling flow inside of finite-length pipes with Reynolds numbers greater than 100,000. The results concluded that divergence promotes the appearance of vortex-breakdown states at lower levels of the incoming swirl [15]. They also saw that pipe contraction delays the appearance of the vortex breakdown to higher levels of swirl and promotes the formation of wall-separation states [15].

The final paper examined in this literature study was written by R.F. Huang and F.C. Tsai (2001) [14]. This paper forced on the flow characteristics of swirling double concentric jets. For this experiment a dual jet stream was created where an outer swirling jet and a central jet stream were separated by a blockage wall. The swirl number of the outer jet stream could be adjusted

from 0.125 to 0.850 based on the *Re* of the flow and the angle of the vanes. Both the internal and external jet streams had separate velocity controls [14]. For this experiment flow visualization was achieved using a hot wire in conjunction with a laser sheet. Video was taken at 30 *fps* for these images. To measure the streamline patterns two-component laser Doppler velocimeter and particle seeding was implemented [14]. This system took data for 0.3s at 10 *kHz* sample rate [14]. The hot wire images and streamline patterns show that the blockage between the central nozzle and the outer nozzle create a standing vortex swirl on the blockage wall [14]. As the Reynolds number increase for the outer nozzle the vortex starts to breakdown and at even high Reynolds numbers the vortex sheds from the wall [14]. However, when the central jet stream Reynolds number was increased the vortex ring was more stable and prevents the vortex breakdown and shedding [14]. Their conclusion was that larger blockages create better flow mixing than smaller blockages which may be useful in some engineering applications.

The information that was examined in each of these experiments, [2] [5] [6] [14] and [15], aided in determining the impingement swirl variables as well as the proper setup to obtain valuable results. The setups were studied to find the configuration that would represent the conditions seen on the aircraft carrier the closest.

1.4 Specific Research Objectives

The objective of this research will be to characterize the flow behavior of a vortex flow on an impingement surface. To accomplish this task there will be four steps taken to achieve this goal. First, the existing diverging/ converging jet stream system will be characterized. This will be accomplished by comparing the jet stream centerline velocity profile of the turbulent jet stream to the results compiled from previous paper with similar configuration and the use a trip ring [6]. Second, flow visualization techniques will be developed to capture the flow field. Smoke generation will be developed to capture a cross section of the flow, while Schlieren imaging will capture the boundary layer and outer sections of the flow. Third, three different swirl nozzles will be characterized by measuring the cross-section velocity profile at different distances. The fourth objective will be a series of experiments with the three swirl nozzles and an impingement surface set to a specified distance away. This impingement surface will be set at three different angles. Finally, the measurements of the flow field velocity, in conjunction with the visualization data, will be discussed to explain airflow changes from one configuration to the next.

2. Experimental Setup

2.1 Experimental Facility

All experimentation was performed in the Micro Air Vehicles Laboratory of the University of Arizona at the AME Building. The pre-existing jet stream system [6] was modified for the use of this study as shown in Fig. 2.1.1, which has not been used in many years. Air from the blower (*B*) passes through a radiator (*E*), which has cold water from the facility circulating through it. The blower is a Boeing BC528989 with a 4-inch exit diameter. A Hitachi X200 variable draw power supply is used to operate the blower. This power supply uses 208V and 50A draw from building facilities. The power supply allows the blower to operate from 0 to 60 rpm and is controlled with a manual nob allowing for 0.1 rpm setting accuracy. The radiator is a 6" by 6" system that drops the temperature of the air inside of the system from 25°C to 17°C. The air then enters the 10-inch cubic seeding chamber (*A*) used for the Schlieren imaging system. The air proceeds, passing through a long diffuser (*F*) of 6° half-angle into a plenum chamber (*C*), 36" long and 12" in

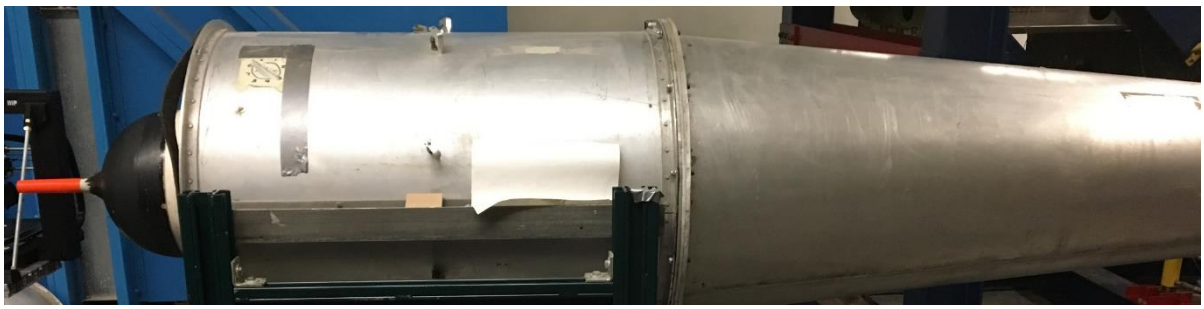

Figure 2.1.1: Facility jet system.

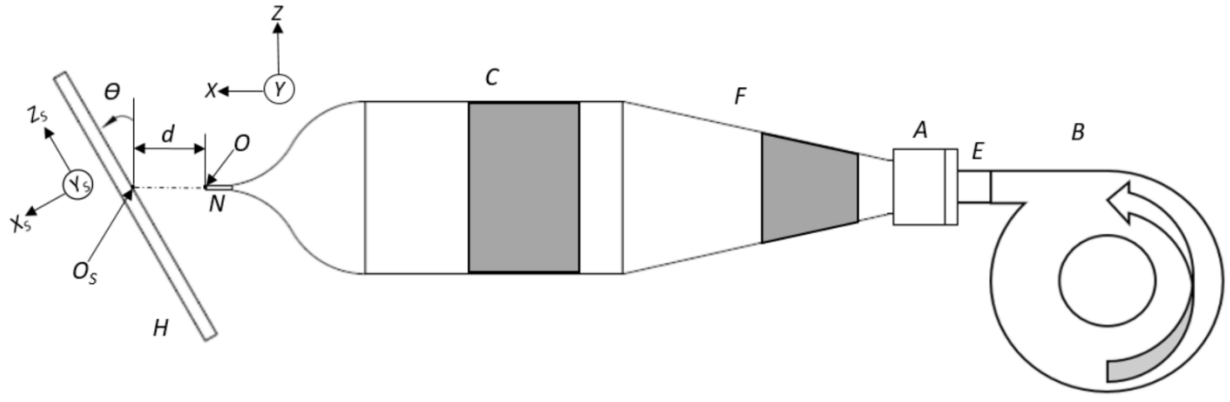

Fig 2.1.2: Schematic of the jet facility. The gray sections represent grids or screens, and the labelled parts are described in the text.

diameter. The plenum chamber has a grid of filters used to straighten the turbulent flow from the diffuser into a laminar stream. A nozzle (*N*) having a 12:1 dimeter contraction was used with the exit diameter D = 1". The nozzle has a removable attachment at is 6" long and has a constant diameter of D =1". Throughout the experiment multiple 3D printed inserts were placed into this attachment such as vortex forming geometries as well as a boundary layer trip. These will be covered in more detail in their respective sections.

Finally, the air exists the nozzle and interacts with the 24" by 36" impingement wall (*H*). The impingement wall will have a constant distance d of 2 inches for all experiments where *H* is used. For normal jet stream flows there is a laminar boundary layer surrounding the jet column, which exists with a top-hat velocity profile and a 0.1% turbulence level. The jet can be driven up to a maximum velocity U_e of 73 ft/sec.

2.2 Measurement Technique

A single wire probe mounted on a probe holder was used as the sole sensor for these experiments. The hot wire measures velocity through a voltage sent from the Constant Temperature Anemometry (CTA) hardware to the Streamline Pro from Dantec dynamics. The probe as well as the hardware that configures the sensor are off-the-shelf equipment. The system is configured via the associated software SteamWare pro, this was used to calibrate the hot wire setup, acquire and process measurements, and export the results. In this case calibration is achieved

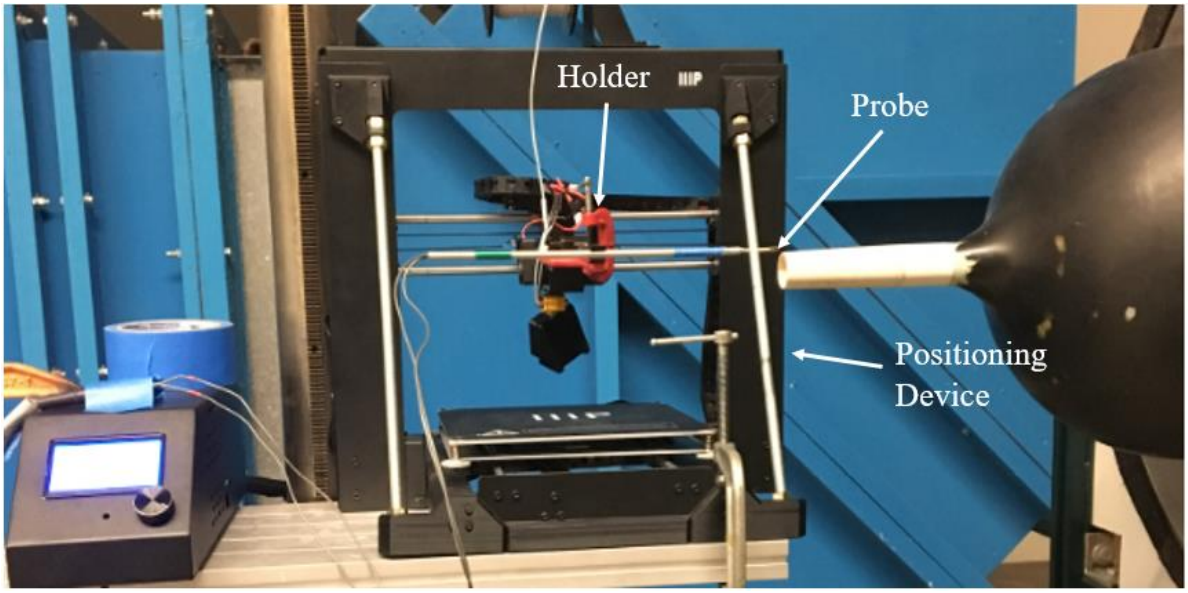

Fig 2.2.1: Hot Wire Measurement Setup.

by using the Dantec Dynamics StreamLine Pro Automatic calibrator. This calibrator used air set at a regulated pressure and a computer interface in the same software to create a jet of air at a well-known velocity. To allow for extended use of the probe the resistance overheat ratio and the current was reduced to 30% and 0.3 mA, respectively. The calibration system does not allow for the hot wire to be calibrated below 1 m/s. Because of this uncalibrated range from 0 m/s to 1 m/s the data that is collected during experimental tests need to be post processed. The raw voltage data from each run is examined to determine which data to keep and which to omit from the results. The hot wire anemometers have a -10V to +10V response range but typically does not use this full range. By looking at the calibration raw voltage file the bottom of the calibration range can be set. If the hot wire measures a voltage below this set limit than the data is omitted from the results because the conversion software outputs erroneous velocity readings.

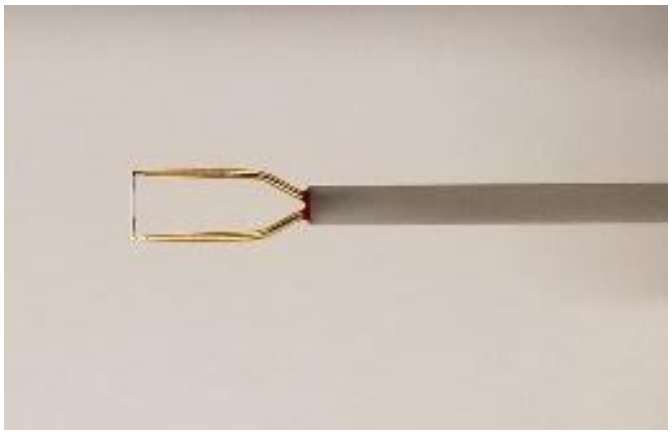

Fig 2.2.2: One-Dimensional Hot-Wire Anemometer

The output from the Streamline pro goes through an Analog to Digital Converter (ADC) to be used by the StreamWare Pro software and all its automatic calibration and data processing abilities. To achieve this a Data Acquisition system (DAQ) from National Instruments (NI) was used to allow for acquisition triggering needed by the CTA system. The system was set to sample at 1 kHz and a sampling duration of 1 s for each position of the probe. An experimental setup was developed inStreamWare Pro to run the data acquisition. The system was setup for manual triggering of the DAQ and would allow for position data to be entered between each event. Once all the positions were measured the experiment was manually stopped.

To acquire accurate position location a model IIIP V2 3D printer was modified so that the CTA probe could be mounted to the extruder head. This printer had manual axial and vertical movement

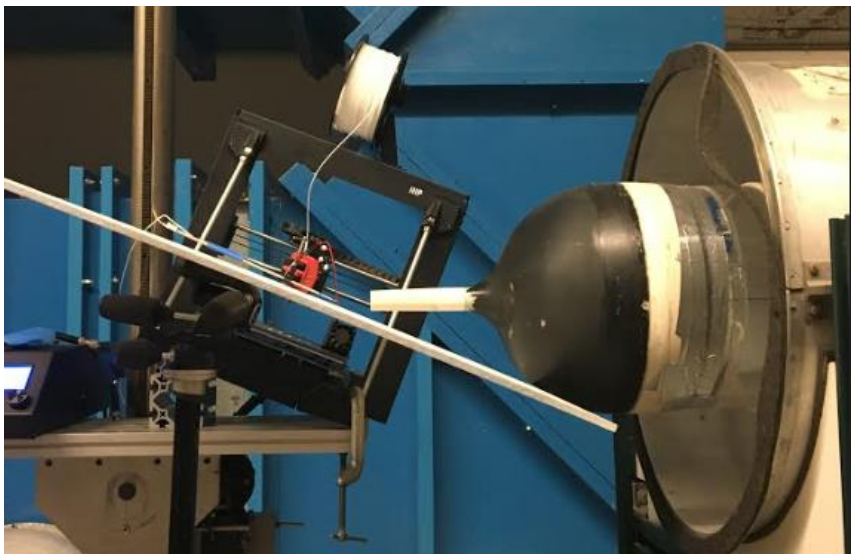

Figure 2.2.3: Axial measurement setup for tripped nozzle at station 0D where θ = 67.5°

control using the knob controller seen in Fig. 2.2.1. The printer has a positional accuracy of 0.01 mm. To measure the cross-section velocity profile for each of the nozzles the probe was moved along the centerline of the nozzle in the vertical direction.

The StreamWare Pro software was then used to post process the data. Each trigger event was averaged over the duration of the acquisition time to get the mean voltage measured from the CTA. The process discussed previously was then used to find measurements below 1 m/s and omitted them from the results. Finally, the calibration data is applied to the mean voltages to obtain axial mean velocities. To measure the azimuthal mean velocity the probe would need to be rotated 90º so that the one-wire probe is perpendicular to the azimuthal direction, see Fig. 2.2.2.

Table 1: Total Hot Wire Measurements Error

Device	Measurement	Accuracy	% Error
1D Hot Wire Probe	Velocity	0.05m/s	5
3D Printer X Axis	Distance	.01mm	0.1
3D Printer Y Axis	Distance	.01mm	0.1
3D Printer Orientation	Angle	5°	0.4
		Total % Error	5.6

The total estimated error of the hot wire probe measurements is shown in Table 1. This error measurement is based on 1m/s, the lowest velocity that the probe was calibrated for. The hot wire probe and data acquisition system has an accuracy of ±0.5m/s. While the positional accuracy of

the 3D printer in both the *X* and *Y* direction is ±0.01mm where the measurements were taken in millimeters. Finally, the positional angle of the probe was positioned to be perpendicular to the probe by hand and is estimated to be around ±5° true to position. While the total error of 5.6% seems to be high this is at the smallest measurement taken. These means that is it the maximum error and most measurements have a much smaller component of error. For example, at 30m/s the error is than 1%.

To measure the flow interacting with the impingement wall the probe was setup to be perpendicular to the wall, see Fig 2.2.3 for an example. The velocities are also measured in the orientation of the impingement wall, *Xs, Ys, Zs* where the nozzle measurements were taken in the nozzle coordinates, *X*, *Y*, and *Z*. For the impingement wall measurements, the origin is the wall surface for *Xs* and the centerline of the nozzle for *Ys* and *Zs*. For the nozzle coordinates the origin is the exit plane for *X* and the centerline of the nozzle for *Y* and *Z*.

2.3 Flow Visualization Technique

Although velocity measurements from the hot wire anemometer provide valuable data about a jet stream profile, discrete measurements miss vital information for understanding the overall behavior of the flow. In an effort to observe the larger picture of the jet stream, multiple flow visualization techniques was developed. The previous works performed, [6] were analyzed as a starting point for the visualization system requirements. A camera was set to 5 kHz to match that of the example setup [6]. The baseline jet stream settings were chosen to be 1 in diameter (*D*), see

(a) **(b)**

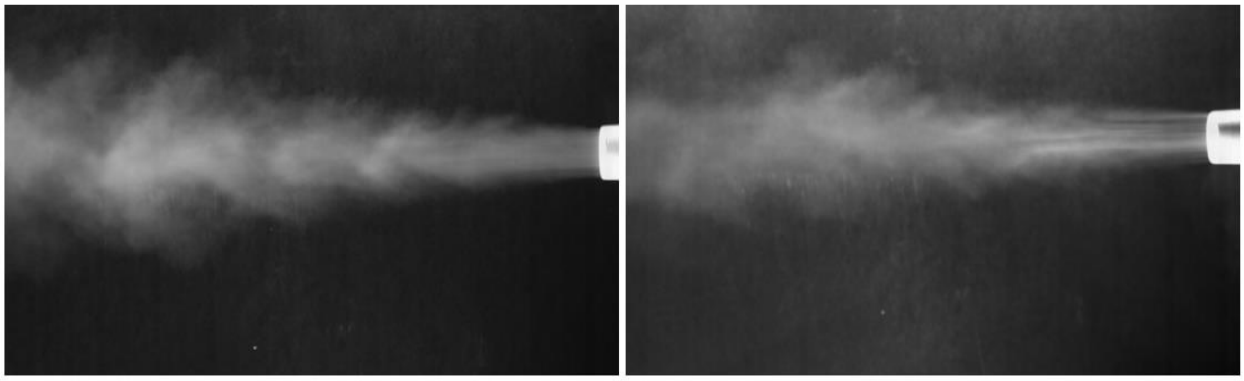

Fig 2.3.1: Smoke injection of 1in jet. The Reynolds numbers range from (a) 3.7 x 10^4 (b) 8.5 x 10^4.

Fig 1.2.1, and the nozzle did not have the trip ring or any other flow disturber for these series of tests.

Once the system was setup the easiest flow visualization technique to experiment with was smoke injection. A smoke generator was connected to seeding box (*A*) in Fig. 2.1.1. The smoke then traveled through the diffuser, chamber, and out the nozzle. The results for two different velocities, 27 ft/s and 62 ft/s can be seen in Fig. 2.3.1.

The results that yielded from the experiment showed that it was possible to get clean results for the range that was shown in Fig. 2.3.1. However, once the Reynolds numbers exceeded 9.0 x 10^4 the smoke generation system became very faint, to the point that the characteristics of the flow was no longer discernable. This was a major concern for vortex flow because the jet stream would be much more dispersed compared to the pipe flow used for the initial testing.

The next flow visualization technique that was tested was the Schlieren imaging system. While the smoke injection system provides an external view of the flow, the boundary layer prevents one to see how the centerline flow field is interacting. For the setup of this system see Fig. 2.3.2. A cellphone flashlight with a pin-hole cover acted as the point light source (*L*). This light source was directed at a parabolic mirror (*G*) with a 40” focal length and the mirror was configured behind the existing jet stream (*K*). The light reflects off *G* and at the focal point of the reflection a razor blade edge (*I*) was setup to block half of the reflected light, acting as a filter. The high-speed camera (*J*) was then situated behind the knife edge using the aperture, focus, and distance from the knife edge until there was a clean and focused image. CO_2 was injected into the seeding box (*A*)

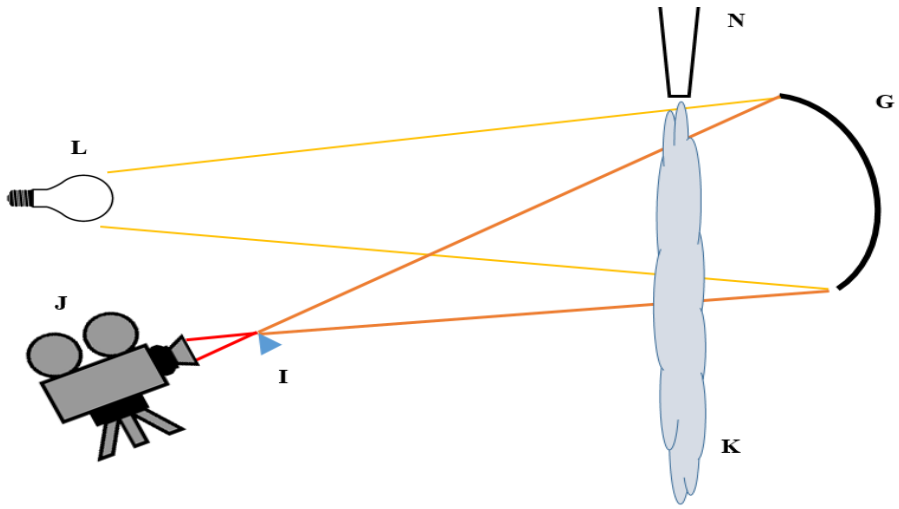

Fig 2.3.2: Schlieren Imaging System Diagram.

Fig 2.3.3: Boundary layer trip ring installed in nozzle at 1" from the exit (left); 3D model of the trip ring (right).

through a 5/16" flexible pipe at a pressure of 30psi. This changed the density of the income air to approximately 1.50 greater than the surrounding air. This density differential makes the images from the Schlieren system much cleaner. Also, the Reynolds number for the 30m/s air flow is 4.87 x 10^4 while the jet stream flow that is seeded with CO_2 has a Reynolds number of 6.16 x 10^4. This is closer to the 40m/s air flow which is 4.87 x 10^4, which is well within the range of Re being studied in this paper.

3. Measurements

3.1 System Characterization

The jet stream system used for these experiments resembles that of the system used in previous experiments performed [6]. To determine if these systems were indeed comparable a baseline experiment was performed. Other researchers, [6], measured the centerline velocity profile of the jet stream flow at different Reynolds numbers with a trip ring installed in the nozzle. To replicate this setup a 3D printed boundary layer trip ring was fitted tightly into the 1 in. nozzle about 1 in. upstream from the exit, see Fig 3.1.1. Deep axial notches were formed into the ring to break up any organized vortex shedding. The ring is 0.140 in. long and 0.020 in. thick matching the trip ring that was described in other work, [6]. This ring was fitted into the nozzle such that the groves faced the oncoming jet stream.

The exit mean axial speed, *Ue*, (see Fig 1.2.1) of the centerline was measure at Reynolds numbers 6.2 x 10^4, 8.3 x 10^4, 1.03 x 10^5 and 1.24 x 10^5 to verify that the system remained constant. The *Ue* was calculated by taking discrete measurement along the cross section of the nozzle and taking the mean of these values. The results were then compared to the plots provided by [6], seen in Fig. 3.1.2. While the data does not march perfectly with the results measured by [6], the general profile trends match. It is also worth noting that the main concern for this measurement was to verify that the Reynolds number did not change the jet stream shape while the trip ring was installed. It can be observed that for the range shown in Fig. 3.1.2 no significant change is profile shape occurred. The largest deviation from the mean profile was 3.2% which could be caused by the hot wire anemometer not being exactly perpendicular to the jet stream. With this data it has shown that the two systems are similar enough that the data collected should be comparable. The characterization also serves as a validation of the measurement techniques used and shows that the experiments performed in [6] were repeatable. With the completion of this experiment the setup is ready to move to swirl jet streams.

The next step to ensuring that the hot wire setup will work for the swirling jet stream is to measure the axial and azimuthal velocity profiles as a function of the tripped jet stream, the *U* and *V* directions respectively (see Fig 1.2.1). This will show how the jet stream is transforming as it moves forward from the exit of the nozzle. Based on the results seen in Fig. 3.1.2 it has been

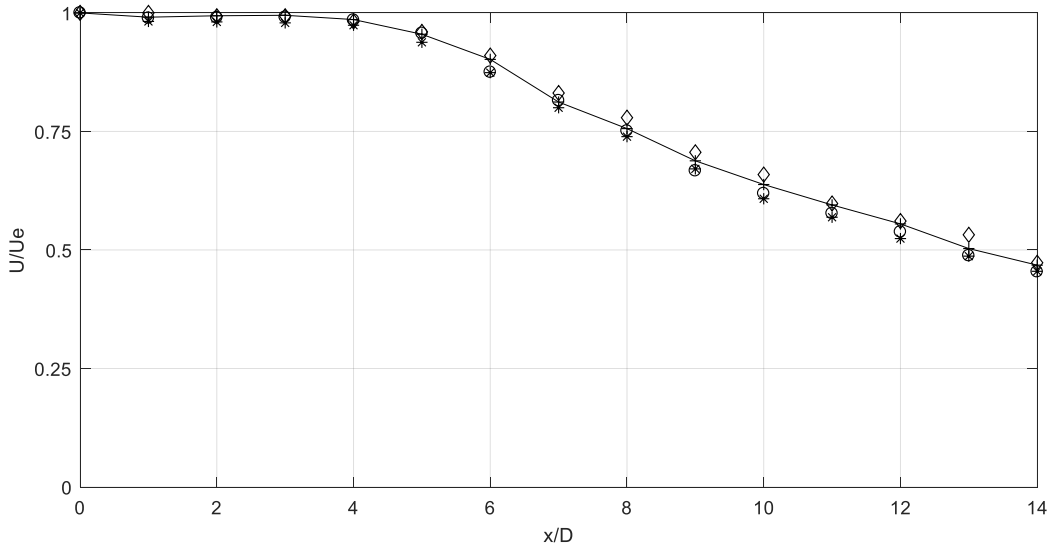

Fig 3.1.1: Profile of the mean axial speed on the centerline at several Reynolds numbers, as denoted by the following data symbols: ◊, 6.2 x 10^4; +, 8.30 x 10^4; ○, 1.02 x 10^5; *, 1.24 x 10^5, --, [6].

determined that the Reynolds number and velocity of the tripped jet stream nozzle will not affect the results as long they fall within the boundaries of the Reynolds number previously studied. For the axial profile measurements the system was set to a Reynolds number of 6.2×10^4. The same measurement system seen in Fig. 2.2.1 was used for this experiment where the hot wire was setup at the center of the nozzle and was moved upward to take to axial samples. A data set was collected for five different stations from the exit of the nozzle; $x = 0, 2D, 4D, 6D$ and $8D$. The data was then normalized to the mean velocity of the exit and was then combine in a single plot seen in Fig 3.1.3 for the axial velocity U. The vertical lines for Figs 3.1.3 and 3.1.4 are to indicate where zero is for each of the stations measured. They were offset by 0.5 U/Ue to fit them all on the same plot.

Fig. 3.1.3 has an almost identical shape to the azimuthal profile measured by [6]. In this plot R represents the radius of the nozzle exit. The exit profile has a uniform top hat shape where the U velocity is consistent across the entire diameter of the nozzle then reduces to zero immediately after the lip of the nozzle. As the stations progress from the exit the mean velocity reduces slightly and the jet stream increased in diameter. The shape becomes a much wider and more evenly distributed profile. This confirms that the tripped nozzle system and hot wire measurements taken for the U directions are accurate because we were able to repeat the previous setup so closely.

Fig. 3.1.4 is the measurements of the V-velocity component of the jet stream at each of the five stations. The measurements were taken at the same interval and method as the U-direction but the 1-dimensional hot wire was positioned perpendicular to the exit stream. Again, the measurements started at the center of the nozzle and moved upward. All the data was normalized to the mean velocity (Ue) of the x- direction allowing for a comparison between the U and V velocities. Just like Fig. 3.1.3, Fig. 3.1.4 had very similar results to the measurements taken by [6]. At the nozzle exit there is relatively minimal V direction velocity except for the small peak that formed right at the edge of the nozzle. As the stations progress from the exit the peak stays at the same magnitude but becomes wider in both directions. The center of the peak also moves from the $r = 1R$ location and drifts closer to the centerline of the stream. Again, this confirms the tripped nozzle system and hot wire measurements taken for the V directions are accurate. This provides us with confidence that the data we will collect for the swirling nozzles in both the U and V directions will be true.

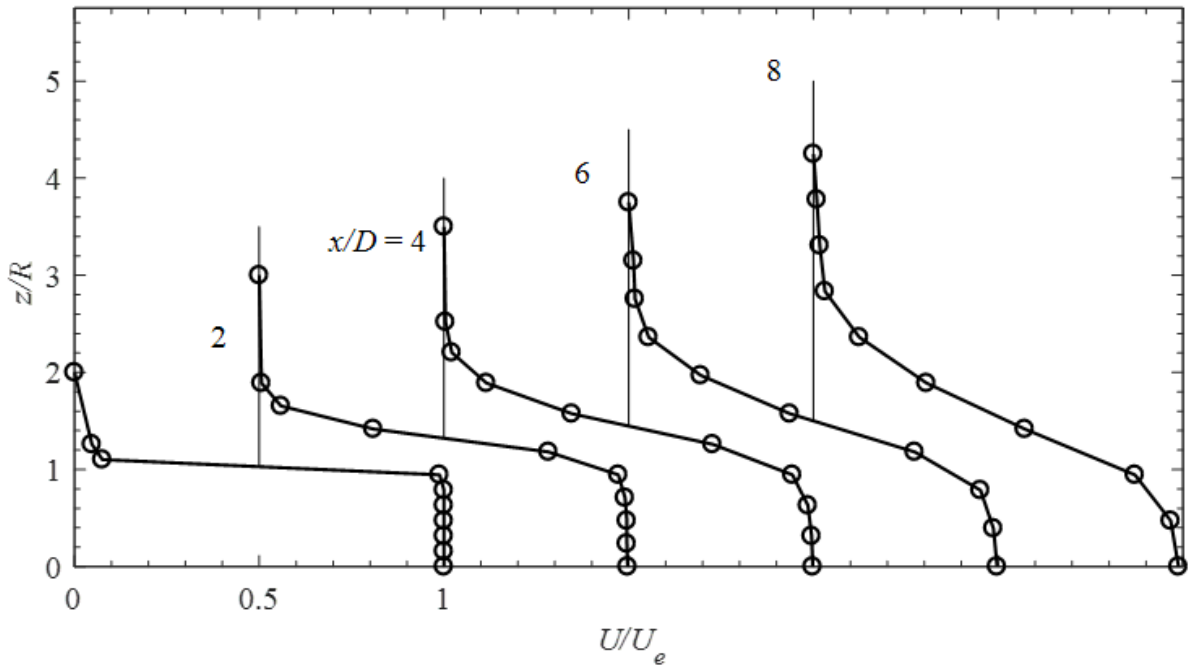

Fig 3.1.2: Axial mean velocity profile (*U*) at five stations along the jet axis. Tripped jet stream nozzle.

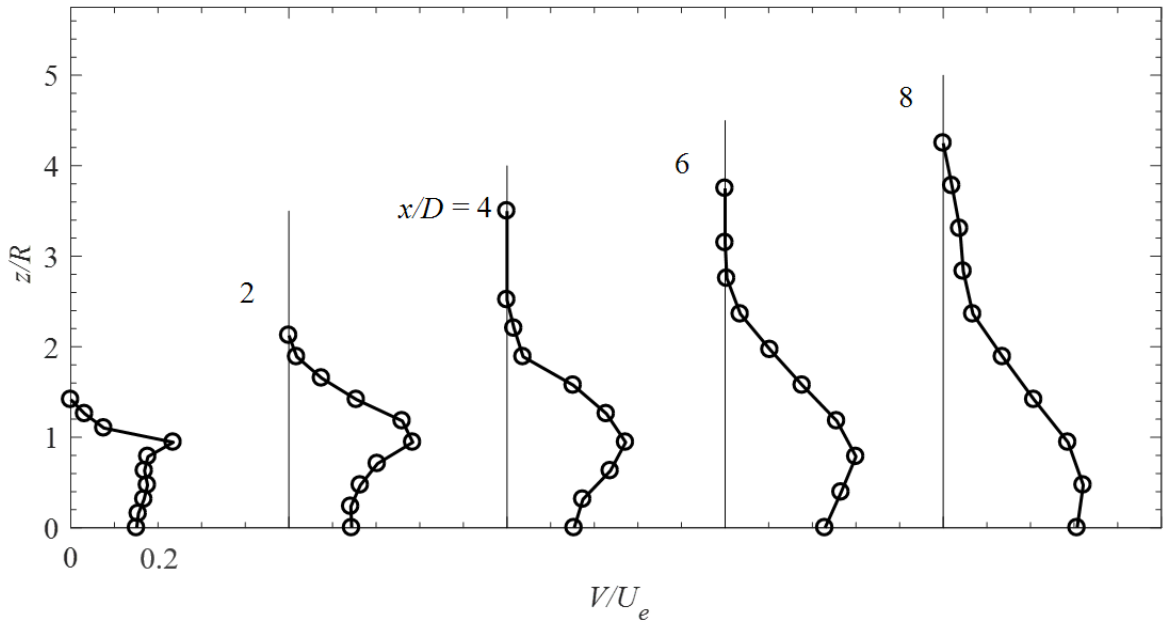

Fig 3.1.3: Azimuthal velocity profile (*V*) of the axial component of turbulent velocity; Tripped jet stream nozzle.

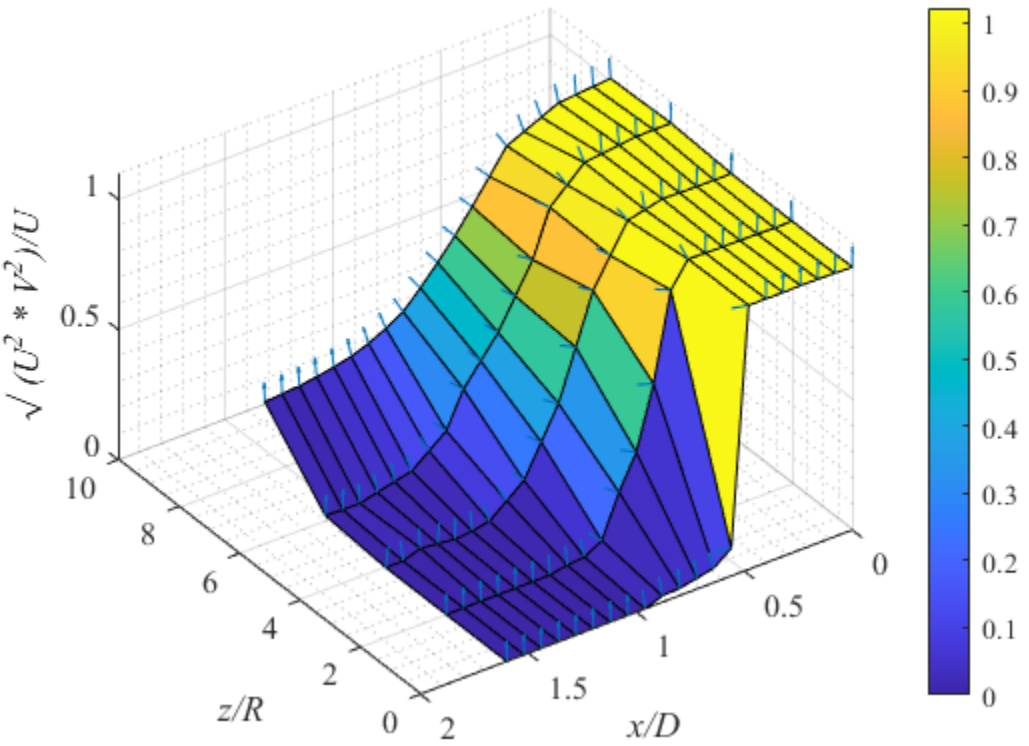
√ (U² * V²)/U
1
0.5
0
10
8
6
4
2
0
z/R
2
1.5
1
0.5
0
x/D
1
0.9
0.8
0.7
0.6
0.5
0.4
0.3
0.2
0.1
0

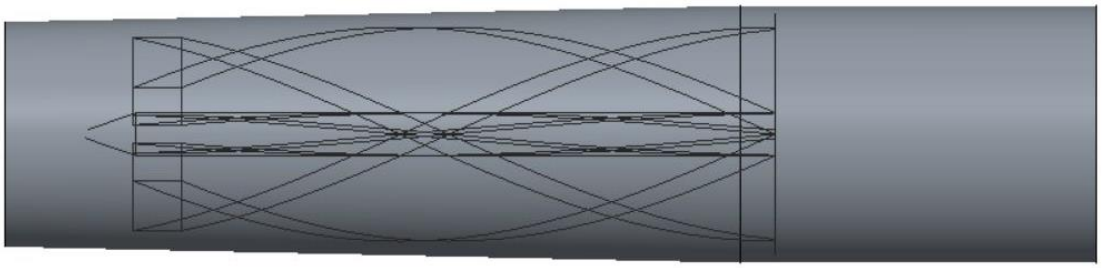

Fig 3.1.4: Swirling Jet Nozzle Overview

This concludes the system characterization for collecting hot wire data. The two comparisons to [6] have been successfully made. The first is the centerline profile of the tripped jet stream at different Reynolds numbers. It was demonstrated that in the ranges compared there was little to no effect on the centerline profile. This comparison confirmed that the jet stream system is similar enough to the one used by [6] to achieve the same results. The second comparison made was the velocity profile for both the *U* and *V* direction. The results showed that the tripped jet stream had little to no axial velocity and that the velocity profile spread axial as it moved forward away from the exit. The results validated the hot wire measurement setup for both directions.

3.2 Swirling Nozzle Characterization

For this research a vortex jet stream needed to be generated using the setup seen in Fig. 2.1.1. To accomplish this vortex stream new nozzles needed to be designed and characterized. The nozzle dimensions were kept the same as the original jet stream nozzle where the exit diameter is 1in and the length of the nozzle was 5in. To generate the swirling flow the general concept of a turbine engine was utilized where there is a central core with four blades inside of the nozzle, as seen in Fig. 3.2.1. The first 1.5in of the nozzle were unchanged so that it could be properly mounted onto the jet stream system. The next 3in of the nozzle had the central core and blade configuration and the final 0.5in near the exit was also left unchanged to allow for the flow to recombine prior to exiting the nozzle.

Three different blade pitches were selected to give a range of swirl numbers. The lowest pitch was three inches where the blade rotates 180 degrees along the length of the nozzle. The air flow from the jet stream travels along the path of the blades which generates a corkscrewing flow. This corkscrew path created an azimuthal component to the jet stream velocity vector. The flow then

exits the blades where it can mix with the other separated streams before it exits the nozzle. The other two nozzles have a pitch of 5.0 ad 7.0 inches respectively. This translates to the blades rotating 300 degrees and 420 degrees over the 3in. length of the nozzle. All other features are identical to the first swirling nozzle described above. A visualization of the blades for each nozzle can be seen in Fig. 3.2.2 where the external of the nozzle is removed.

These swirling nozzles were modeled in a Computer Aided Design (CAD) software and 3D printed because of their complicated internal geometry. Because the nozzles were not subjected to extreme temperatures or high loads the Polylactic Acid (PLA) filament from the 3d printers was a suitable material for fabrication. Once printed the nozzles needed to be characterized to determine if they would have a sufficient amount of swirl generated by the pitched blades.

The characterization of the swirling nozzles was performed in the same way as the baseline jet stream nozzle. Both the *U* and *V* velocity components of the jet stream were measured at five *x*-stations along the jet stream creating a profile of the flow. For these measurements the system was set to a Reynolds number of 6.2 x 10^4. The hot wire was setup at the center of the nozzle and was moved upward to take the measurements. A data set was collected for five different stations: the nozzle exit, 2*D*, 4*D*, 6*D* and 8*D* from the exit of the nozzle. The data was then normalized to the mean velocity of the exit and then was combine in a single plot.

The *U* and *V* profiles for the swirling nozzle with a pitch of 3 can be seen in Fig. 3.2.3 and 3.2.4 respectively. Fig. 3.2.3 shows that the profile for the *U* direction is a completely different

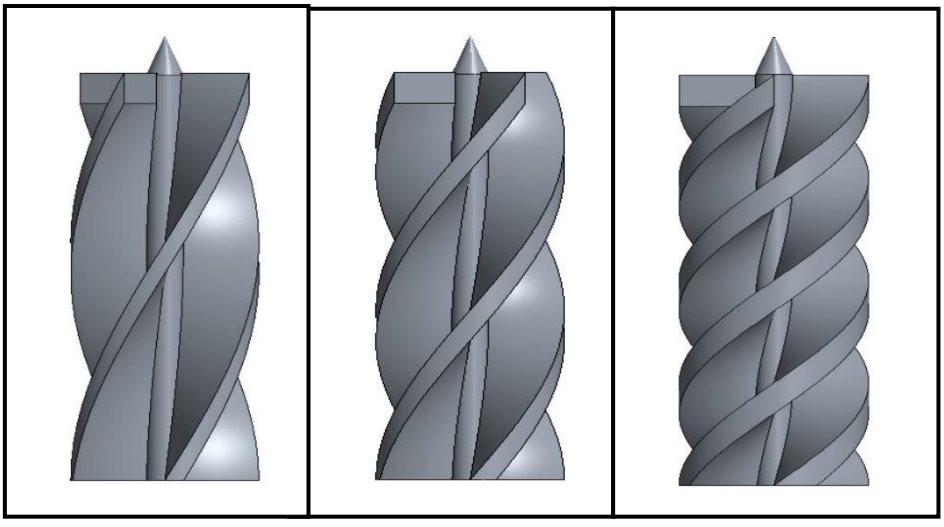

Fig 3.2.1: Swirling Jet Nozzle Interior; (a) 3.00" Pitch (b) 5.00" Pitch (c) 7.00” Pitch.

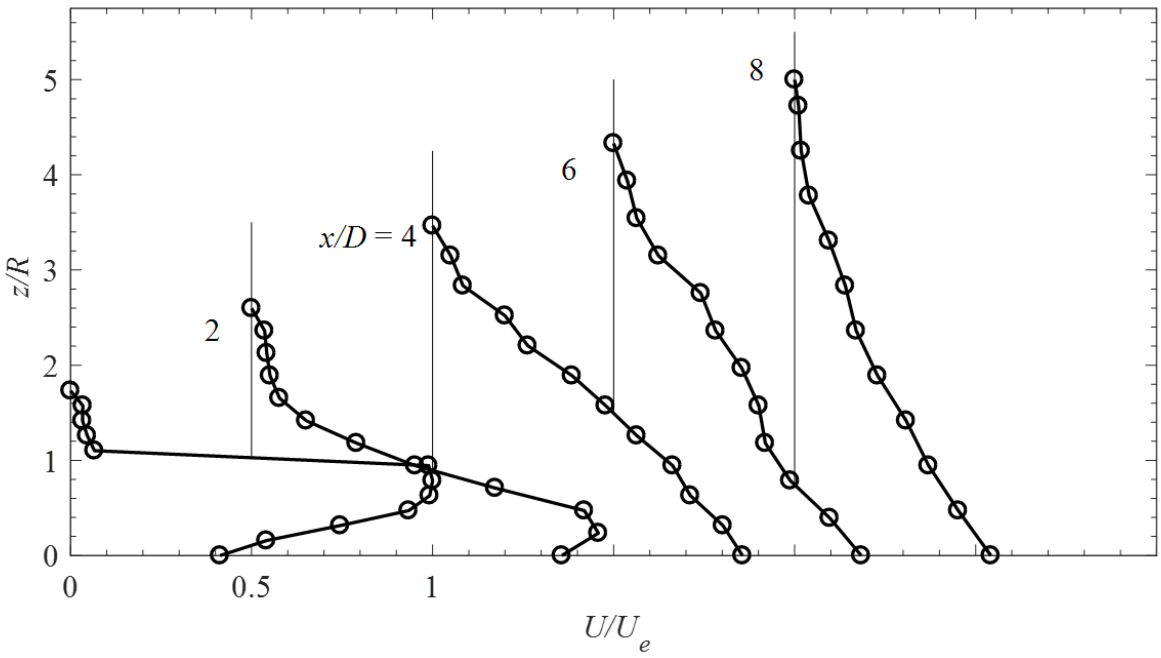

Fig 3.2.3: Axial mean velocity profile (*U*) at five stations along the jet axis. Swirling Nozzle with Pitch 3".

shape than that of the tripped nozzle. At the exit of the nozzle the center of the profile has about half the velocity as the outer portion. This is due to the center core of the nozzle generating a low-pressure area and forcing the flow around it. The *U* direction at the nozzle does maintain a consistent velocity from 0.5 R to 1.0. As the jet stream moved forward along the stations the peak of the profile moved toward the center axis. The profile also grows in diameter to be about five times larger at station 8*D* compared to the exit of the nozzle. The overall speed of the flow slows down at each station and the profile becomes much more uniform creating a cone like structure. At station 8*D* the peak speed has reduced to just half of the speed at the exit plane.

The *V* direction of flow, as seen in Fig. 3.2.4, has taken on a different shape than that of the tripped nozzle. At the exit plan the profile resembles that of the *U* direction but with about a third of the velocity. However, as the flow moves along the stations the peak does not moved toward the center of the flow but rather moved out to 1.5*R* and maintains that peak location. The axial component of the flow does dissipate in strength and widen in circumference at each of the stations. At x/D= 6*D* and 8*D* the axial component of the flow has become very uniform for the majority of the profile and reduced in strength at the edge. This swirling nozzle reduces in velocity in both the *U* and *V* direction much quicker than the tripped nozzle. This is caused by the stronger azimuthal

component that is generating the swirl of the flow pushing the airflow outwards instead of in a tightly formed jet stream normal to the nozzle.

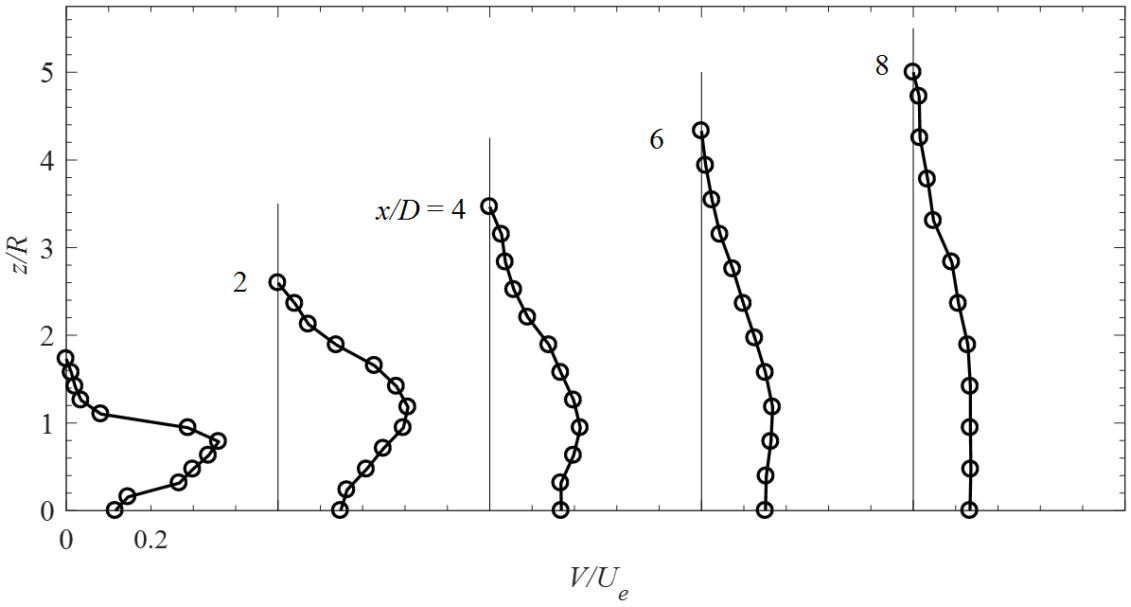

Fig 3.2: Azimuthal velocity profile (*V*) of the axial component of turbulent velocity; Swirling nozzle with Pitch 3".

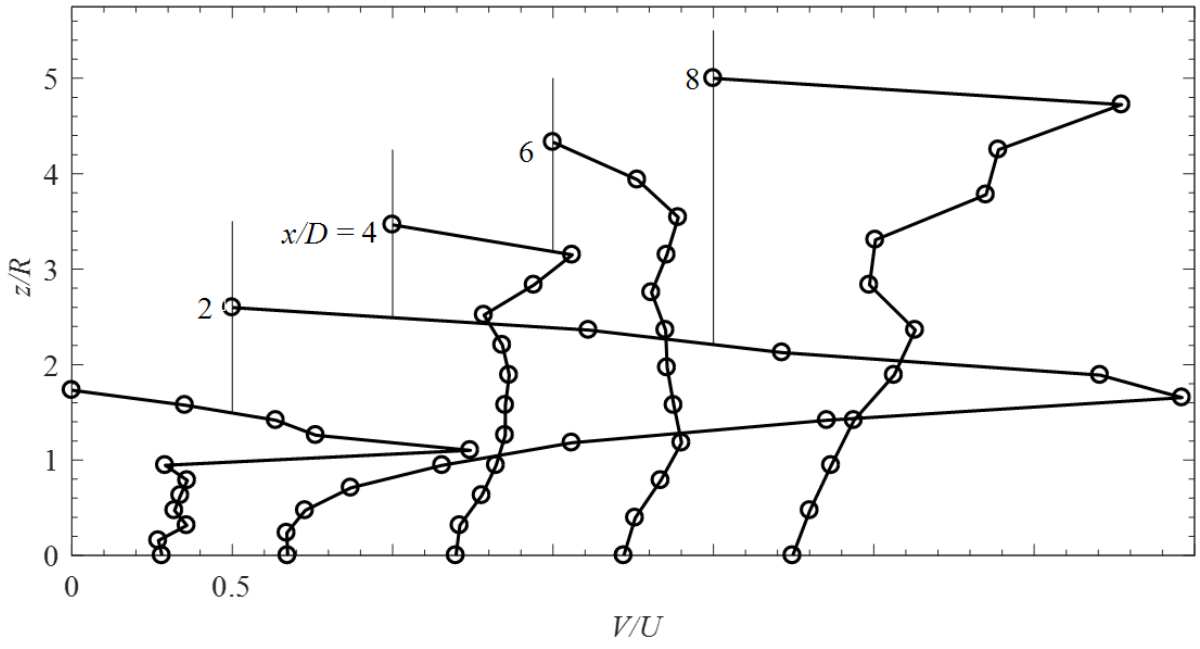

Fig 3.2.5: Swirl intensity profile at 5 stations along the jet axis; Swirling nozzle with Pitch 3".

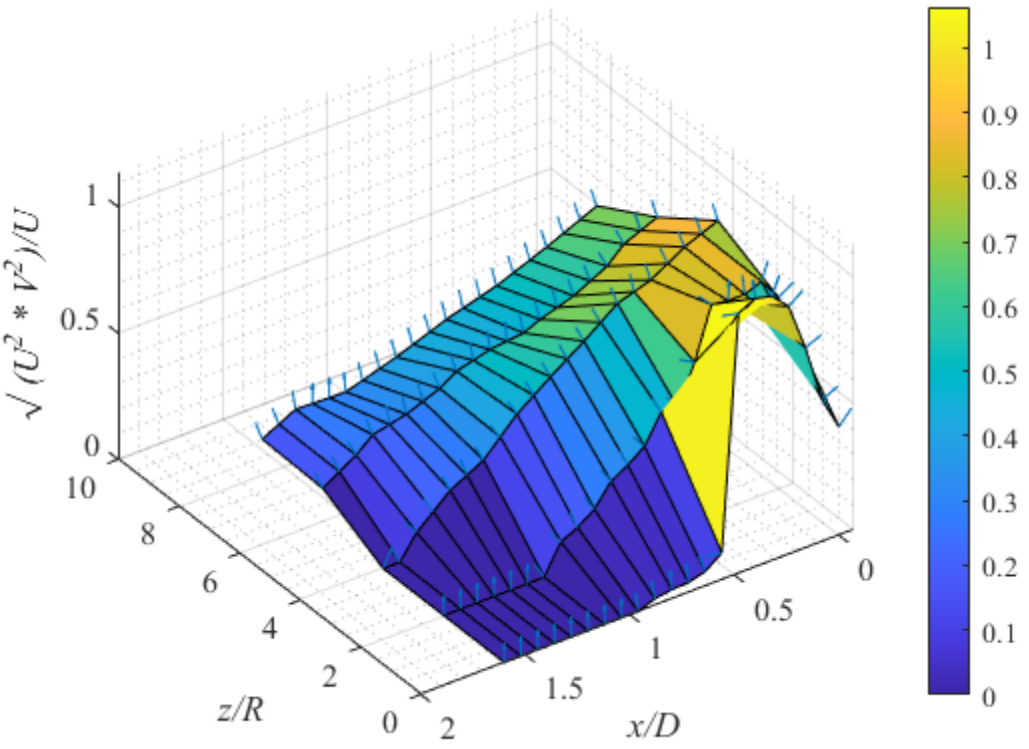

The *U* and *V* data was combined to generate an intensity profile for each station measured, seen in Fig. 3.2.5. This graph gives a general idea of how much swirling is being generated by the nozzle and where the maximum swirling is occurring along the azimuthal length of the stream. It is worth noting however that some of the data in the swirl intensity plots can be devising. For example, at station *x/D* =8 there appears to be a large peak out at *r/R* = 4.75. But in the *U* and *V* plots at this same location there are very small intensities of flow. The swirl values are divided from equation (15) where the *V/U*. So, at these small values it is not uncommon for *V* to be equal or greater than *U*. Because of this, the outer edges of the swirl profiles will not be discussed since their magnitude is less than 10% of the maximum magnitude of the swirling jet stream.

For the swirling nozzle with pitch 3" it can be observed that the greatest swirling effect occurred approximately 2*D* from the exit of the nozzle with a peak of 2.96. At the exit of the nozzle, the swirl number on average is .31 however, once this stream reaches 2*D*, the swirl number increases to 1.18. Past 2*D* the swirl profile returns to about .35 for the remaining stations measured. As discussed earlier, it is thought that the axial velocity is so great at 2*D* that the majority of the swirling dissipates outwards at 2*D* leaving a more uniform jet stream that flows further down the axial direction.

The *U* and *V* profiles for the swirling nozzle with a pitch of 5” can be seen in Fig. 3.2.7 and 3.2.8 respectively. Fig. 3.2.7 shows that the profile for the *U* direction has a similar shape to Fig 3.2.4. At the exit of the nozzle the center of the profile has about half the velocity as the outer portion but quickly increases to its full magnitude. Again, it is due to the center core of the nozzle generating a low-pressure area and forcing the flow around it. The *U* direction at the nozzle does maintain a consistent velocity from 0.3 *R* to 1.0 and resembles that of the top hot profile at *x/D* = 0. As the jet stream moved forward along the stations the peak of the profile moved toward the center axis but much more gradually compared to the 3” pitched nozzle. The profile also grows in diameter like the previous nozzle but has more of a rounded shape instead of the cone structure earlier observed. At station 8*D,* the peak speed has reduced to just under half of the speed at the exit plane. Overall, the *U* direction velocity of the 5” pitch nozzle is quite like the 3” pitch nozzle. The major difference is that the flow does not seem to merge back to the center of the jet stream as quickly creating a more evenly distributed profile.

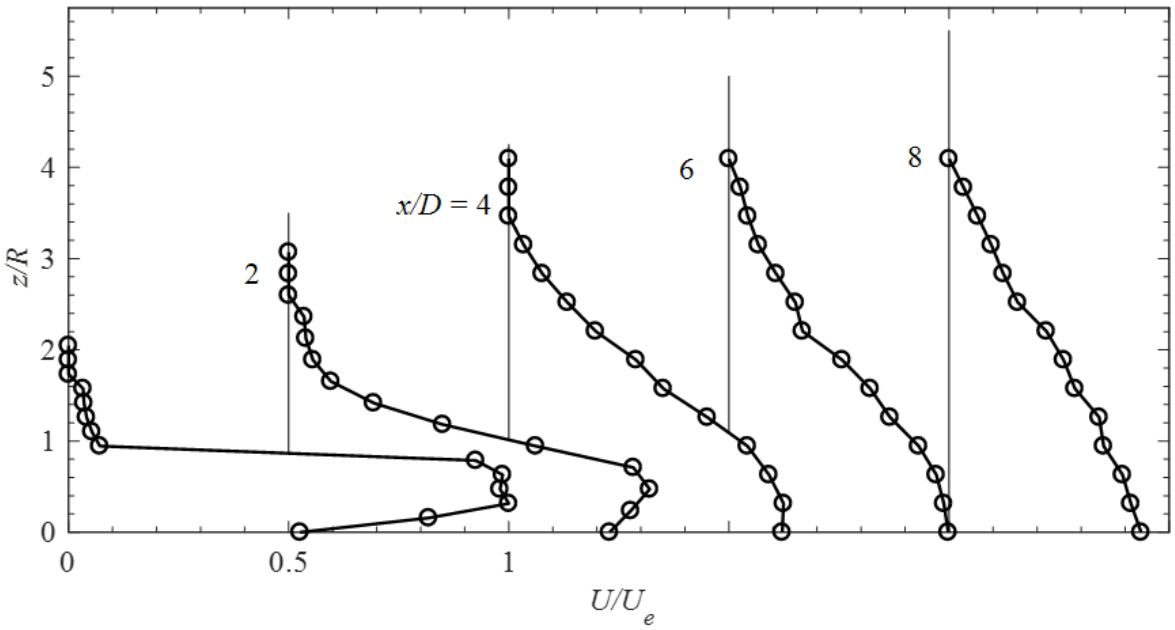

Fig 3.2.6: Axial mean velocity profile (*U*) at five stations along the jet axis; Swirling Nozzle with Pitch 5”.

The *V* direction of flow, as seen in Fig. 3.2.8, again resembles that of the 3” pitch nozzle shown in Fig. 3.2.5. At the exit plan, the profile is accelerating as it approaches the edge of the nozzle

much more sharply than the 3” pitch nozzle. As the flow moves forward to the next station the peak maintains is position near *r/R*=1 where the 3” pitch nozzle moved further outward. The overall profile does decrease in magnitude as it moves forward and becomes more uniform in shape. At *x/D* = 8 the axial profile is almost completely singular in magnitude. Overall, the azimuthal profile of the 5” pitch is like the 3” pitch azimuthal profile in both shape and behavior. The major differences are the initial shape and the transformation as the flow moves downstream.

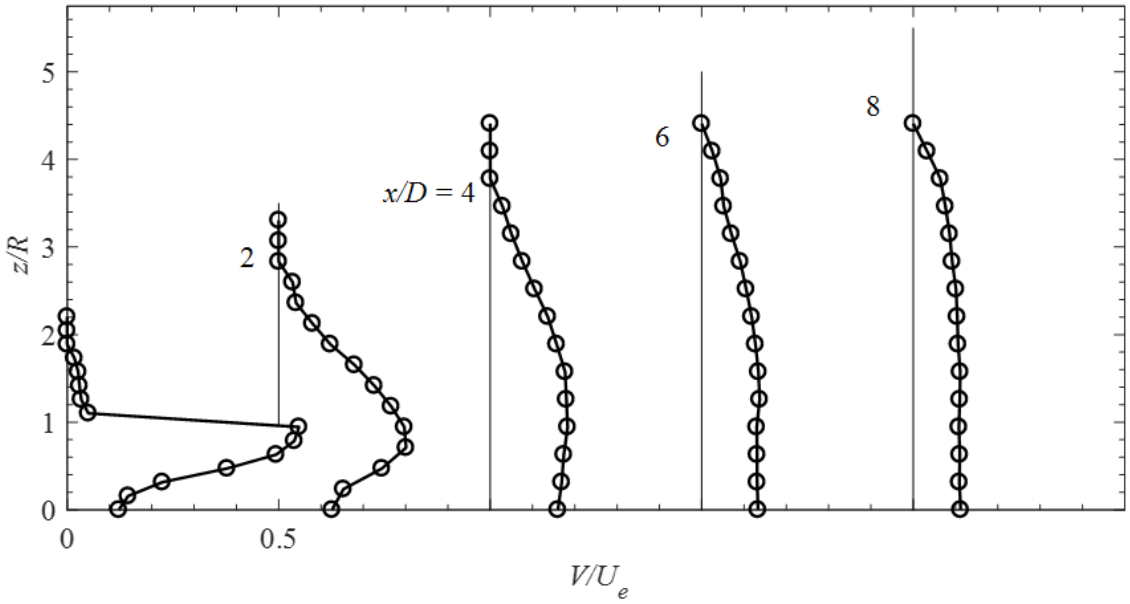

Fig 3.2.7: Azimuthal velocity profile (*V*) of the axial component of turbulent velocity; Swirling nozzle with Pitch 5".

For the swirling nozzle with pitch 5” it can be observed that the greatest swirling affect occurred, just like the first swirling nozzle, at approximately 2*D* from the exit of the nozzle with a peak of 2.71. At the exit of the nozzle the swirl number is on average .59 however, once this stream reaches 2*D* is increases to 1.16. So, although the peak of the swirling profile was not as great as the 3” pitch nozzle overall the profile had a higher swirl number. Past 2*D*, the swirl profile returns to about .60 for the remaining stations measured. The major differences that can be observed when comparing Fig. 3.2.8 with Fig 3.2.6 are the shape of the profile after 2*D*. Because the azimuthal velocity of the jet streams maintains its shape much further out along the *r/R* direction than the axial velocity. The swirl number spikes as the outer limits of the jet stream are reached. This seems to indicate that, unlike the 3” pitch swirl nozzle, the axial component of the stream is maintained even after it reaches its peak at 2*D*.

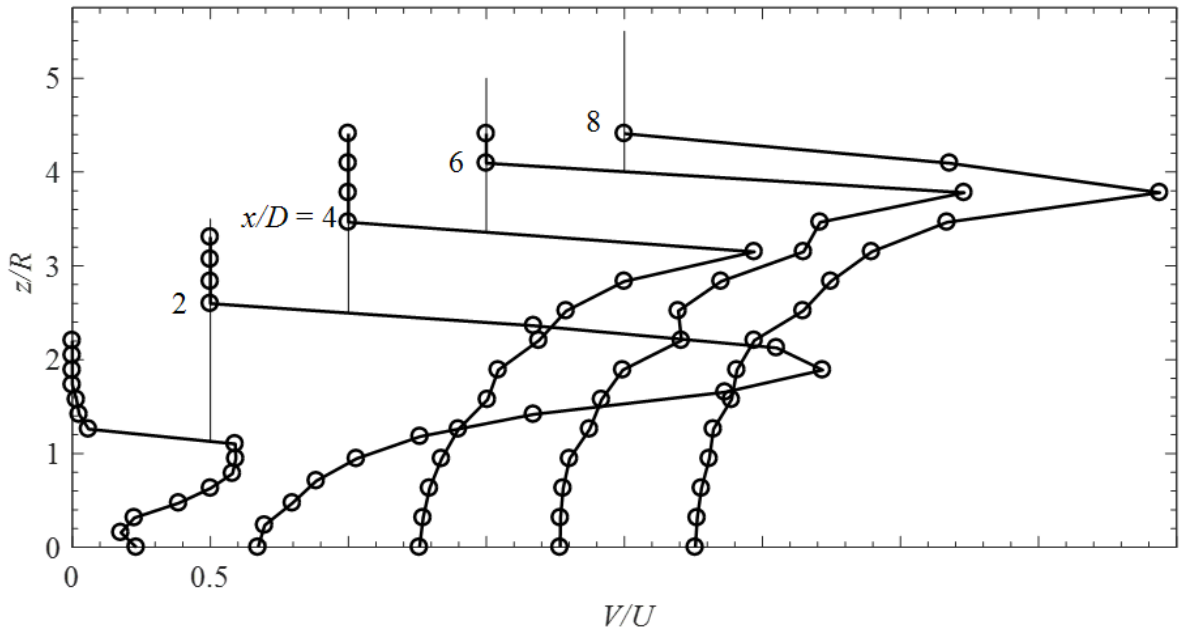

Fig 3.2.8: Swirl intensity profile at 5 stations along the jet axis; Swirling nozzle with Pitch 5".

The *U* and *V* profiles for the swirling nozzle with a pitch of 7" can be seen in Fig. 3.2.10 and 3.2.11 respectively. It is shown from Fig. 3.2.10, that the profile for the *U* direction has a similar shape to Fig 3.2.4. At the exit of the nozzle the center of the profile has about a quarter of the velocity as the outer portion and sharply increases to its full magnitude. Again, it is due to the center core of the nozzle generating a low-pressure area and forcing the flow around it. The *U* direction at the nozzle does not maintain any uniformity like the other two nozzle profiles. As the jet stream moved forward along the stations the peak of the profile moved away the center axis which is quite different when compared to the other nozzles. The profile also grows in diameter like the previous nozzles but has a much flatter profile after $x = 2D$. At station $4D$ the peak speed has reduced to a quarter of the velocity seen at the exit plane. Overall, the *U* direction velocity of the 7" pitch nozzle is initially like the other nozzles but afterward it behaves completely different. The 3" and 5" pitch nozzles have a normal flow to merges back to the center of the flow. For the 7" pitch nozzle, the axial velocity moves outwards and then quickly reduces in speed and the peak dampens as it moves forward.

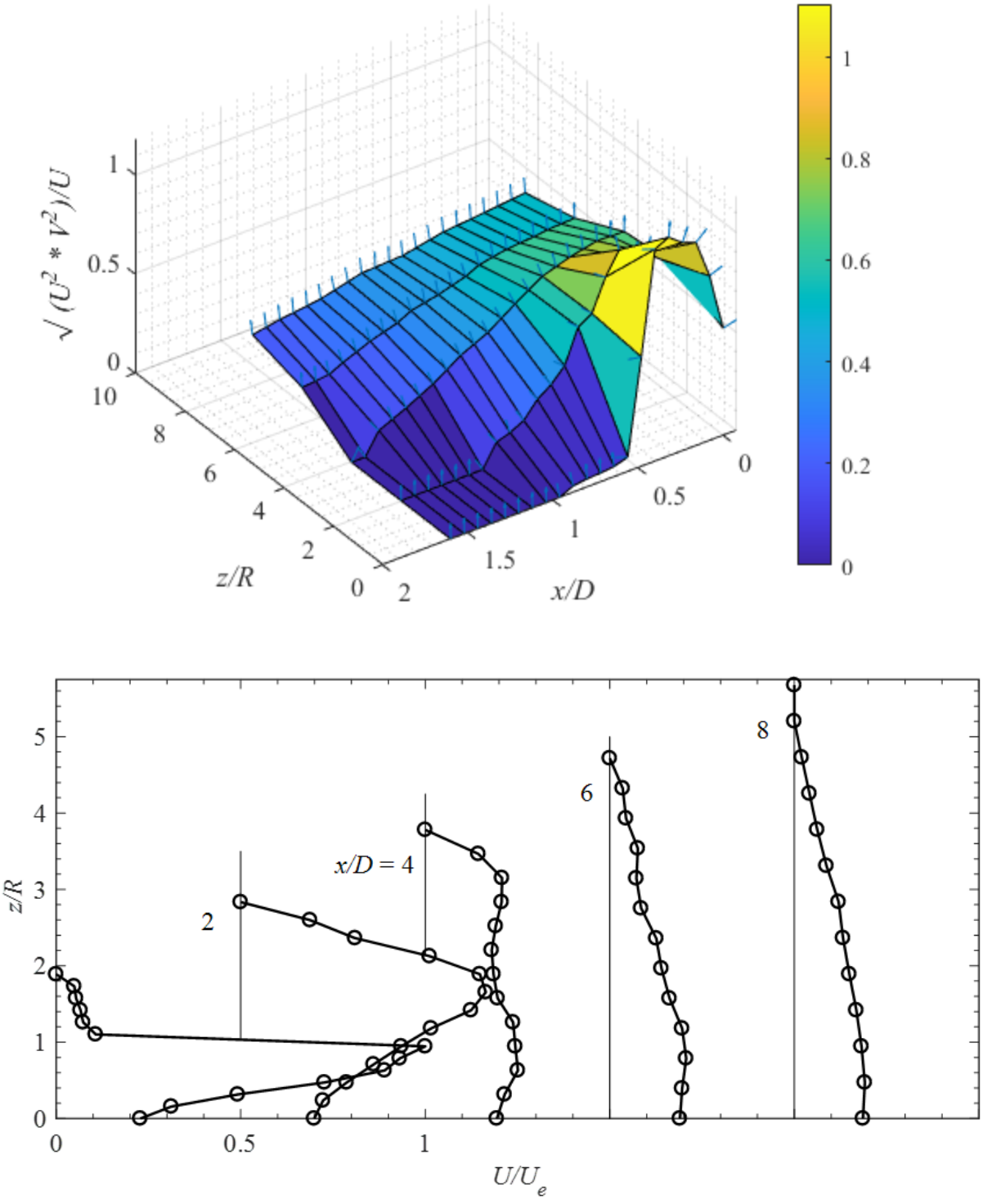

Fig 3.2.9: Axial mean velocity profile (*U*) at five stations along the jet axis; Swirling Nozzle with Pitch 7".

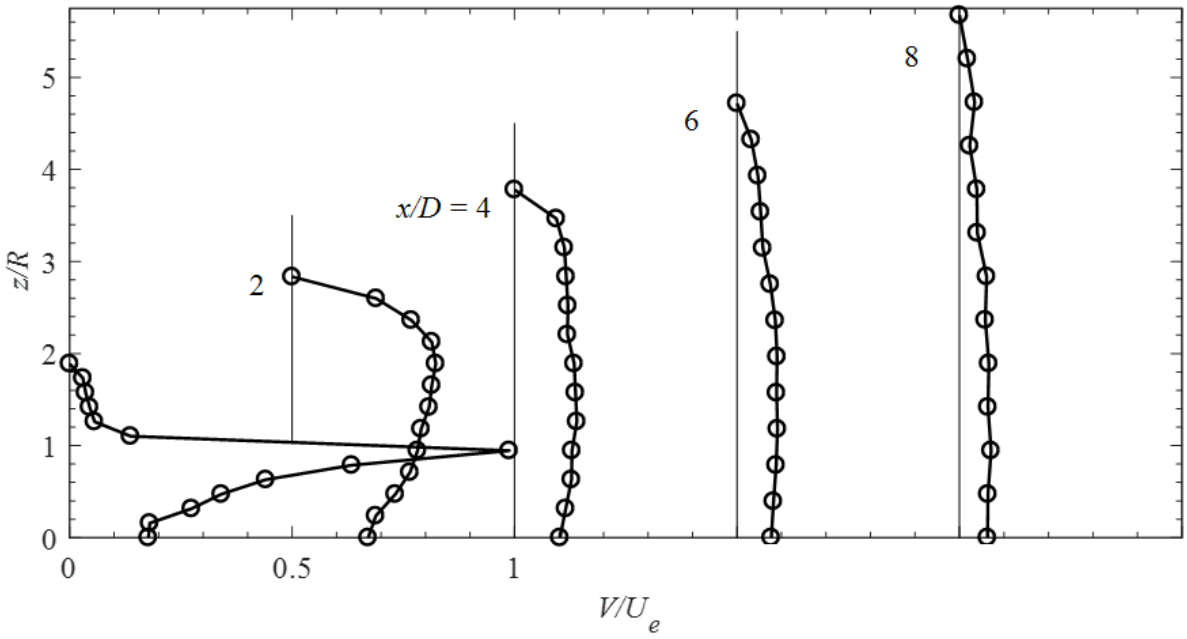

Fig 3.2.10: Azimuthal velocity profile (*V*) of the axial component of turbulent velocity; Swirling nozzle with Pitch 7".

The *V* direction of flow, as seen in Fig. 3.2.11, again resembles that of the 3" and 5" pitch nozzle profiles. At the exit plan, the profile is accelerating as it approaches the edge of the nozzle much more sharply than either of the other nozzles. As the flow moves forward to the next station the peak moves outward like the 3" pitch nozzle. The overall profile does decrease in magnitude as it moves forward and becomes more uniform in shape. At *x/D* = 8 the axial profile is almost completely singular in magnitude; however, the magnitude is much lower than the other nozzles. Overall, the azimuthal profile of the 7" pitch is like the 3" pitch azimuthal profile in both shape and behavior. The major differences are the initial shape and the transformation as the flow moves forward.

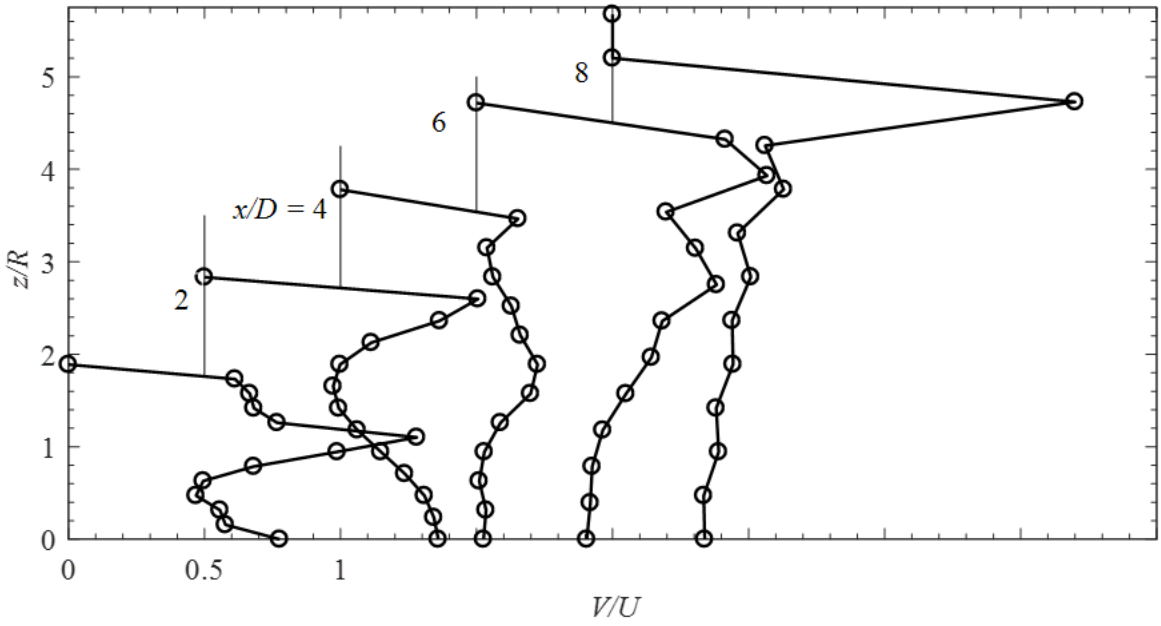

Fig 3.2.11: Swirl intensity profile at 5 stations along the jet axis; Swirling nozzle with Pitch 7".

For the swirling nozzle with pitch 7" it can be observed that the greatest swirling affect occurred at the exit of the nozzle with a peak of 1.28. At the exit of the nozzle, the swirl number on average is .71 however once this stream reaches 2*D* is increases to 1.2. Unlike the other two nozzles, no large peak was observed at 2*D*. Looking at the *U* and *V* profiles, it is apparent that the peak for the azimuthal direction does not align with the peak of the axial velocity direction. This is the same for all of the swirl nozzle but the 7" pitch seems to have a much smaller peak at 2*D*. Past 2*D*, the swirl profile returns to about .60 for the remaining stations measured. The major differences that can be observed when comparing Fig. 3.2.8, Fig 3.2.6 and Fig. 3.2.12 is the shape of the profile after 2*D*. Both the *U* and *V* velocity components maintain a somewhat uniform shape resulting in a semi-uniform shape for the swirl profile. It is worth noting however that both the *U* and *V* components after 2*D* are quite small when comparing them to the exit velocities. Also, because no major peak was observed at 2*D* it is thought that the peak occurred before the 2*D* station. Both velocity components move outward very quickly indicating that there was a significant amount of axial energy that dissipated outward before the 2*D* station.

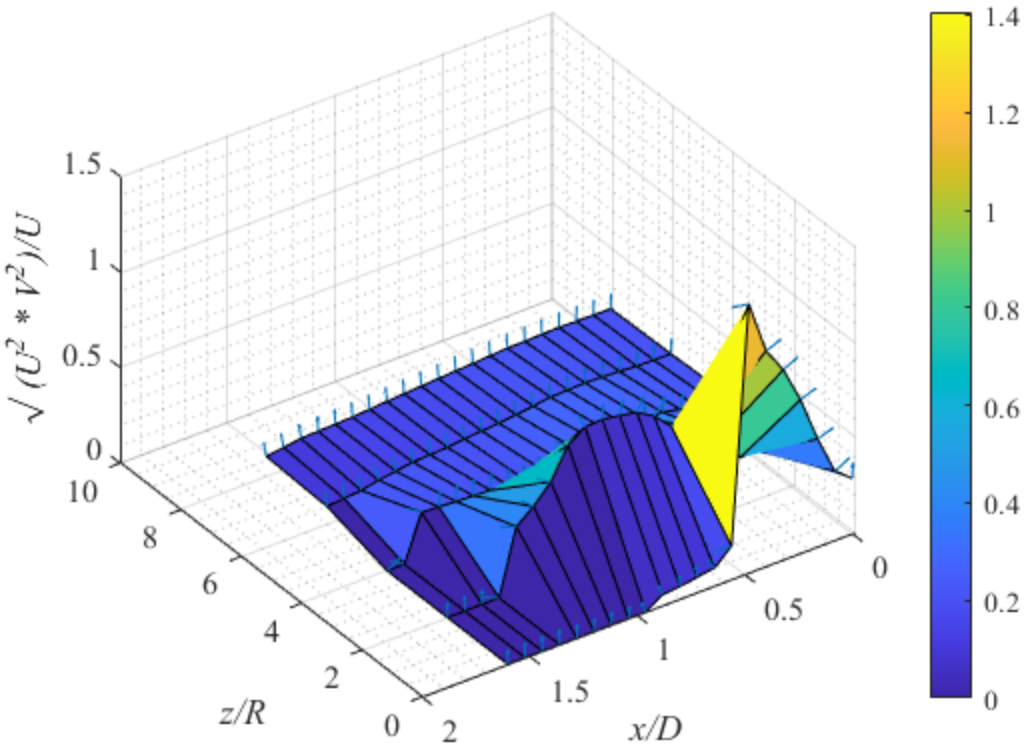

Based on the results generated in this section a table has been put together to classify each of the three swirl nozzles, see Table 1. The mean swirl number at the exit plane of the nozzle was chosen to be the defining swirl number for each of the nozzles. A general correlation of higher pitch translates to higher swirl number. However, it was also observed that that if the pitch was too great than most of the jet stream velocity dissipated quickly and there was relatively no downstream flow. Because of this discovery it was decided that for impingement testing the wall would be placed at the 2*D* station to ensure that swirling jet maintained its form and velocity during its interaction with the wall.

Table 2: Swirl Nozzle Characteristics

Nozzle Reference Name	Mechanical Swirl (Pitch)	Swirl Number
Nozzle 3	3.00″	0.31
Nozzle 5	5.00″	0.59
Nozzle 7	7.00″	0.71

Overall, this section of the experiment proved to be a valuable step in the swirling jet impingement characterization. The swirling nozzles were designed and tested to identify the general jet stream profiles generated. The swirl numbers and test location were also determined for the next step in the experiment.

3.3 Tripped Jet on Impingement Surface

To maintain a comparison between the tripped nozzle and the swirling jet nozzles the impingement experiments were first performed on the tripped nozzle. This allowed for a baseline of the setup with a well-defined system. As stated in the last section, the impingement wall was placed 2 inches from the centerline of the nozzle. The impingement wall was oriented at three angles of θ, 22.5°, 45° and 67.5°. The impingement wall oriented to the perpendicular position to the jet stream nozzle represents a 0° of θ. At each angle of θ the experiment was performed at three different mean exit velocities of the tripped nozzle, 30m/s, 40m/s and 50 m/s. Measurements were taking in both the *Us* and *Vs* by measuring the jet stream at seven centerline stations along the *Zs* axis. These measurements were taking by starting as close to the impingement surface as practically possible without breaking the hot wire probe. Then moving the probe along the *Xs* axis by a measured distance for the *Us* and *Vs* data. To capture but directions the probe was oriented in two different configurations to ensure that the hot wire was perpendicular to the flow being measured. The data was then reviewed to ensure that the entire velocity profile was captured.

The first set of data that will be presented is the *Us* and *Vs* data for each of the different impingement angles where the three different velocities are compared to one another. This data is normalized by dividing the raw *Us* data by the maximum *Us* measurement taken at the 0D station. Also, the distance from the impingement surface was normalized by dividing the distance measured by the nozzle radius.

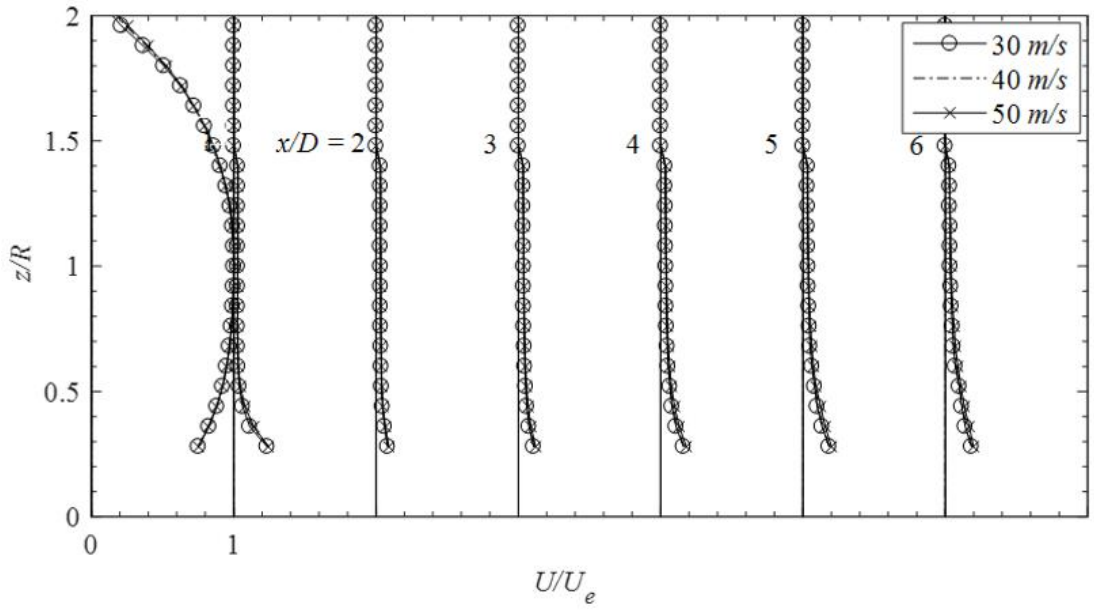

Fig 3.3.1: Axial mean velocity profile (*U*) at six stations along the jet axis; Tripped nozzle with impingement wall at *d* = 2" & *θ* = 22.5°.

The results presented in Fig 3.3.1 show that there is little to no change in the results between the three different velocities tested. This is somewhat expected since the profiles in Fig 3.1.2 matched quite similarly without an impingement wall. The profile for the 0*D* however is not a top hat profile since the data was collected in the *Xs* orientation. The data measured by starting where the centerline of the nozzle intersects with the impingement wall and moves slightly towards the nozzle because of the angle of the impingement wall. This gives the 0*D* cross section more of a dome shape than a top hat. The remaining five stations has a very similar profile shape to each other where there appears to be a strong velocity close to the surface of the impingement wall but dissipates very quickly. Because of the limitations of the hot wire probe the full shape of the velocity profile near the impingement surface could not be defined.

The data for the azimuthal velocity in relation to the impingement surface looks very similar to that of the axial data, see Fig 3.3.2. The 0*D* cross-section has a domed profile and the remaining five stations are much more reduced in magnitude. However, because of the orientation of the hot wire probe used to take the azimuthal data, it was possible to get 5mm closer to the impingement surface. This allowed for a better view into the azimuthal profile downstream. As the flow moves away from the nozzle exit, the profile's peak amplitude decreases, and overall profile widens. At or near the surface of the impingement surface the velocity approaches zero. Basic fluid dynamics

verifies that the velocity of any moving fluid is zero at the surface of a boundary. The flow stays close to the impingement surface initially then slowly moves away and slows down as it does so.

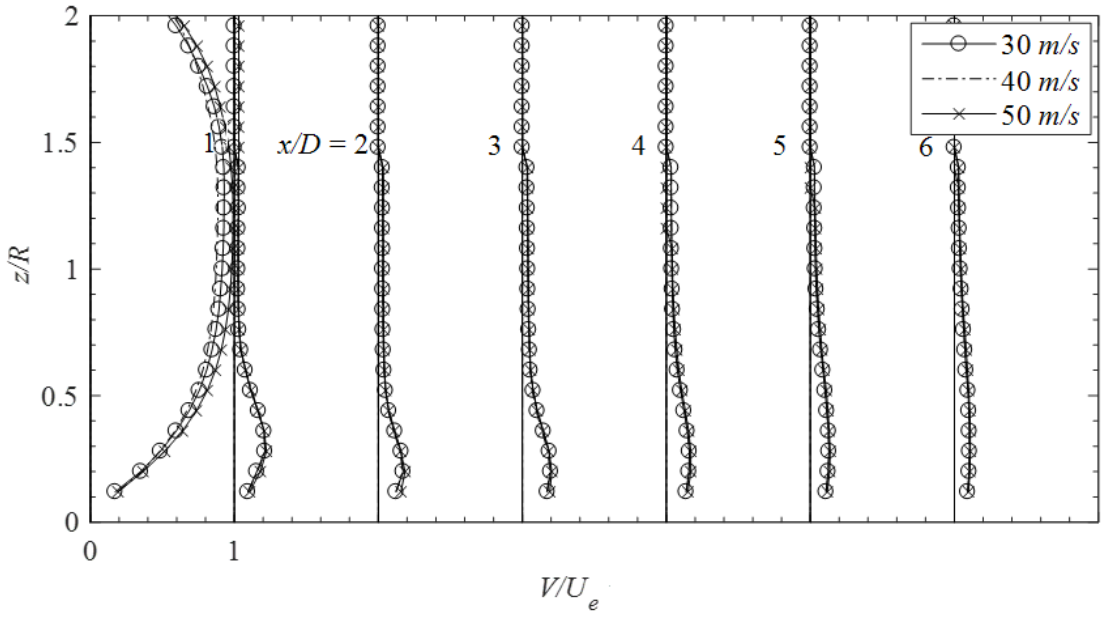

Fig 3.3.2: Azimuthal velocity profile (*V*) at six stations along the jet axis; Tripped nozzle with impingement wall at *d* = 2" and *θ* = 22.5°.

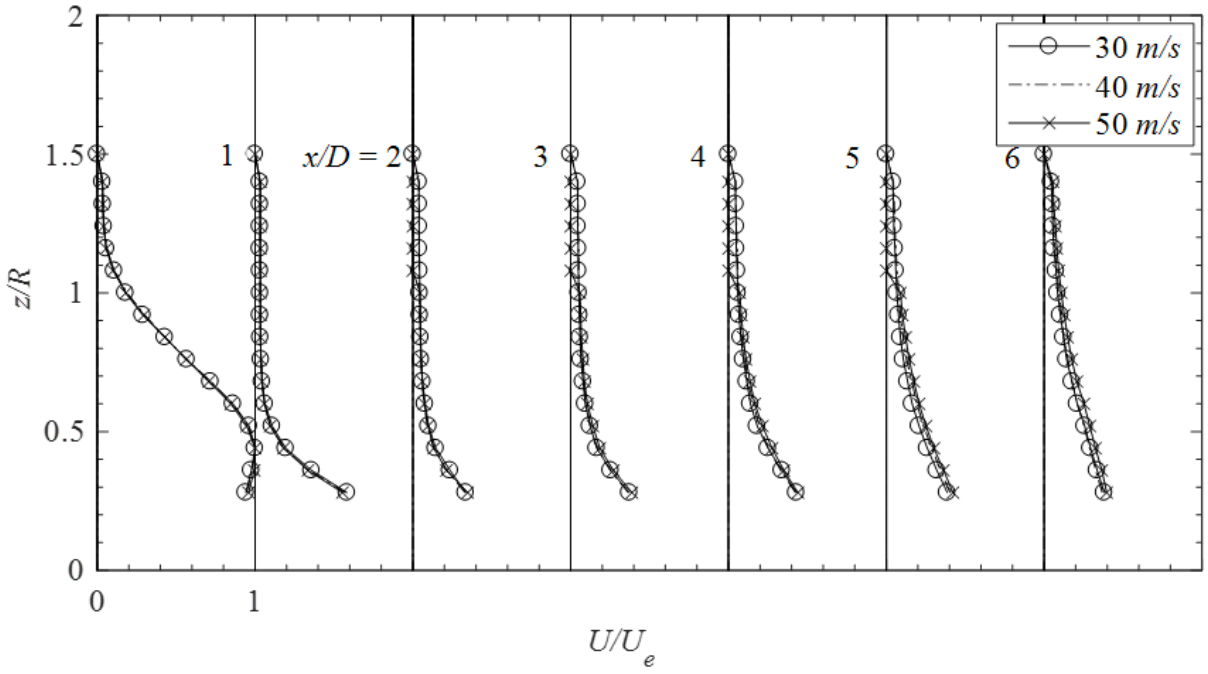

Fig 3.3.3: Axial mean velocity profile (*U*) at six stations along the jet axis; Tripped nozzle with impingement wall at *d* = 2" & *θ* = 45°.

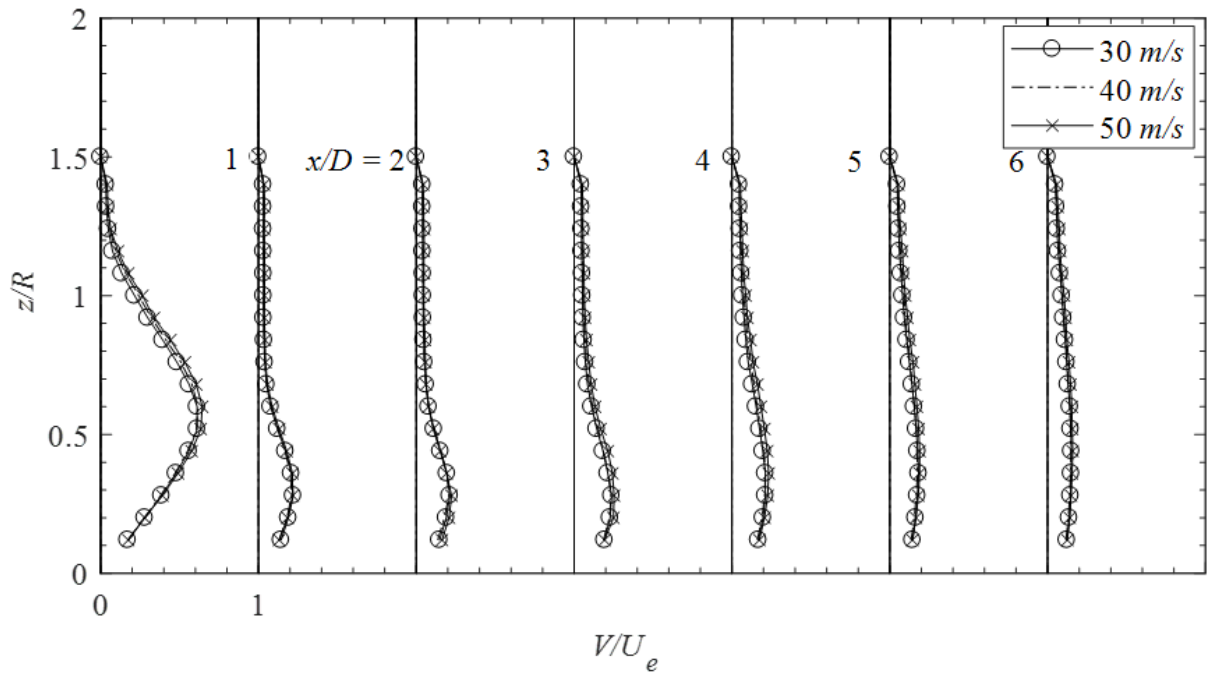

Figure 3.3.4: Azimuthal velocity profile (*V*) at six stations along the jet axis; Tripped nozzle with impingement wall at *d* = 2" and *θ* = 45°.

The overall shape at 0*D* has changed quite a bit for the *Us* and *Vs* profile when comparing them to the 22.5° impingement angle profile, see Fig 3.3.3 and Fig 3.3.4. The profile is more like a hill verse the dome shape of the previous plots. It is also worth noting that the *Vs* profile has a smaller amplitude and is wider than the *Us* profile for the 45° angle. The axial profile starting at 1*D* station has a large amplitude and is close to the surface. As the flow moves along the impingement surface the overall amplitude reduces and the flow moves away from the wall. The azimuthal profile has a similar shape as the axial but seems to be an order of magnitude lower.

The final pair of plots to compare is Fig 3.3.5 and Fig 3.3.6, the *Us* and *Vs* profiles where the impingement wall has an *θ* angle of 67.5°. This is the first set of measurements where the profiles for the three different velocities measured do not fall into family. The 30m/s axial and azimuthal profiles differ from the 40m/s and 50m/s profiles. However, the 40m/s and 50m/s profiles align close enough to consider them the same. There are a few possible reasons for this difference on profile shape. The first could be that the test setup for the 30m/s data collect runs where different than that of the 40m/s and 50m/s data runs. If the impingement wall was not setup at the same angle or distances as the other runs than the data could have been skewed out of alignment. The other possibility is that when the impingement angle is at such a large oblique angle the profile of

the flow is susceptible to changes in the velocity. However, because the 40m/s and 50m/s data match very closely and because all other data that will be reviewed in a later section match closely, the most likely cause of this difference is a configuration inconsistency. For the sake of defining the velocity profile the 40m/s and 50m/s shape will be considered as the profile for the 67.5° angle of θ flow.

The profile at the 0*D* station for the axial and azimuthal velocities look similar to the 45° profile. The azimuthal amplitude does appear to be more damped while both profiles look to have moved further away from the centerline of the nozzle. The profile's location of the maximum amplitude from station one to six remains constant while the peak decreases. Also, the profile widens away from the impingent for both directions of flow.

Except for the 30m/s data set for θ = 67.5°, it was noted that a change in the exit velocity of the jet stream had no signification change to the overall velocity profile. Because of this observation it has been decided that the 40m/s data sets will stand as the profile shape for each of the impingement angles. To make a better comparison of how the profiles change with the different impingement angles a separate set of plots has been made of each of the 40m/s data sets.

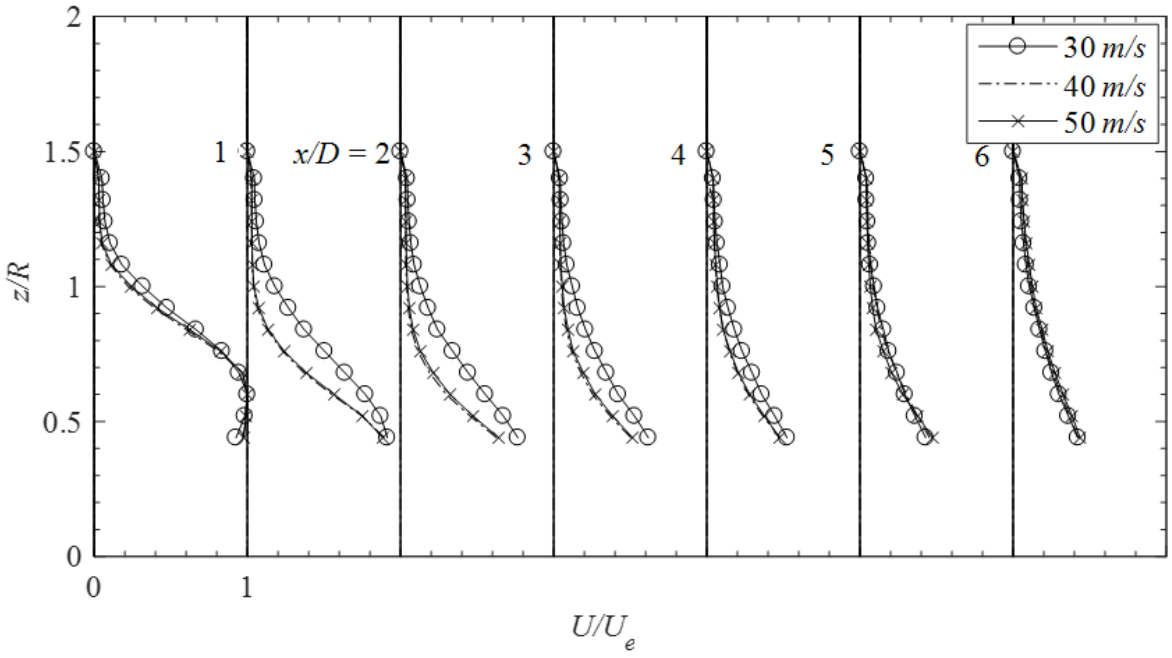

Fig 3.3.5: Axial mean velocity profile (*U*) at six stations along the jet axis; Tripped nozzle with impingement wall at *d* = 2" & θ = 67.5°.

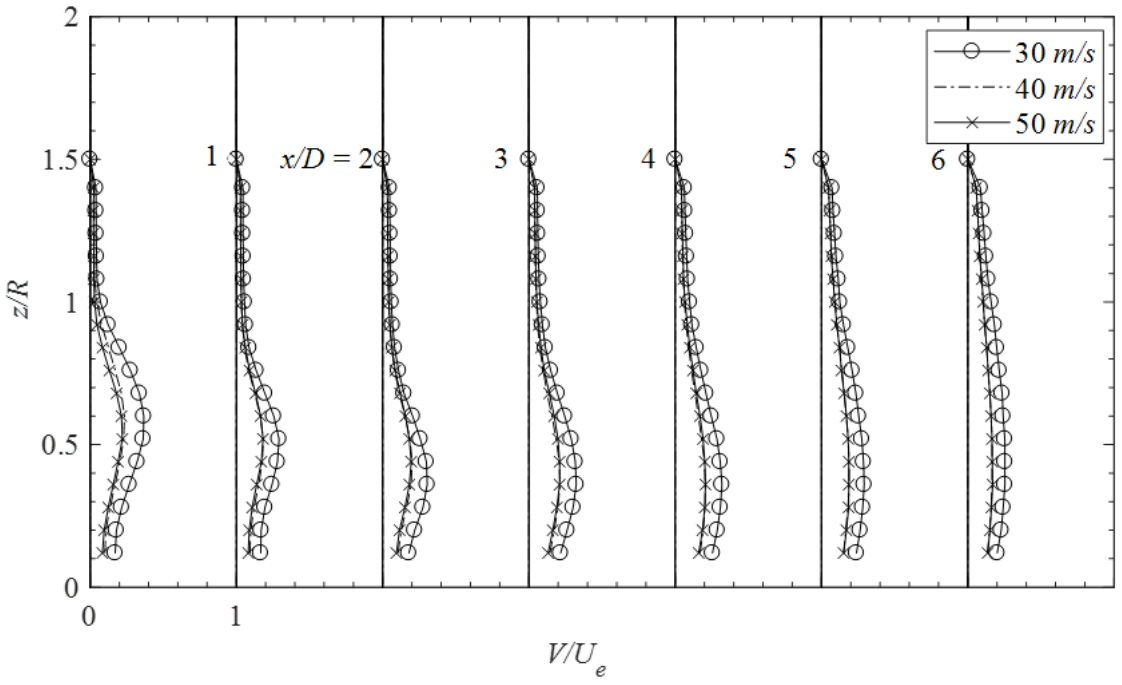

Fig 3.3.6: Azimuthal velocity profile (*V*) at six stations along the jet axis; Tripped nozzle with impingement wall at *d* = 2" and *θ* = 67.5°.

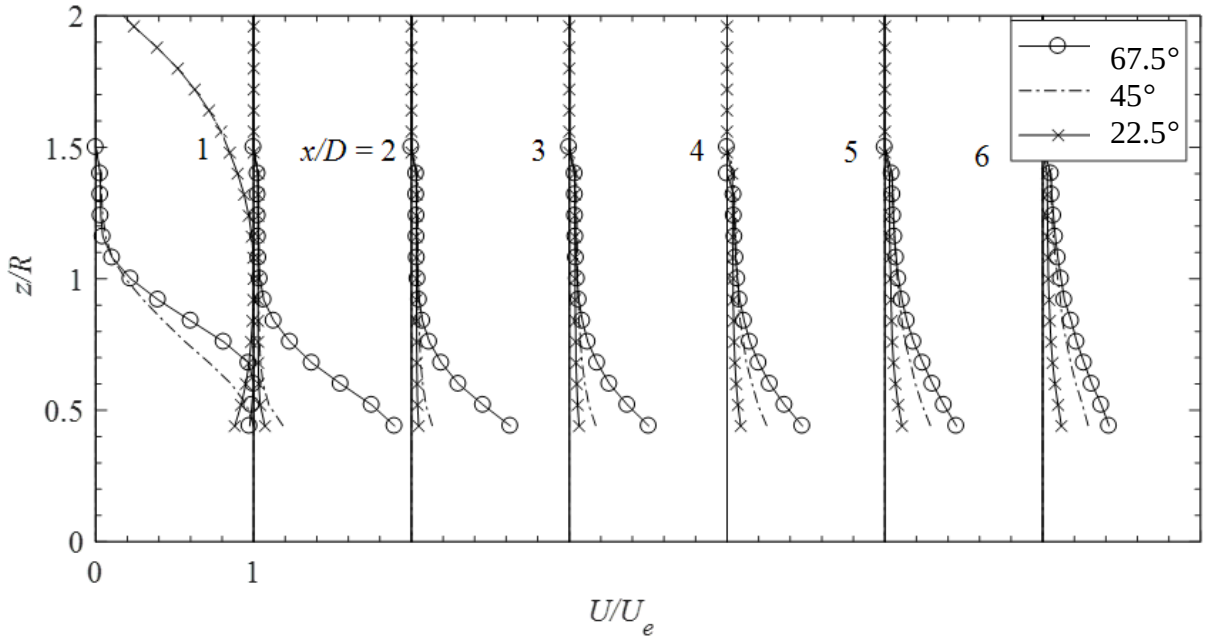

Fig 3.3.7: Axial mean velocity profile (*U*) at six stations along the jet axis; Tripped nozzle with impingement wall at *d* = 2" & *Ue* = 40m/s.

Comparing the jet stream profile with the different impingement angles has yielded some interesting results, see Fig 3.3.7 and Fig 3.3.8. While the 0*D* station seem to be out of order the remaining six stations show an ordered trend when observing the axial jet stream profile. As the impingement angle becomes more oblique or trending away from a perpendicular wall the effect it has on the jet stream appears to decrease. While the jet stream profile of the θ = 67.5° is far removed from the unimpeded profile it could be said that it resembles the shape in Fig 3.1.3 more than the profile of θ = 22.5°. Especially at station 1*D* there seems to be a drastic difference between 67.5° and 45° shape, where the difference between 45° and 22.5° profile's is minimal. As the jet stream moves forward the opposite seems to be the case as the flow reaches station 6*D*. At this station however the jet stream for all three impingement angles flows has slowed significantly from the original exit velocity.

For the azimuthal profile the only drastic difference noted between the three jet stream profiles appears to be at 0*D*. While there are some minor jet stream profile differences, they all appear to have similar magnitudes and trends. The 22.5° azimuthal jet stream stays closer to the impingement surface throughout the stations measured. As the angle increase so does the distance away from the impingement wall. Also, the larger angle has a slightly larger mean jet stream velocity at the later stations.

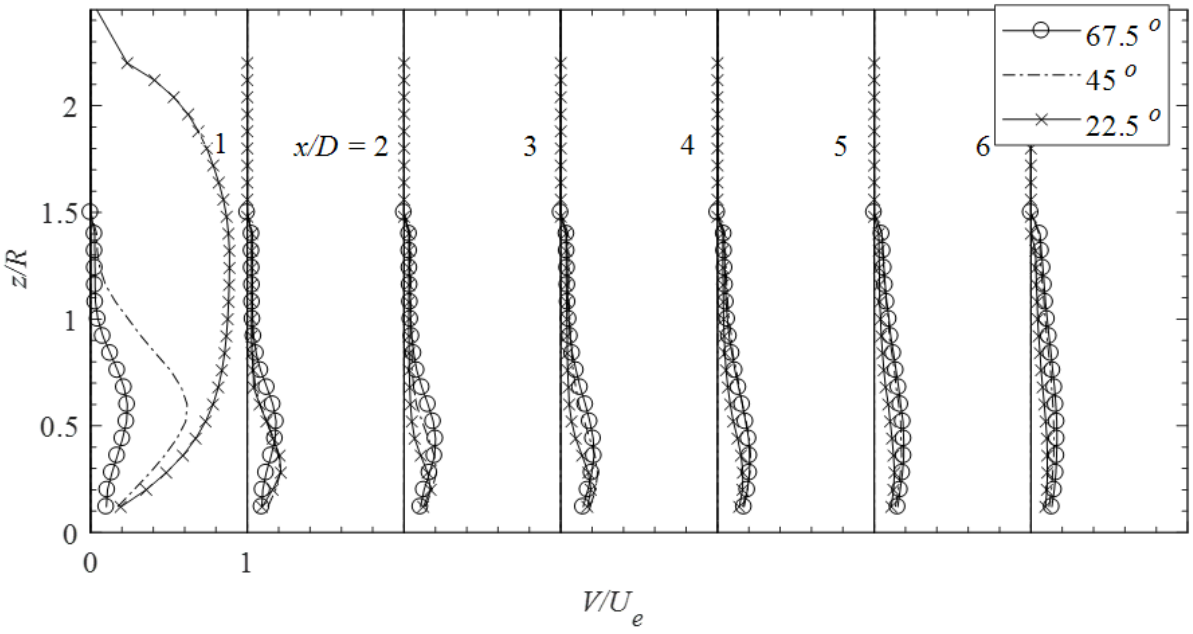

Fig 3.3.8: Azimuthal velocity profile (*V*) at six stations along the jet axis; Tripped nozzle with impingement wall at *d* = 2" & *Ue* = 40m/s.

3.4 Swirling Jets on Impingement Surface Velocity Comparison

Now that the tripped nozzle impingement data has been reviewed the data for the three swirling jet nozzles will be analyzed. The experimental setup remains the same as section 3.3 where the nozzles remain the only change. As stated in the last section the impingement wall was placed 2 inches from the centerline of the nozzle. The impingement wall was oriented in three angles of θ, 22.5°, 45° and 67.5° and where the impingement wall being perpendicular to the jet stream nozzle represents a 0° of θ. At each angle of θ the experiment was performed at three different mean exit velocities, 30m/s, 40m/s and 50 m/s. The blower motor for the experiment were set to the same rotation frequency as the tripped nozzle in the experiments performed in section 3.3. This was done to maintain overall Reynolds number of the flow since the swirling jet stream has such high azimuthal components. Measurements were taking in both the *Us* and *Vs* by measuring at seven centerline stations along the *Zs* axis. These measurements were taking by starting as close to the impingement surface as practically possible without breaking the hot wire probe. Then moving the probe along the *Xs* axis by a measured distance for the *Us* and *Vs* data. The data was then reviewed to ensure that the entire velocity profile was fully captured.

The nozzle with a 3" pitch, which will be referred to as Nozzle 3, data sets will be reviewed first. Each of the different impingement angles, with the three speeds, will be plotted to see if change in velocity has an effect of the jet stream profile. Based on the θ = 22.5° jet stream profiles in Fig 3.4.1 and Fig 3.4.2 there does not show any significant changes between the profiles for the different velocities tested for the *Us* or *Vs* directions. Like the tripped nozzle the 0*D* shape resembles a dome like structure. However, the velocity close to the wall is much more diminished which trends in line with the data collected from the nozzle characterization, Fig 3.2.4 and Fig 3.2.5. The slope of jet stream profile for the axial direction that was measured at around 0.25*R* decreases at every station measured. This indicates that the overall amplitude of the profile is reducing as the jet streams moves along the impingement wall. The same trend is seen more clearly in the azimuthal direction where a clear shape reduces to essentially zero at station 6*D*. Overall the jet stream, regardless of the exit velocity, seems to dissipate rapidly after the initial interaction with the wall.

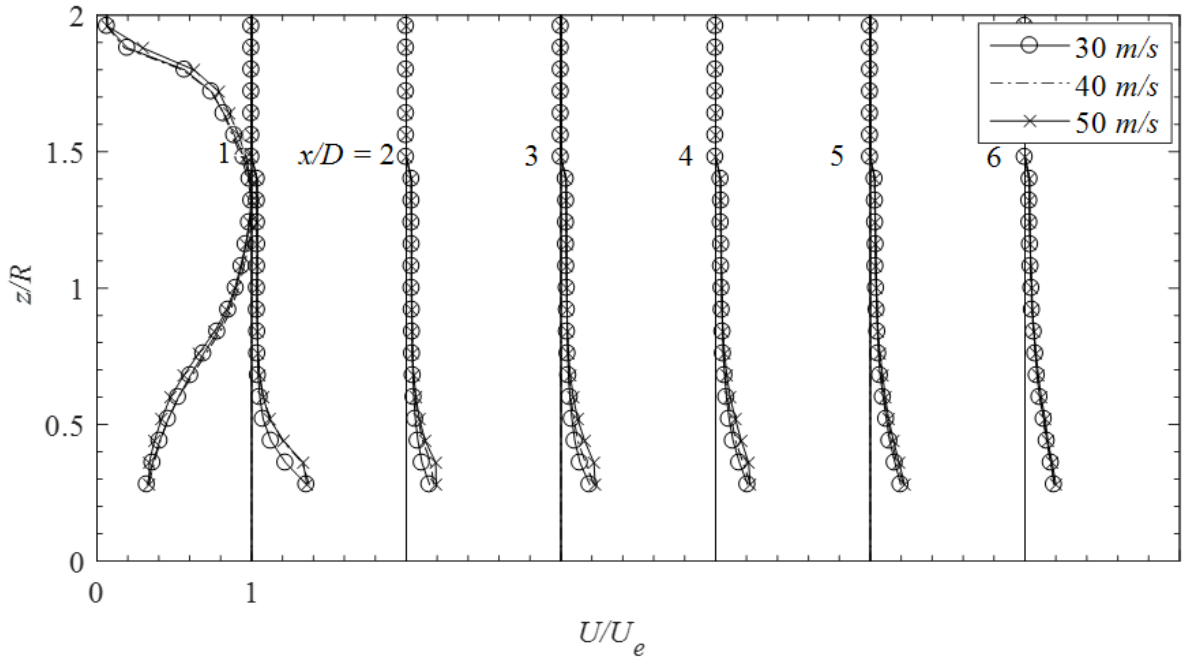

Fig 3.4.1: Axial mean velocity profile (*U*) at seven stations along the jet axis; Nozzle 3 with impingement wall at *d* = 2" & *θ* = 22.5°.

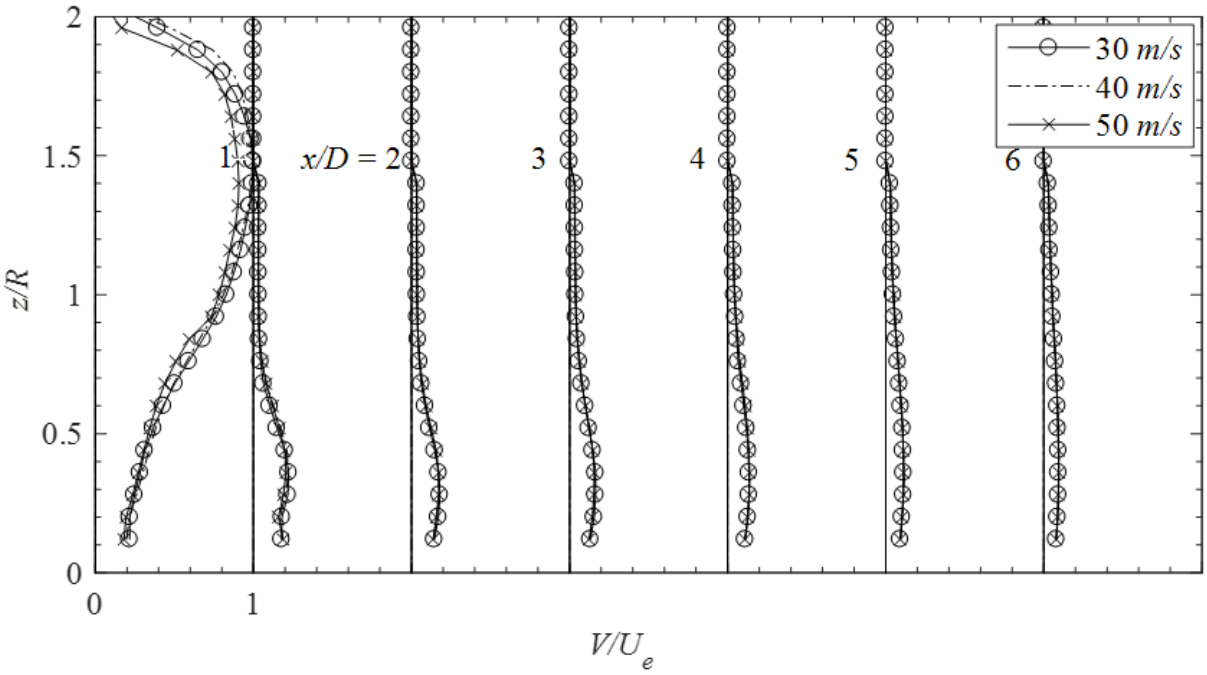

Fig 3.4.2: Azimuthal velocity profile (*V*) at seven stations along the jet axis; Nozzle 3 with impingement wall at d = 2" and θ = 22.5°.

The jet stream profiles for the θ = 45° experiment can be seen in Figs 3.4.3 and 3.4.4. These plots show that the change in velocity does not transform the profile in a noteworthy way. At 0*D* the axial shape is much more compressed than the 22.5° profile and the azimuthal amplitude is about half that of the axial. At the 1*D* station the shapes are like the previous impingement angle, but the amplitude is approximately double. The remaining stations are also larger in amplitude but still maintain the same overall shape.

The θ = 67.5 axial and azimuthal profiles can be seen in Figs 3.4.5 and 3.4.6. This final set of data for the Nozzle 3 experiments verifies that a change in velocity has no significant effect on the azimuthal or axial profiles. At 0*D,* the profile shape is much closer to the impingement wall for both directions. Much like the θ = 67.5° plots for the tripped nozzle in the axial direct, the overall profile resembles that of the unimpeded tripped nozzle. Also, while the axial direction does dissipate some over the seven stations it is much more reduced than the other two impingement angles. The azimuthal direction however is much broader at 1*D* station than the other two angles. But the profile also transforms into the same overall shape as it moves through the stations.

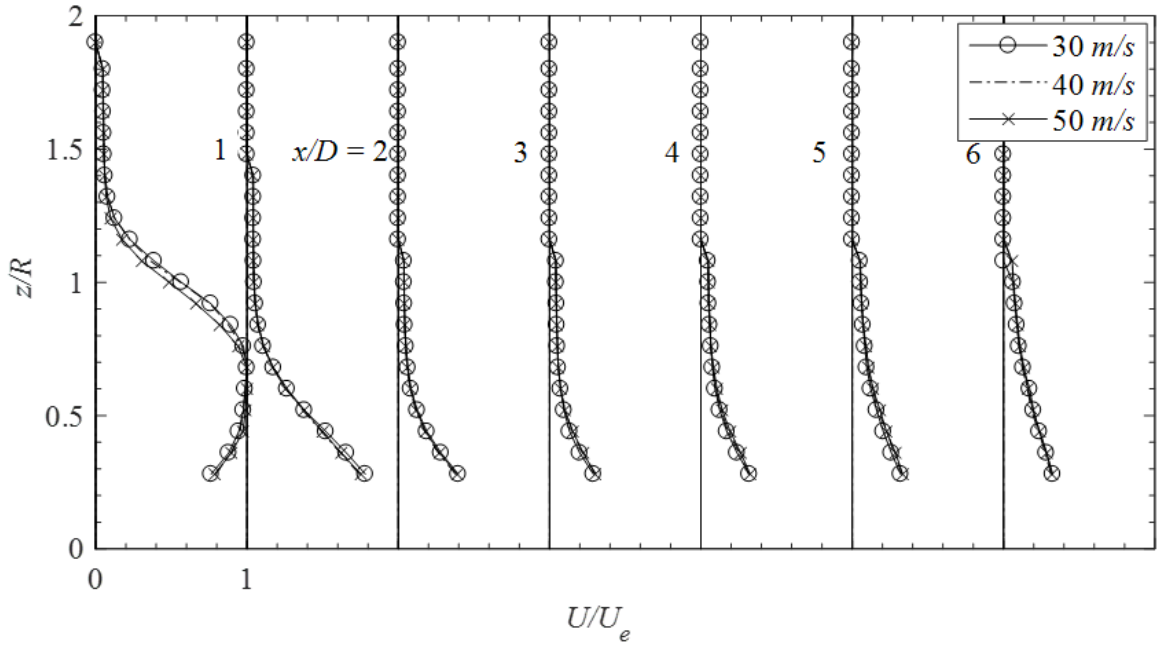

Fig 3.4.3: Axial mean velocity profile (*U*) at seven stations along the jet axis; Nozzle 3 with impingement wall at *d* = 2" & θ = 45°.

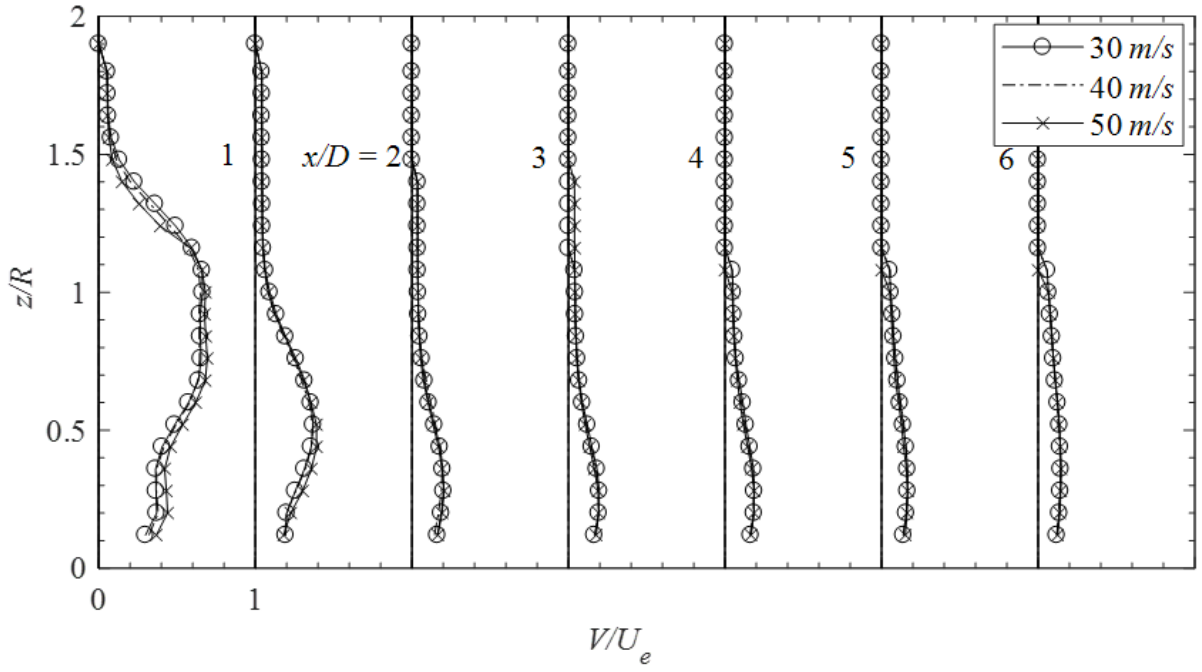

Figure 3.4.4: Azimuthal velocity profile (*V*) at seven stations along the jet axis; Nozzle 3 with impingement wall at *d* = 2" and *θ* = 45°.

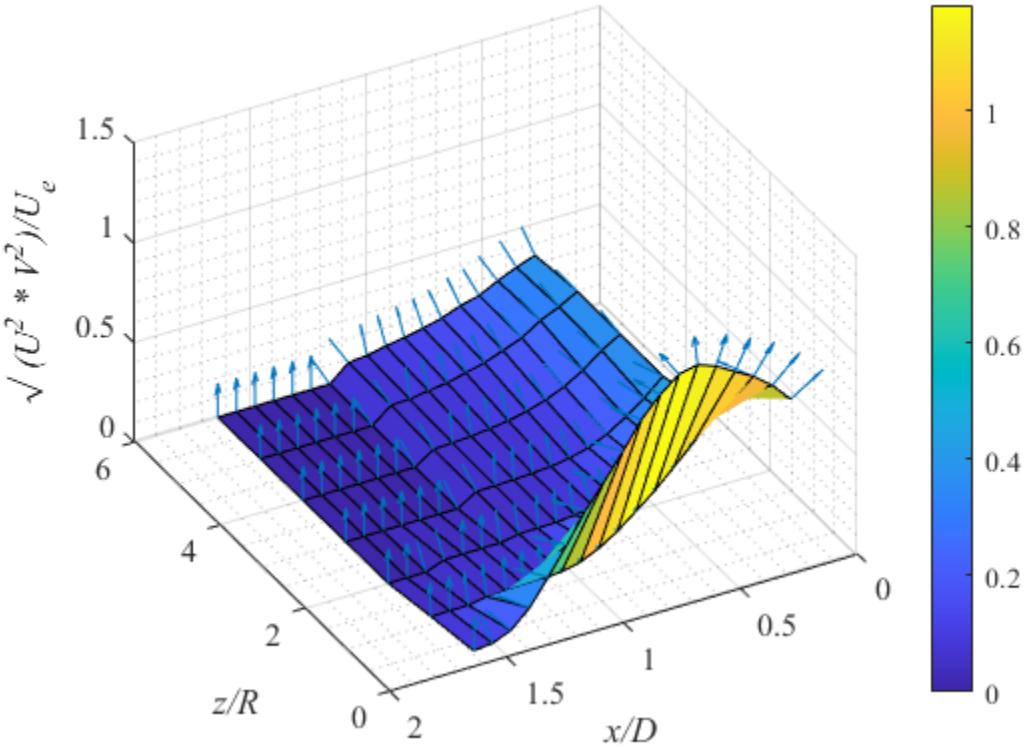

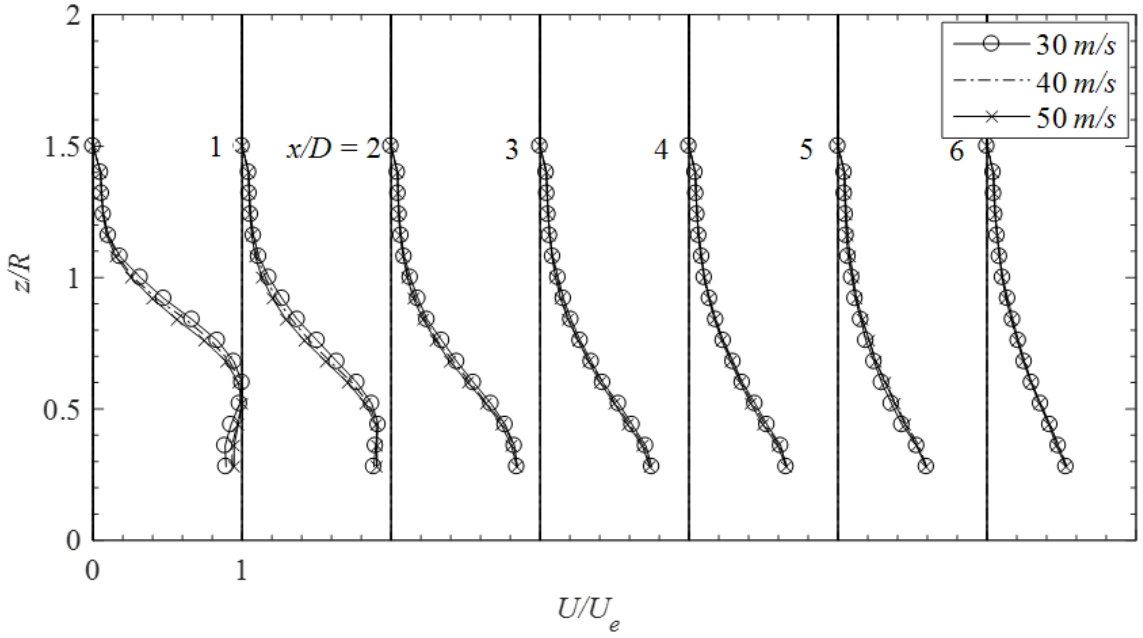

Fig 3.4.5: Axial mean velocity profile (*U*) at seven stations along the jet axis; Nozzle 3 with impingement wall at *d* = 2" & θ = 67.5°.

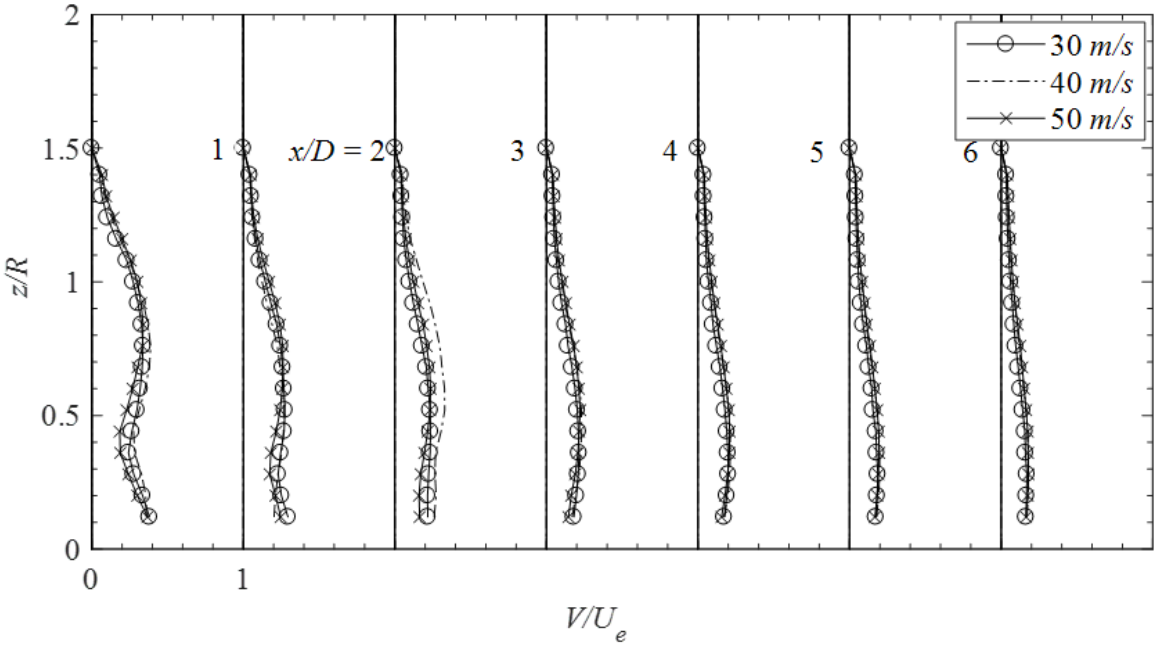

Fig 3.4.6: Azimuthal velocity profile (*V*) at seven stations along the jet axis; Nozzle 3 with impingement wall at *d* = 2" and θ = 67.5°.

Next the nozzle with the 5” pitch, which will be referred to as Nozzle 5, data sets will be reviewed. Each of the different impingement angles, with the three speeds, will be plotted to see if change in velocity has an effect of the jet stream profile. Based on the jet stream profiles in Fig 3.4.7 and Fig 3.4.8, the 22.5° impingement angle plots, there does not show any significant changes between the profiles for the different velocities tested for the *Us* or *Vs* directions. The axial stream slows down and spreads out as it moves along the impingement surface. At station 1*D* the peak velocity measured is twice that of the remaining stations probed. This is an indication that the wall is dissipating the vortex flow quite effectively in the axial direction. The azimuthal jet stream profile also has the same general trends as the axial direction. However, the effects are more gradual. There is a decrease in peak velocity at every station in the azimuthal direction where the profile maintains a similar peak location from stations 2*D* to 6*D*. For the sake of comparing the three different velocities measured it can be said that the profile is stagnate. There are slight differences in the 0*D* profiles for both the axial and azimuthal direction for the 30m/s measurements taken. While this profile difference may be factual it has no effect of the profile where the impingement wall interacts with the jet stream.

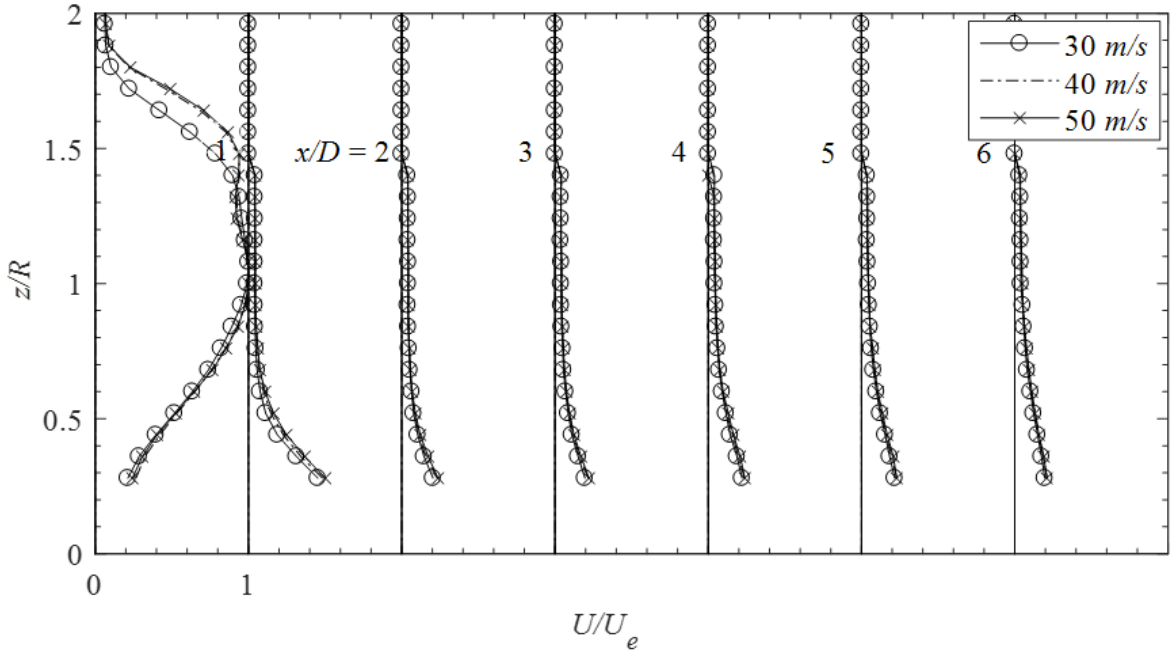

Fig 3.4.7: Axial mean velocity profile (*U*) at seven stations along the jet axis; Nozzle 5 with impingement wall at *d* = 2” & *θ* = 22.5°.

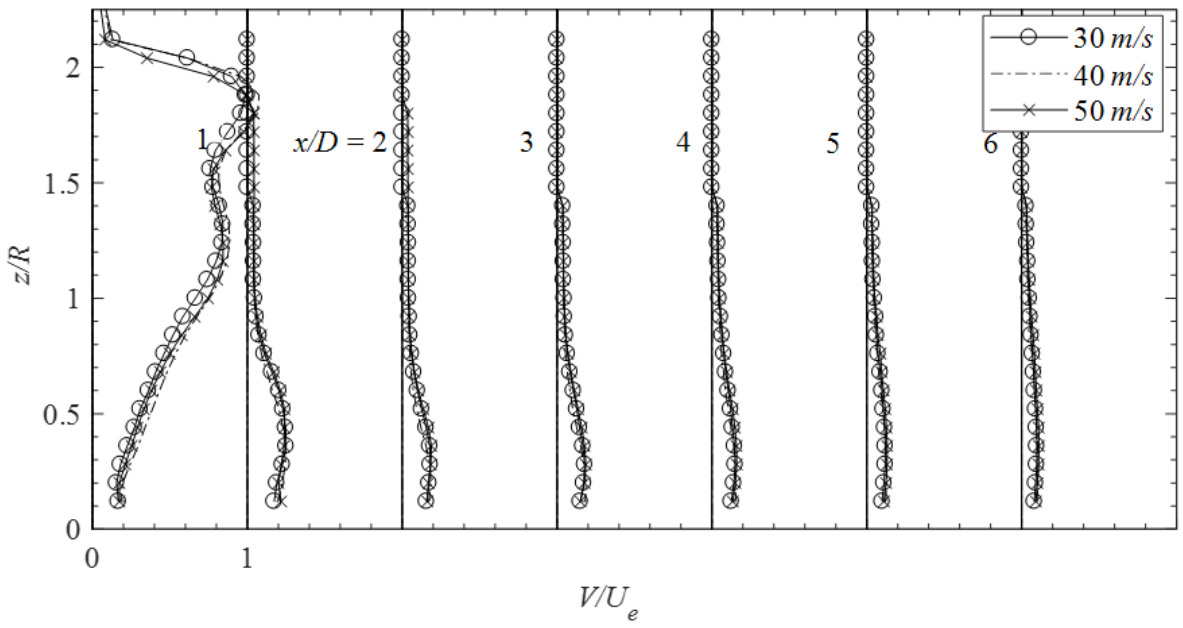

Fig 3.4.8: Azimuthal velocity profile (*V*) at seven stations along the jet axis; Nozzle 5 with impingement wall at *d* = 2" and *θ* = 22.5°.

The profiles for the experimental setup where the Nozzle 5 flow is directed at the impingement wall positioned at a 45° angle is seen in Fig 3.4.9 and Fig 3.4.10. The major similarity to these jet stream flow and the 22.5° profiles is that they also show no significant change due to a variation in velocity. The one outlier is the 0*D* profile for the azimuthal direction which does not have the same shape at the 30m/s as the 40m/s and 50m/s speeds. However, just the like 22.5° jet streams, the profiles align for the other six stations measured. In the axial direction the peak amplitude at 1*D* has only reduced slightly from the nozzle exit peak. At station 6*D* the peak is still at 40% of the original peak measured. The interaction with the impingement wall does not appear to be affecting the jet stream nearly as much as the 22.5° setup. In the azimuthal direction, the peak velocity slowly decreases as the flow moves further away from the nozzle exit. The profile also spreads away the wall slowly. Moreover, there is a dip in the velocity close to the impingement wall at station 1*D* but very close to the wall there is a small increase. This may be an indication of a vortex being generated by the wall. This will be analyzed further in the visualization section, 4.2, to see if there is any further data to validate this assumption. Overall, these figures add to the evidence that the jet stream profile is not affected by a change in speed.

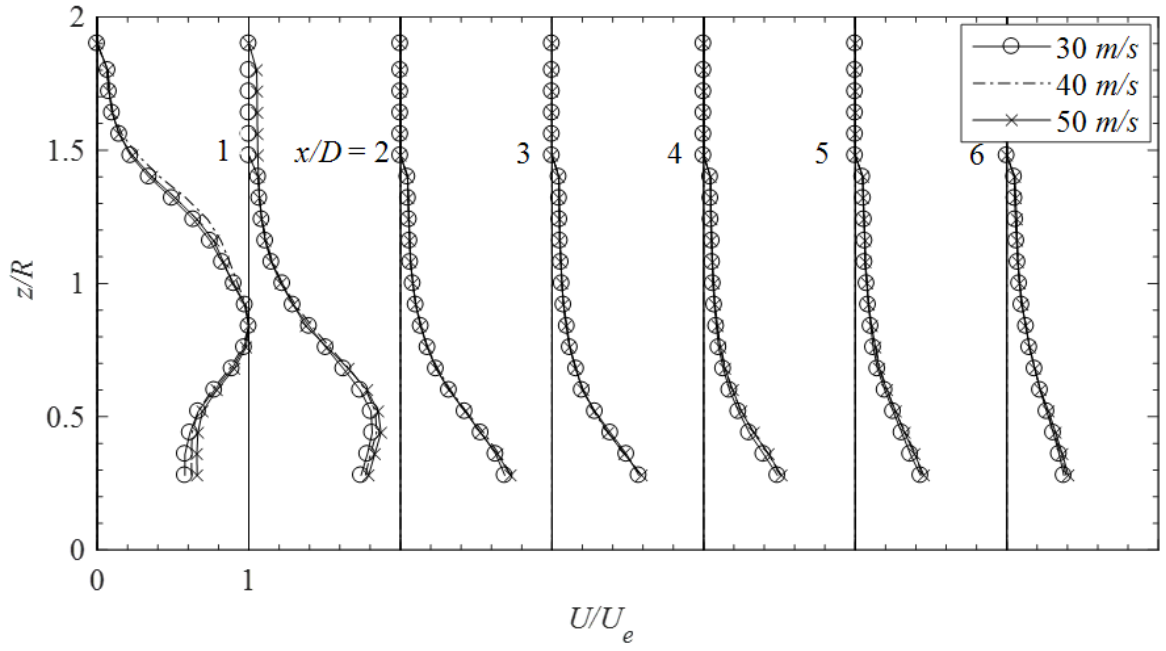

Fig 3.4.9: Axial mean velocity profile (*U*) at seven stations along the jet axis; Nozzle 5 with impingement wall at *d* = 2" & *θ* = 45°.

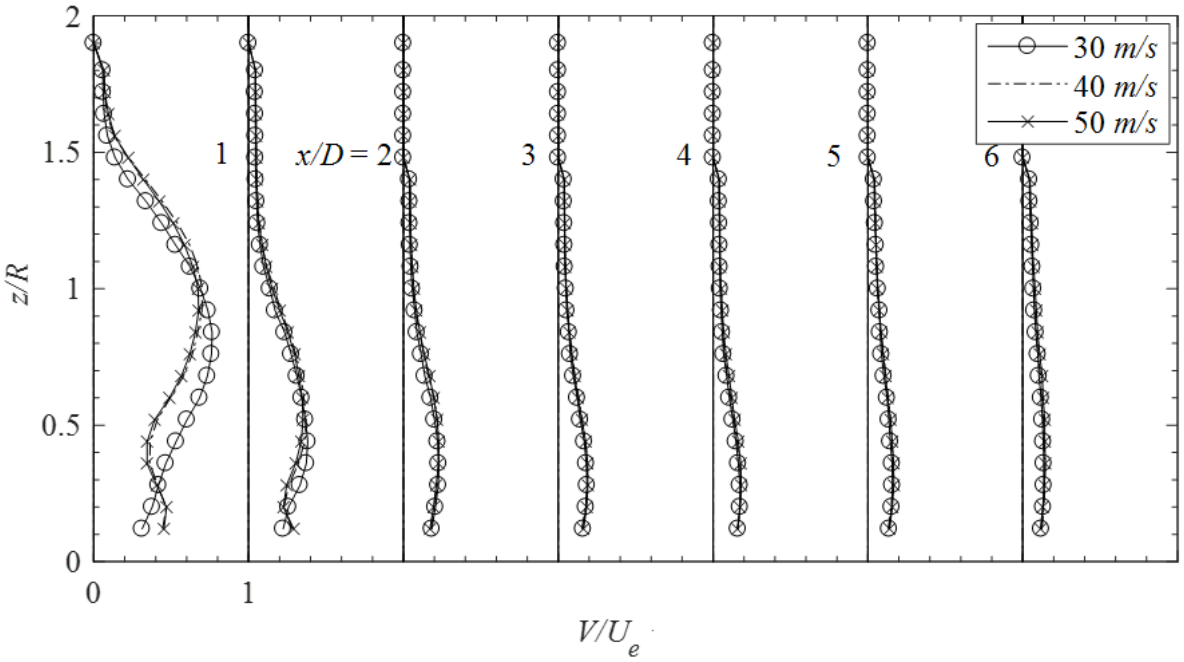

Fig 3.4.10: Azimuthal velocity profile (*V*) at seven stations along the jet axis; Nozzle 5 with impingement wall at *d* = 2" and *θ* = 45°.

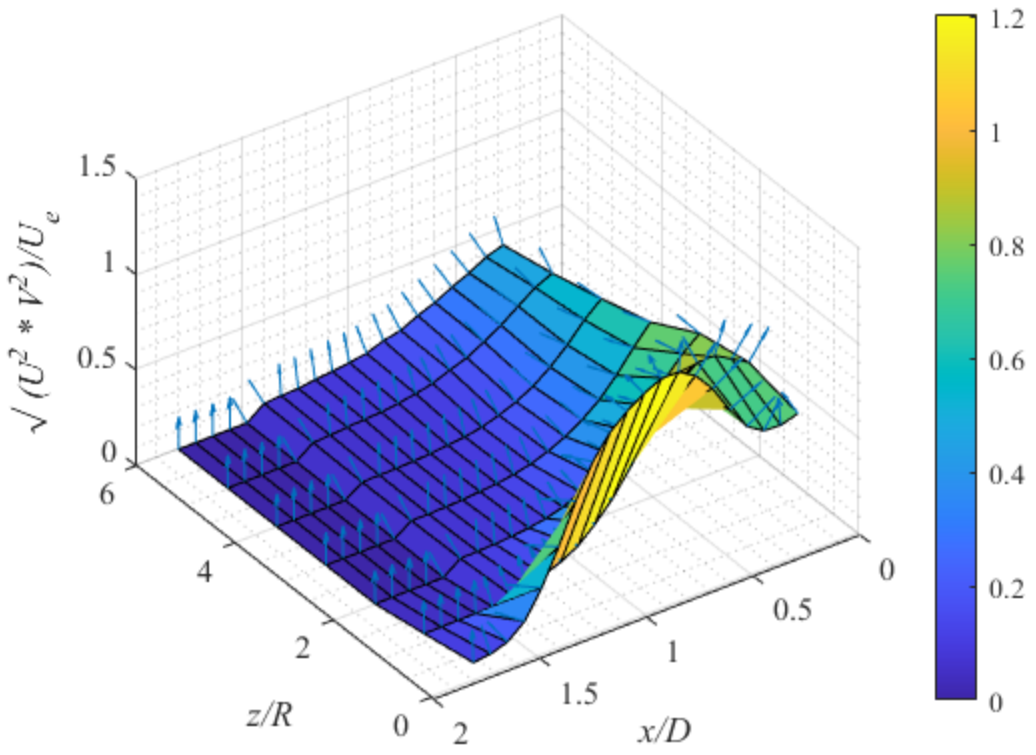

The final impingement wall position is where θ = 67.5° for the Nozzle 5. Again, the jet stream profiles in Fig 3.4.11 and Fig 3.4.12 does not show any significant changes between the profiles for the different velocities tested for the *Us* or *Vs* directions. The only location that deviates from mean more than 5% is at station 0*D* for the axial flow direction. All other measurement locations have consistent recordings regardless of the velocity setting. The axial profile appears to slow down and moved towards the impingement surface as the flow progresses away from the nozzle exit. The profile maintains the same overall shape from 3*D* to 6*D* where the amplitude only reduces by 5% between stations. The azimuthal profile has the same general trend as the axial. From station 4*D* to 6*D* there is less than a 3% difference between locations. There is an interesting feature at 0D and 1D for the azimuthal profile like that of the azimuthal measurement of the 45° impingement wall angle. The velocity seems to have a dip close to the impingement surface and then increase again. The most likely cause for this dip is a vortex that has formed which is reducing the local azimuthal measurement. This is much like the eye of a hurricane where the internal velocities are much lower than the surrounding vortex flow. This concludes the examination of the affects that velocity has on the Nozzle 5 impingement experiments. No sizable difference was noticed for all angles of θ.

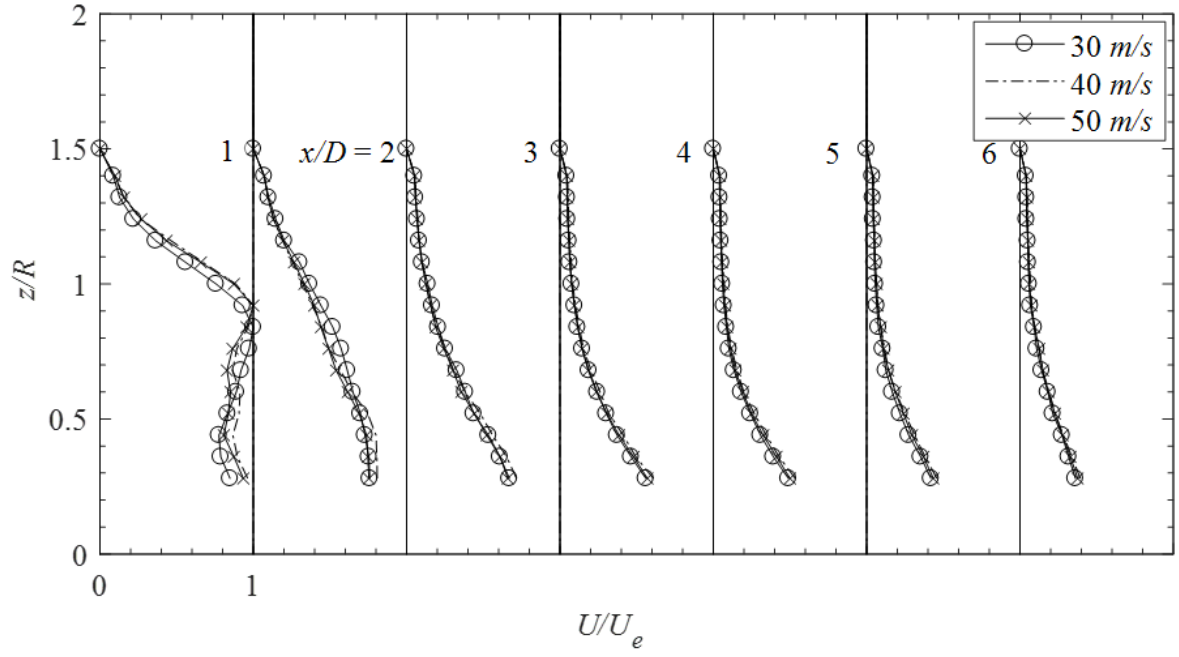

Fig 3.4.11: Axial mean velocity profile (*U*) at seven stations along the jet axis; Nozzle 5 with impingement wall at *d* = 2" & *θ* = 67.5°.

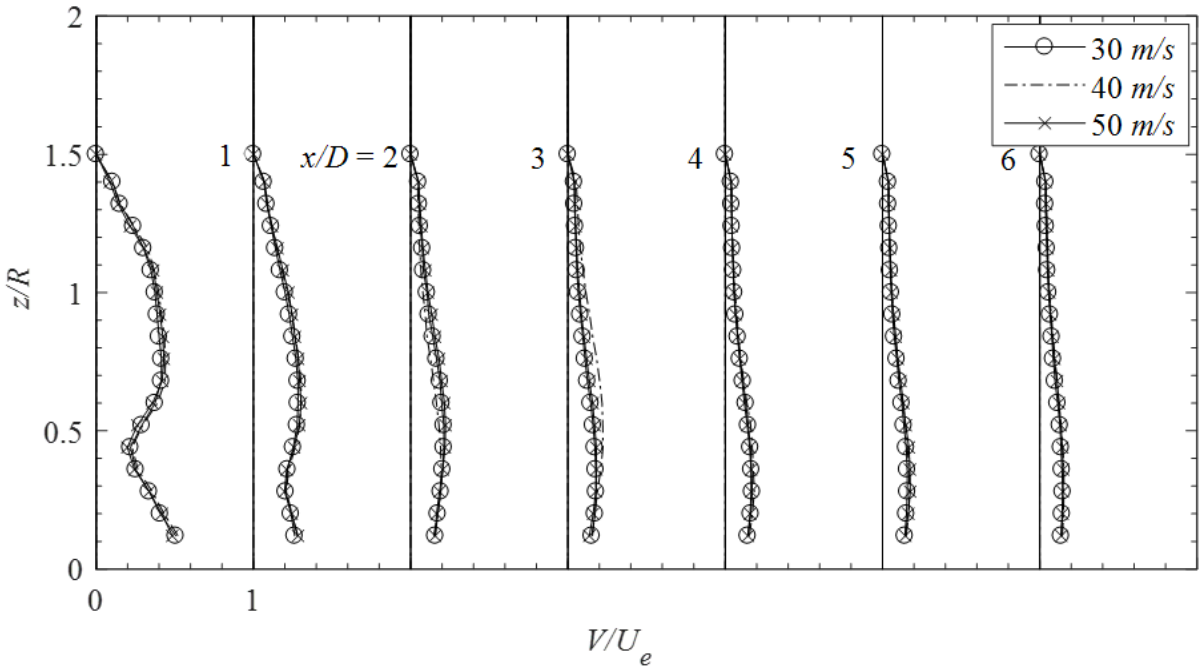

Fig 3.4.12: Azimuthal velocity profile (*V*) at seven stations along the jet axis; Nozzle 5 with impingement wall at *d* = 2" and *θ* = 67.5°.

The final set of velocity comparisons that will be analyzed is from nozzle with a pitch of 7", this will be referred to in the following text as Nozzle 7. The three speeds, 30m/s, 40m/s and 50m/s were overlaid for both the axial and azimuthal directions into two separate plots for each impingement wall angle. The first pair of plots is for when θ = 22.5°, seen in Fig 3.4.13 and Fig 3.4.14. When comparing the overlaid plots these figures tell the same story as the others already reviewed; no significant change in jet stream profile were caused by velocity. The 0*D* station in the azimuthal direction has about a 5% difference in where the peak of the velocity is along the cross section. All other stations do not have a change greater than 3% of the mean profile for each station. For both the axial and azimuthal profiles the 0*D* same is much different than others seen so far. The peak of the profile is much further way from the centerline of the flow. However, the jet stream profile from 1*D* on seems to be normal in terms of shape and trend. For both the azimuthal and axial directions the profile remains constant from 4*D* to 6*D*, less than 3% change from station to station. Both flow directions also show the peak of the profile moving toward the impingement wall as the flow moves forward. Overall, the impingement wall seems to terminate the jet stream effectively.

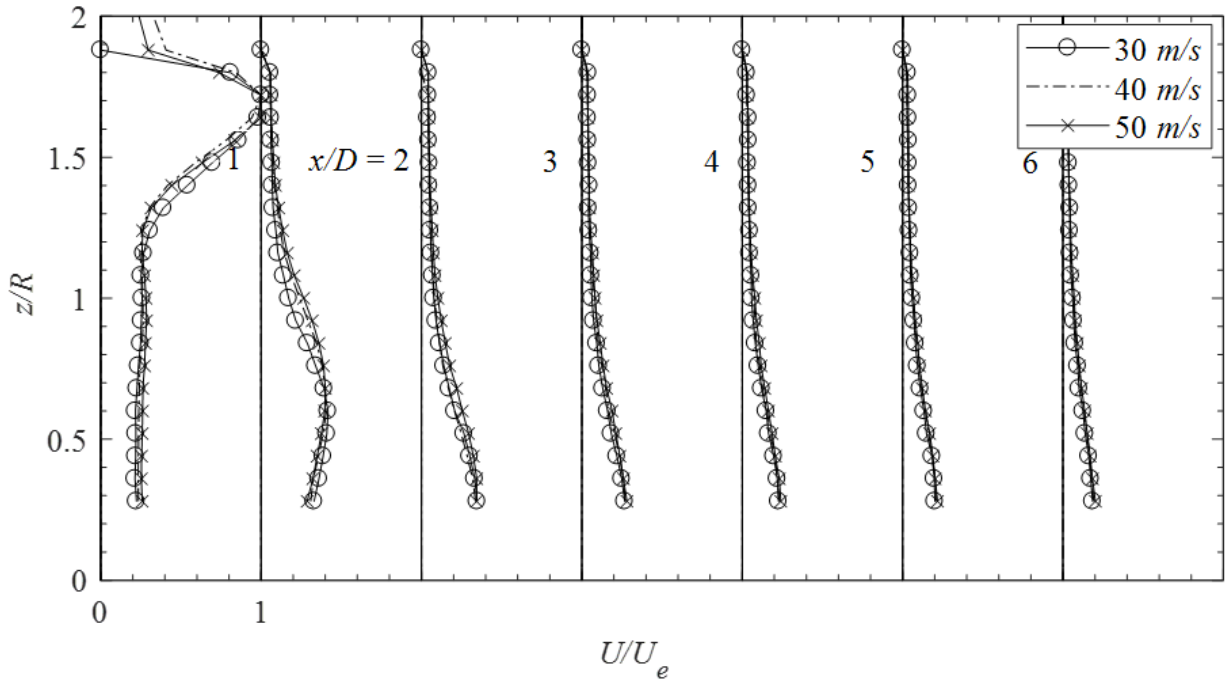

Fig 3.4.13: Axial mean velocity profile (*U*) at seven stations along the jet axis; Nozzle 7 with impingement wall at *d* = 2" & θ = 22.5°.

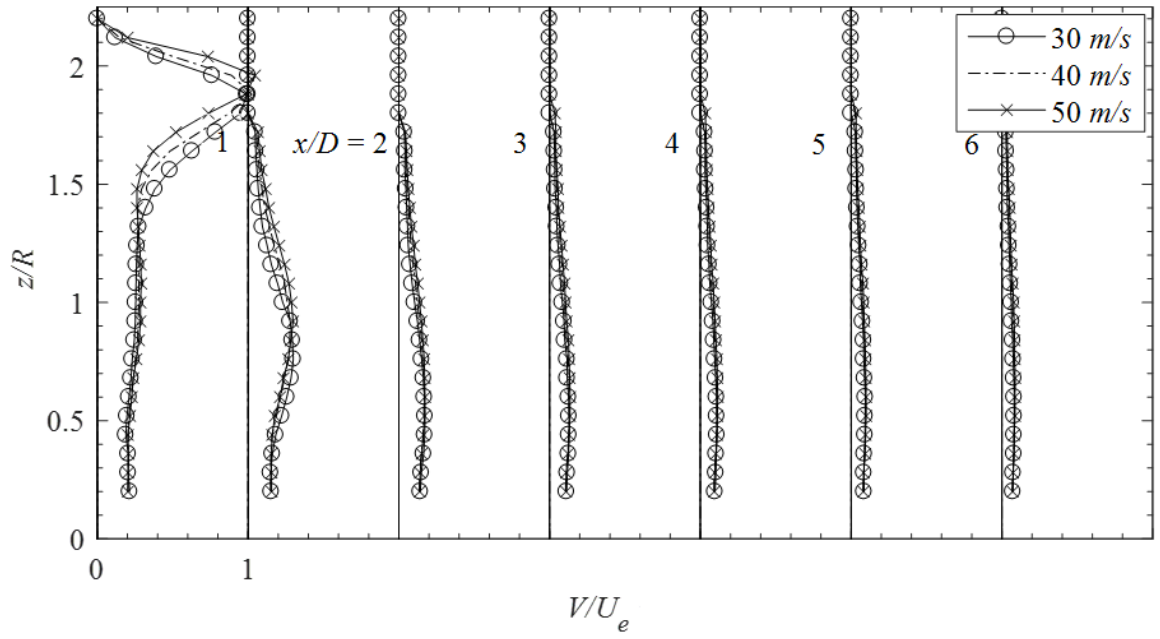

Fig 3.4.14: Azimuthal velocity profile (*V*) at seven stations along the jet axis; Nozzle 7 with impingement wall at *d* = 2" and θ = 22.5°.

The next pair of plots is the impingement wall at θ = 45° for the Nozzle 7, seen in Fig 3.4.15 and Fig 3.4.16. While the axial plot has difference at every station between the velocities the values are still quite small, maximum 4% from mean profile. This is the most significant deviation of any of the plots presented thus far. However, these changes are still so minor that it stands out as an exception when comparing it to the other data samples presented. Like the previous plots seen, 0*D* has the most extreme profile shift for both the azimuthal and axial directions. The axial profile moves further from the centerline as the velocity increase while the peak amplitude of the azimuthal increases. From station 1*D* to 3*D* the axial peak moves towards the impingement wall and flattens out. The azimuthal direction also has the same trend but reduces its peak amplitude by about 50% from that of station 1*D*. Location 1*D* has the characteristic sharp dip near the impingement wall that was seen in the Nozzle 5 azimuthal profiles for θ = 45° and 67.5°. Again, both flow directions show little to no change in jet stream profile from station 4*D* to 6*D*. However, the flow does not appear to dissipate nearly as much as the previous Nozzle 7 plots. A better comparison between the impingement angles will be shown in upcoming plots. Generally, it can be said that velocity has no impactful change on jet stream profile in either the azimuthal or axial directions.

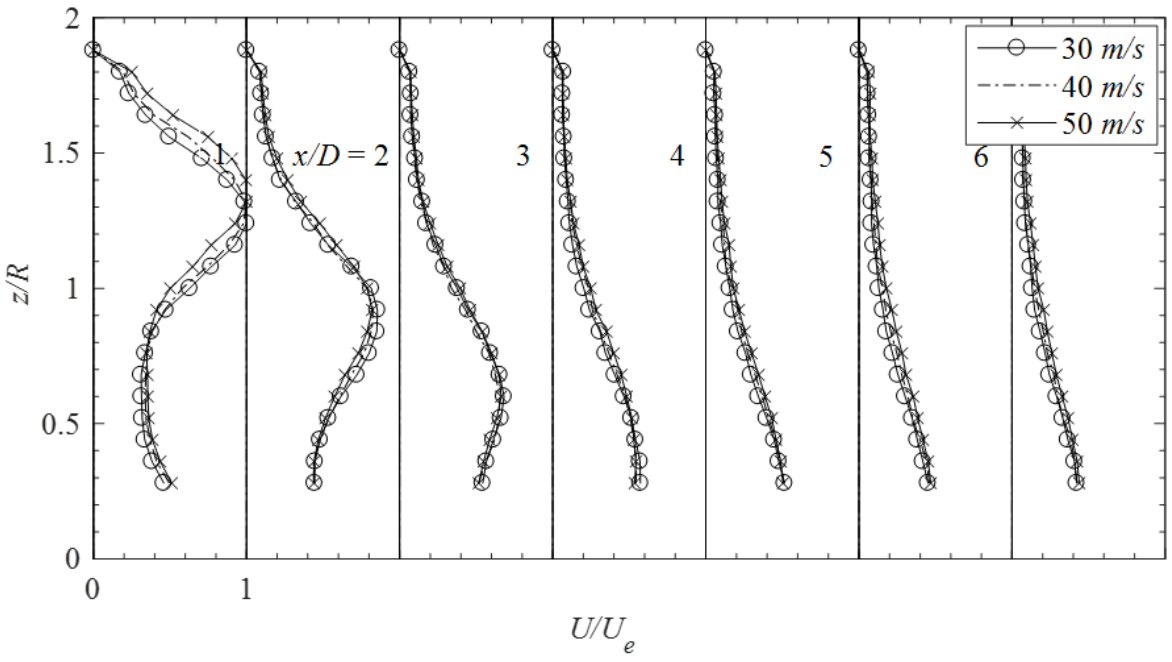

Fig 3.4.15: Axial mean velocity profile (*U*) at seven stations along the jet axis; Nozzle 7 with impingement wall at d = 2" & θ = 45°.

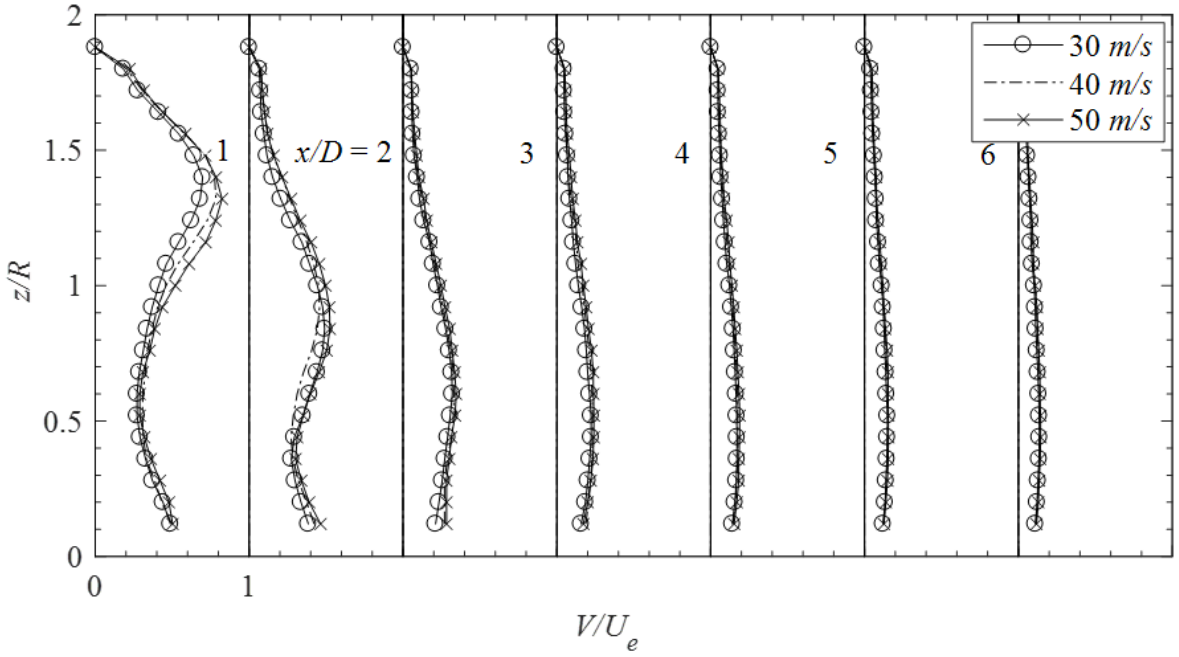

Fig 3.4.16: Azimuthal velocity profile (*V*) at seven stations along the jet axis; Nozzle 7 with impingement wall at d = 2" and θ = 45°.

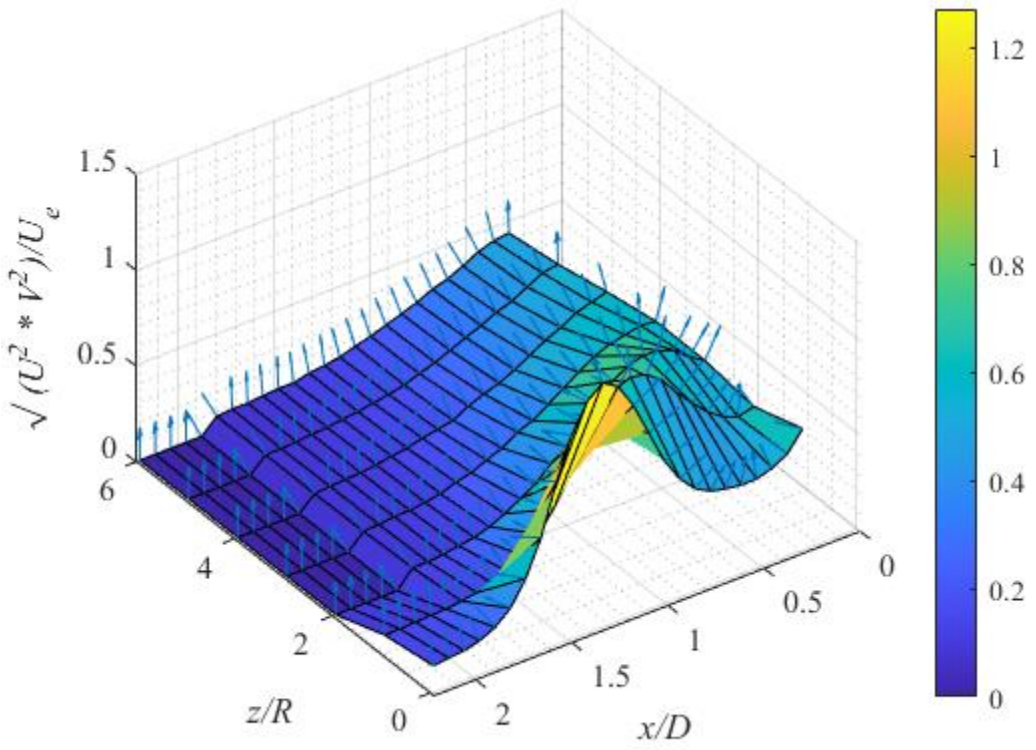

The final pair of velocity comparison plots that will be presented are the Nozzle 7 jet stream profiles for axial and azimuthal flow direction where the impingement wall is at $\theta = 67.5°$, see Fig 3.4.17 and Fig 3.4.18. Just like the rest of the samples shown, both the axial and azimuthal directions do not show a note worth change in profile. The azimuthal direction shows some change for the 30m/s overlay, but it is still less than 8% for the 1*D* station. In the axial direction the peak amplitude shifts toward the impingement wall from locations 1*D* to 3*D* than maintains a relatively constant profile. The magnitude reduces by 30% over the first three stations. The azimuthal direction also undergoes its profile shift from stations 1*D* to 3*D,* flattening out and reducing overall magnitude. The azimuthal direction has the largest dip at the impingement wall for station 1*D* compared to the previous setups. This may be the most likely case to see a vortex if this is truly the cause of this dip in velocity. These final data points complete the velocity comparison section of this report. From all the contrasts for the range of velocities tested there is no significant change on the overall jet stream profile for either the azimuthal or axial direction. The largest differences were observed at station 0*D* for any given nozzle geometry or impingement angle. But for the purpose of this study the stations along the impingement wall were of the most interest and the 0*D* profile was primarily used to define the peak magnitude of the jet stream.

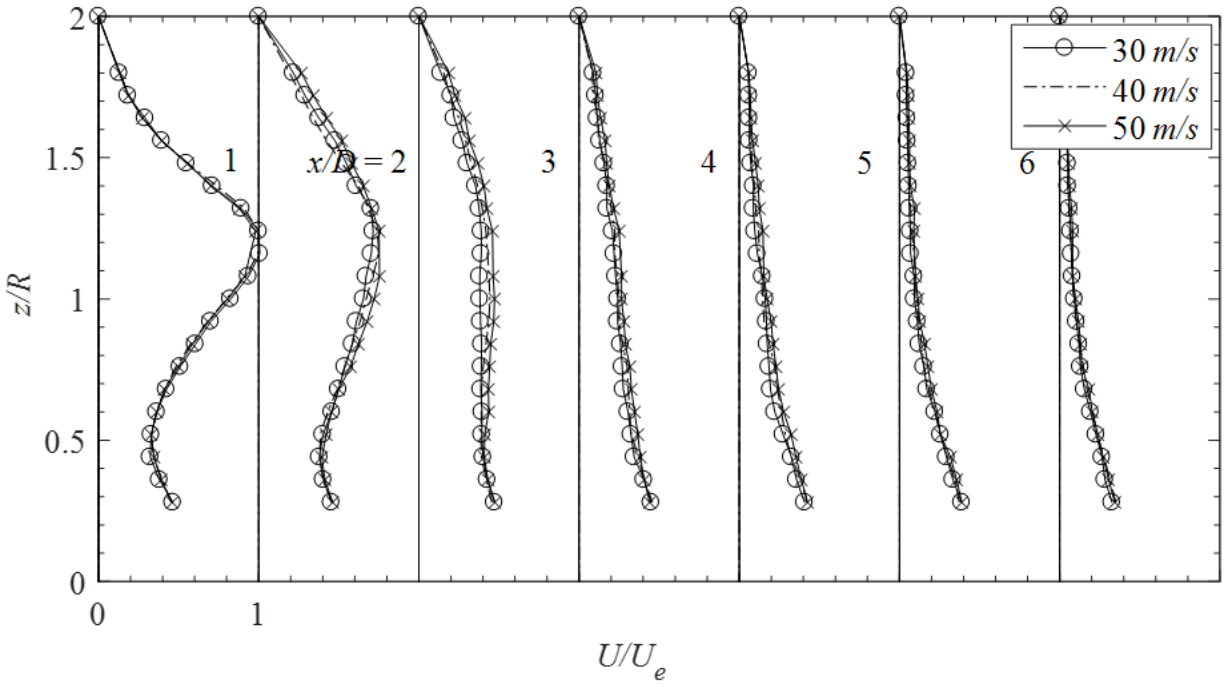

Fig 3.4.17: Axial mean velocity profile (*U*) at seven stations along the jet axis; Nozzle 7 with impingement wall at *d* = 2" & *θ* = 67.5°.

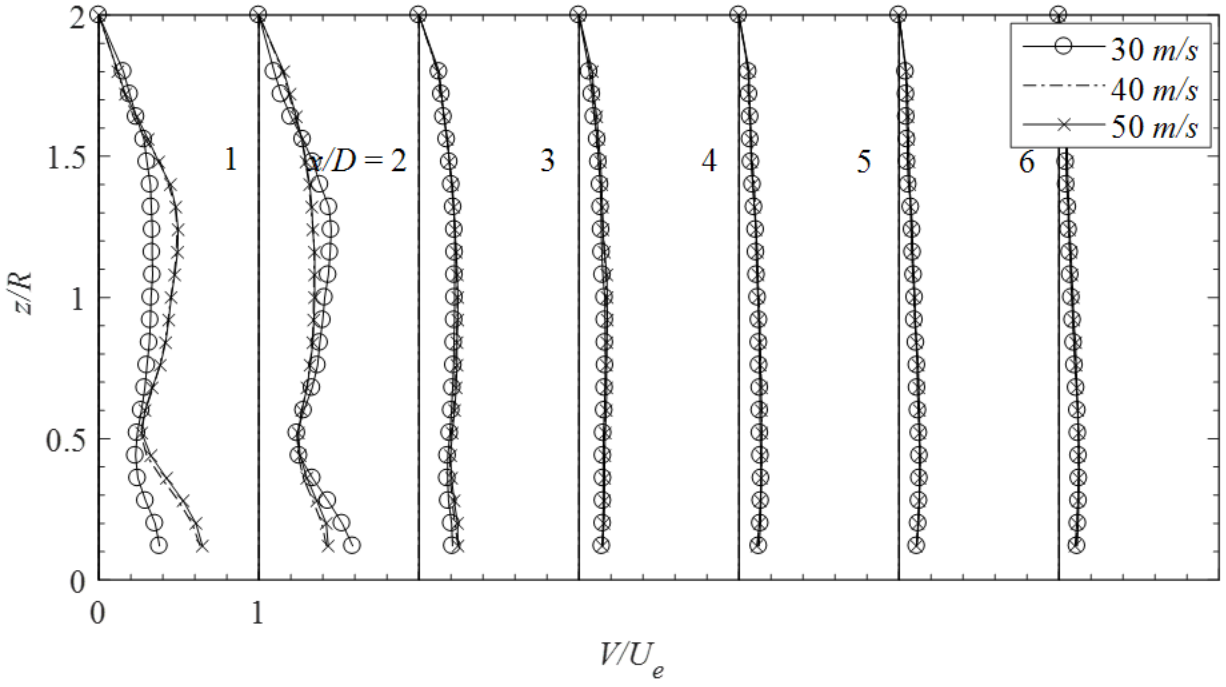

Fig 3.4.18: Azimuthal velocity profile (*V*) at seven stations along the jet axis; Nozzle 7 with impingement wall at *d* = 2" and *θ* = 67.5°.

3.5 Swirling Jets on Impingement Wall Angle Comparison

The previous section has shown that axial and azimuthal jet stream profile doesn't change significantly with a velocity change from 30 m/s to 50 m/s. This will enable the reduction of plots that will be compared in the next section because only one of the three velocities need to be presented. To maintain consistency with Section 3.3 the 40m/s profiles will be used for the remaining plots.

In this section the axial and azimuthal jet stream profiles for each of the swirling nozzles at each of the impingement wall angles will be compared. This will allow for a better understanding of how the angle of the impingement surface effects the downstream flow of the vortex jet. The first profile comparison is from the Nozzle 3 jet stream, see in Fig 3.5.1 and Fig 3.5.2. Looking first at the azimuthal axis, the profile at 0*D* has similar overall shapes for the 67.5° and 45° impingement angles but a much broader profile from the 22.5° angled wall. Some of the difference could be part of the measurement technique used. With the lower angle of the wall the probe moves towards the nozzle exit where the large angles stay relative constant in comparison. At station 1*D* the profiles for the 22.5° and 45° wall change radically from the 0*D* station while the 67.5° profile only changes slightly. For the 22.5° profile the peak amplitude has decrease by 60% while the 45° profile has only reduced by 20%. But the peak for the 45° shifted toward the surface to a point that could not be measured. At station 2*D* the 22.5° jet stream has slowed to only 20% of the original peak velocity and stays there for the remaining stations. The 45° profile reduced to 40% of the 0*D* velocity and only slows slightly more at the other stations. The 67.5° flow however is still at 80% of the exit velocity at station 2*D* and only slows to 60% at the last station. The impingement wall did not seem to have a very large effect on the Nozzle 3 axial jet stream flow at 67.5° angle. While the profile seemed to be drastically slowed when the wall has a smaller angle such as the 45° and 22.5° positions.

For the azimuthal direction the 0*D* amplitude is quite depended on the angle of the impingement wall. The 67.5° peak is equal to the axial direction peak while the 45° profile reaches 60% and the 22.5° has the lowest at 40%. Just like the axial direction the 22.5° azimuthal profile has reduced below the other positions at station 1*D*. The other positions have reduced by about half of the original peak velocity. At station 2*D* both the 22.5° and 45° jet stream profiles only

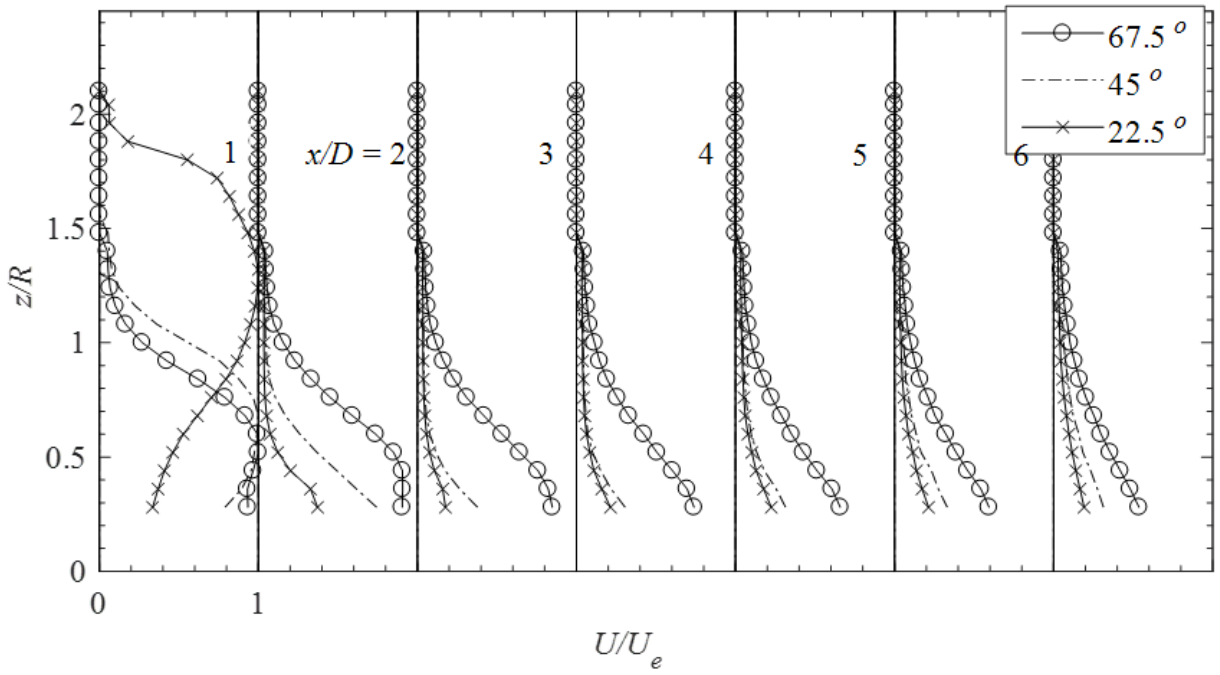

Fig 3.5.1: Axial mean velocity profile (*U*) at seven stations along the jet axis; Nozzle 3 with impingement wall at *d* = 2" & U_e = 40 *m/s*.

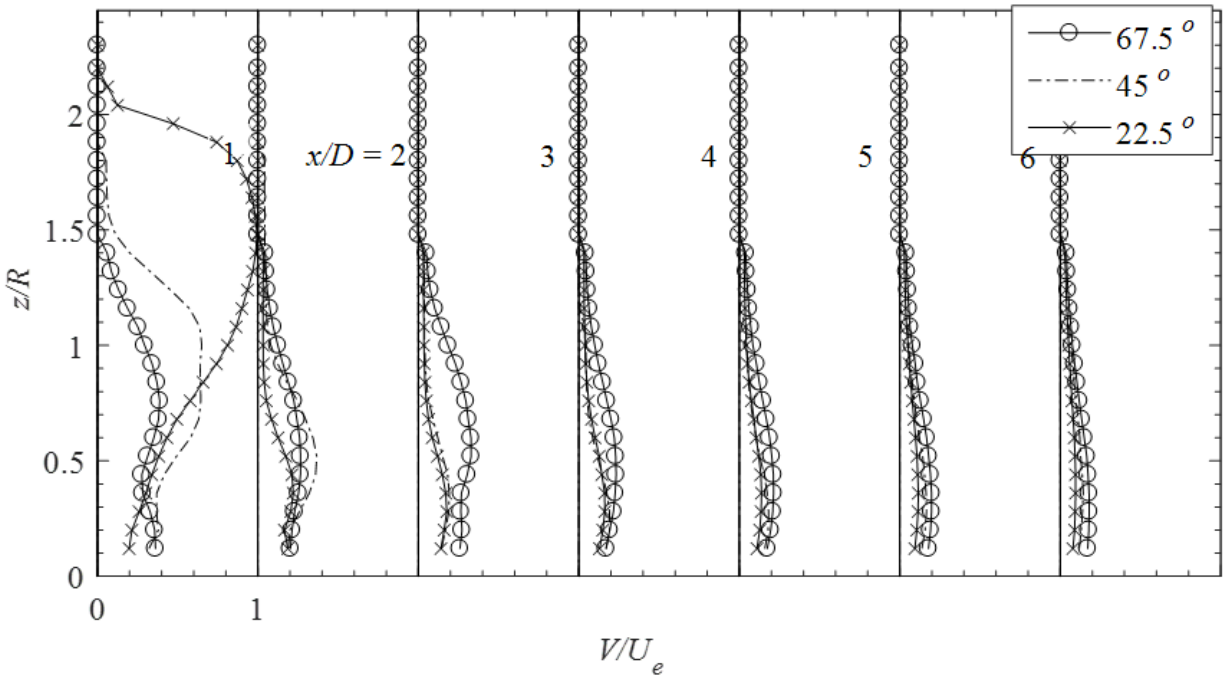

Fig 3.5.2: Azimuthal velocity profile (*V*) at seven stations along the jet axis; Nozzle 3 with impingement wall at *d* = 2" & U_e = 40 *m/s*.

have a peak of 10% of the azimuthal exit speed and stay roughly the same for the remaining five stations measured. The 67.5° profile continues to slow slightly at each station but remains higher than the other positions. These results are like the azimuthal direction where the lower impingement angles reduces the axial flow quickly. The peak velocity for both small angle jet streams dissipate by the 2*D* station. This suggests that for vortex flow with a swirl number near 0.31 the impingement angle needs to be 45° or less to effectively reduce or slow the flow.

The next set of data that will be reviews is the azimuthal and axial data for the three different impingement positions for the Nozzle 5, see Fig 3.5.3 and Fig 3.5.4. The profile at station 0*D* for the axial direction have three distinctive shapes for the different positions. The shape at 45° seems to cut the difference between to the other angles almost perfectly in half. This indicts that the change in the profile are linear, making the profile for an angle between the measured positions predictable. At station 1*D* the peak amplitude of the 22.5° profile has reduced by half while the other two have only slowed slightly. All three jet stream's mean peak have moved toward impingement surface but 22.5° is the most radical. The 22.5° continues to decay as it moves forward to about 20% of the 0*D* peak. The two remaining positions track closely together, where they slow at each station but stay higher than the 22.5° profile. In the axial direction the impingement angle only seems to have an influence on the jet stream flow of Nozzle 5 when the angle is less than 45° and quite effective at 25°. At 45° and greater the profile maintains a strong amplitude out past 4*D* from the exit of the nozzle.

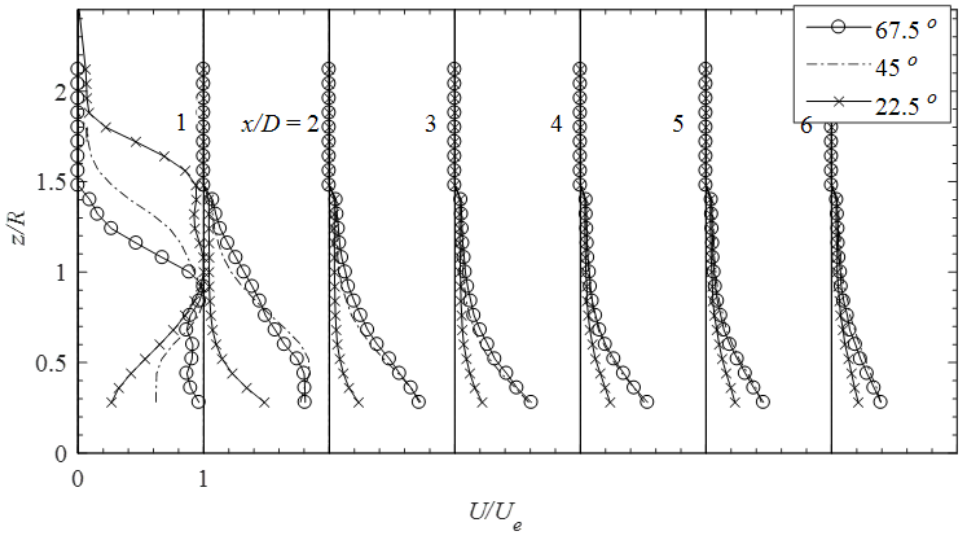

Fig 3.5.3: Axial mean velocity profile (*U*) at seven stations along the jet axis; Nozzle 5 with impingement wall at *d* = 2" & U_e = 40 *m/s*.

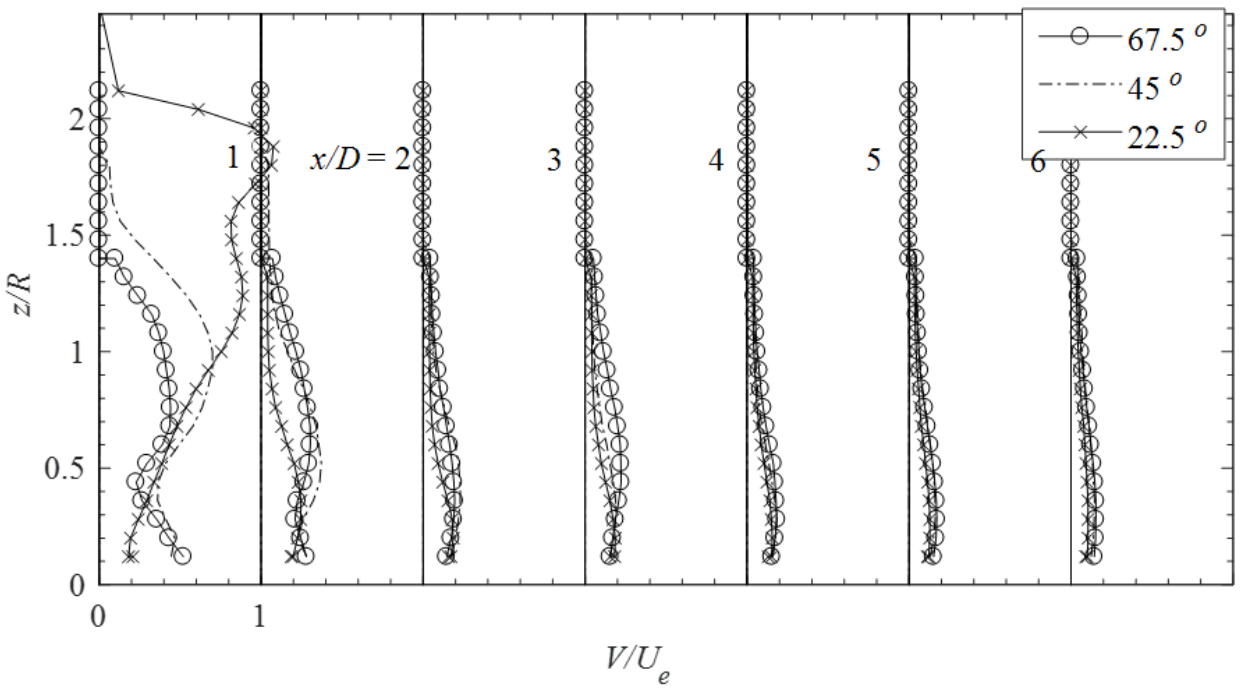

Fig 3.5.4: Azimuthal velocity profile (*V*) at seven stations along the jet axis; Nozzle 5 with impingement wall at *d* = 2" & U_e = 40 *m/s*.

In the azimuthal direction, the 0*D* profiles are again quite different from one another. The 22.5° profile has a peak higher than the axial direction while the others are at 60% and 40% for the 45° and 67.5° profiles respectively. At station 1*D* all three profiles have reduced where the most extreme change was from the 22.5°**,** slowing to only 25% of the axial exit velocity. The other positions have similar shapes. At station 2*D* the 22.5° jet stream has continued to slow and the profile flattened, the profile remains unchanged for the other stations measured. The 45° and 67.5° profiles continue to track closely for the remaining stations, where the jet stream decays at each station until they align with the 22.5° profile at station 6*D*. While the 22.5° impingement wall position is changed the most, the other two positions also reduce in amplitude quickly. At 2*D* all three profiles have dissipated significantly compared to the original shape. This suggests that for vortex flow, with a swirl number near 0.59, the impingement angle needs to be less than 45° to effectively reduce or slow the flow in the azimuthal axis.

The final impingement wall positions that will be compared is for the Nozzle 7, the data for the azimuthal and axial flow directions are seen in Fig 3.5.5 and Fig 3.5.6. For the azimuthal axis at 0*D* the three jet stream profiles are similar in shape but the peak of the profile is shifted further

away from the impingement surface as the angle reduces. This shift does not appear to be linear as the 67.5° and 45° peaks are much closer together than the 45° and 22.5° peaks to one another. At station 1*D* each profile changes in a different way, the 67.5° jet stream maintains its peak location from the surface but dampens to 80% and broadens in shape. While the 45° profile shifts the peak toward the surface by approximately half and reduces the peak to 80%. The 22.5° flow lastly slows abruptly to only 40% of the exit velocity and shifts the peak to a quarter of the peak position from the surface. At station 2*D* the positions continue to take their own course where the 67.5° profile reduces to 40% of the initial peak but maintains the same peak position. The 45° profile slows to 60% and continues to shift toward the impingement wall and the 22.5° profile reduces only slightly. From stations 3*D* to 6*D* the 45° jet stream has the largest amplitude while the overall shape of the three positions starts to become uniform at station 4*D*. From these results it is difficult to come to any rigid conclusion about how the angle of the impingement wall effects the vortex flow that is generated from the Nozzle 7. It is clear however that at an angle of 22.5° the flow is dissipates quickly in the axial direction. An angle greater than 22.5° however could result in adverse dissipative effects on the downstream flow.

In the azimuthal directions the profiles generated at 0*D,* for three impingement wall positions, seem to be linear. The peak drops evenly and the peak shift towards the wall's surface from one angle to the next. At the next station, 1*D,* what was the strongest profile has become the weakest, reducing in amplitude to 25% of the 0*D* peak. The other profiles have slowed by about half of the original speed. At station 2*D,* all three jet streams have slowed to about the same velocity, 25% of the axial exit speed and broadened in shape. For the remaining stations, 3*D* to 6*D,* all three impingement angle profiles track closely together. Each of them are continuing to decay slowly at each following measurement slowing to 10% at the final station, 6*D*. While the azimuthal direction showed some of the same inconsistencies as the axial direction the overall results were not affected. The azimuthal flow reduced significantly for all impingement wall positions at station 2*D*. This suggests that for vortex flow, with a swirl number near 0.71, the impingement angle needs to be 22.5° or less to effectively reduce or slow the flow in the axial axis while any angle in the azimuthal direction has the desired result.

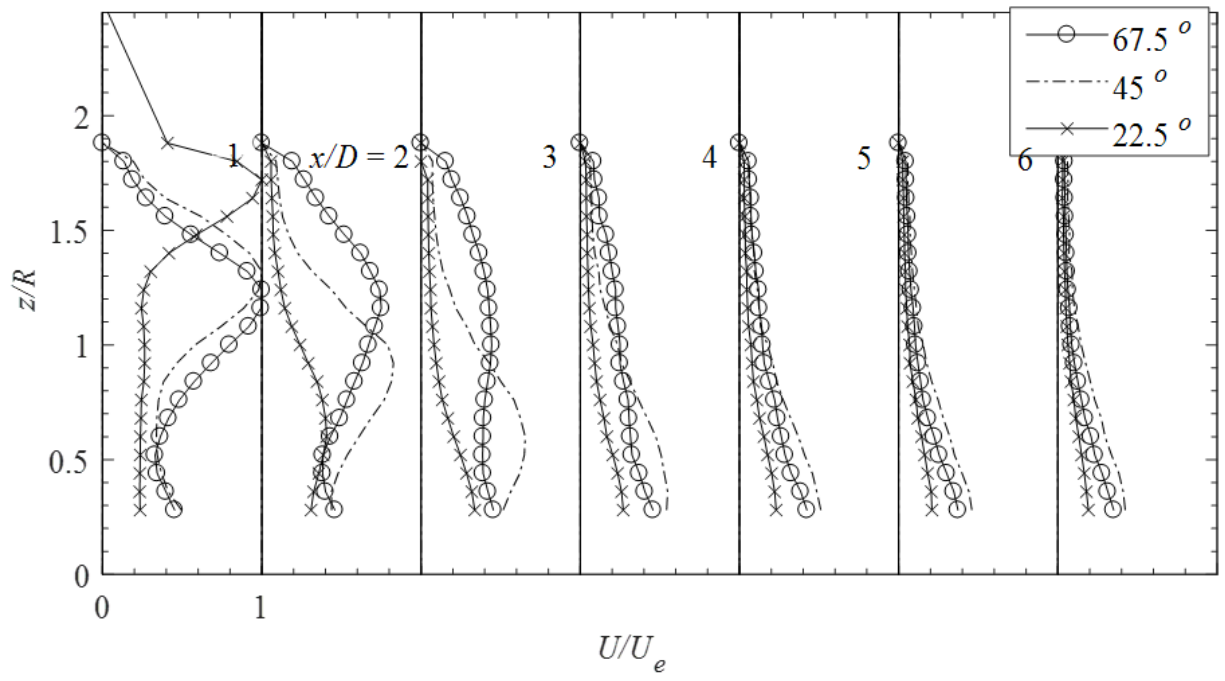

Fig 3.5.5: Axial mean velocity profile (*U*) at seven stations along the jet axis; Nozzle 7 with impingement wall at *d* = 2" & U_e = 40 *m/s*.

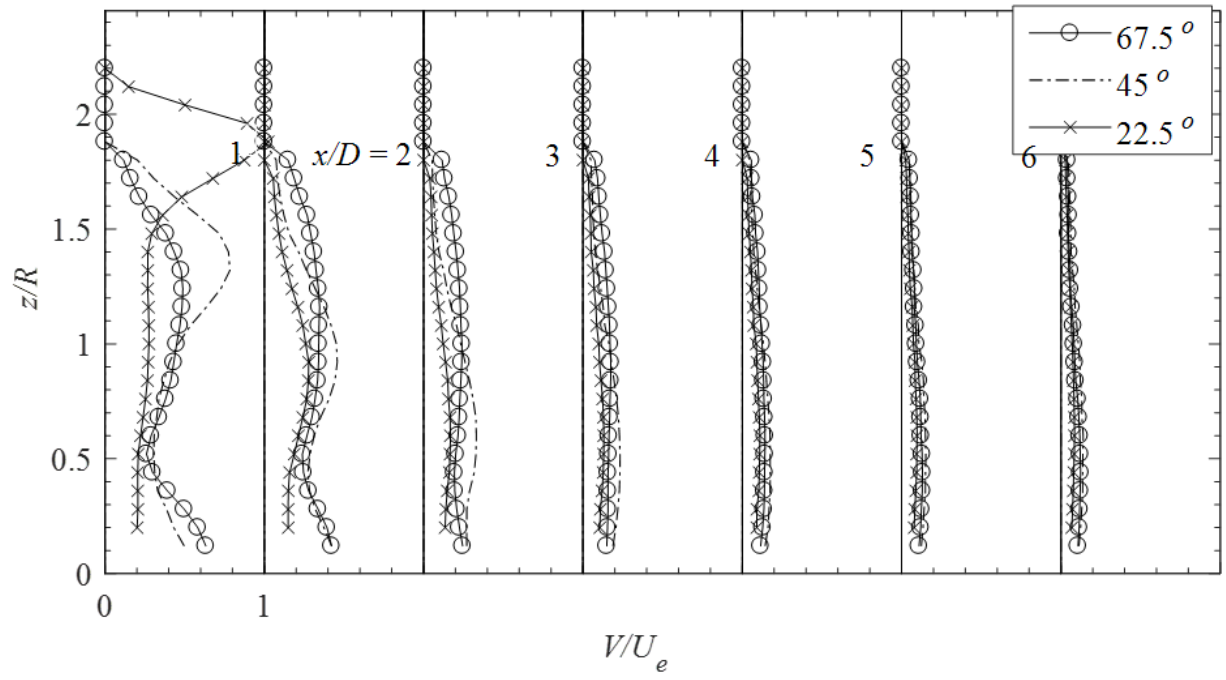

Fig 3.5.6: Azimuthal velocity profile (*V*) at seven stations along the jet axis; Nozzle 7 with impingement wall at *d* = 2" & U_e = 40 *m/s*.

3.6 Swirling Jets on Impingement Wall Nozzle Swirl Comparison

The final comparison that will be made from the hot wire anemometer data will be to overlay the data for each of the vortex swirling nozzles at the different impingement angles. Both the azimuthal and axial flow directions will be presented to determine if there is any general trend that can be revealed. Like the previous section only the data from the 40 m/s runs will be presented as velocity did not show a sizable difference in the jet stream profile over the 6*D* measurement field.

To start, the data from each nozzle was plotted when the impingement wall was angled at 67.5° from vertical, see Fig 3.6.1 and 3.6.2 for the axial and azimuthal plots respectively. At the 0*D* station in the axial axis both Nozzle 3 and 5 resemble that of a top hat profile but Nozzle 5 maintains the full velocity for the whole exit of the nozzle while Nozzle 3 is only 75%. Both nozzles also have the gradual decay that is usually seen with the top hat profile. Nozzle 7 however seems to have a peak further out than the other two and it does not sustain the amplitude as it moves toward the surface. At station 1*D,* Nozzle 3's shape only changes slightly, reducing its amplitude 10% and shifting slightly toward the impingement surface. Nozzle 5's shift is more dramatic to where it now tracks the Nozzle 3 profile. The Nozzle 7 profile slows to 75% of the 0*D* peak and broadens the peak. All three nozzles follow this same type of decay over the next five stations. The Nozzle 7 maintains a high mean velocity than the other two nozzles for stations 2*D* and 3*D* but its peak velocity is much smaller. The jet stream profile generated by the Nozzle 3 vortex is the slowest to decay, with a peak amplitude of 50% at station 6*D*. It can be said that for the axial direction the high the swirl number of the vortex flow is the faster it will decay at when the impingement angle is at 67.5°.

For the vortex flow in the azimuthal direction, the profile at 0*D* for the Nozzle 3 and 5 are quite similar with the Nozzle 5 amplitude only being slightly higher, 5%. The Nozzle 7 profile, while having a similar shape the structure, is elongated stretching out at 1.8R and having a peak velocity of 60% the azimuthal axis. Also, the Nozzle 7 profile has a pronounced dip at 0.5*R* which the other two nozzles only have a small disturbance. At station 1*D* both Nozzles 3 and 5 slow in unison to about 30% axial exit velocity. Nozzle 7 still exhibits the dip at 0.5*R* while the other two profiles no longer show any signs of changes at this location. The profile for Nozzle 7 has reduced to 40% axial exit velocity. As the jet stream progresses through the stations, Nozzle 7 shows the

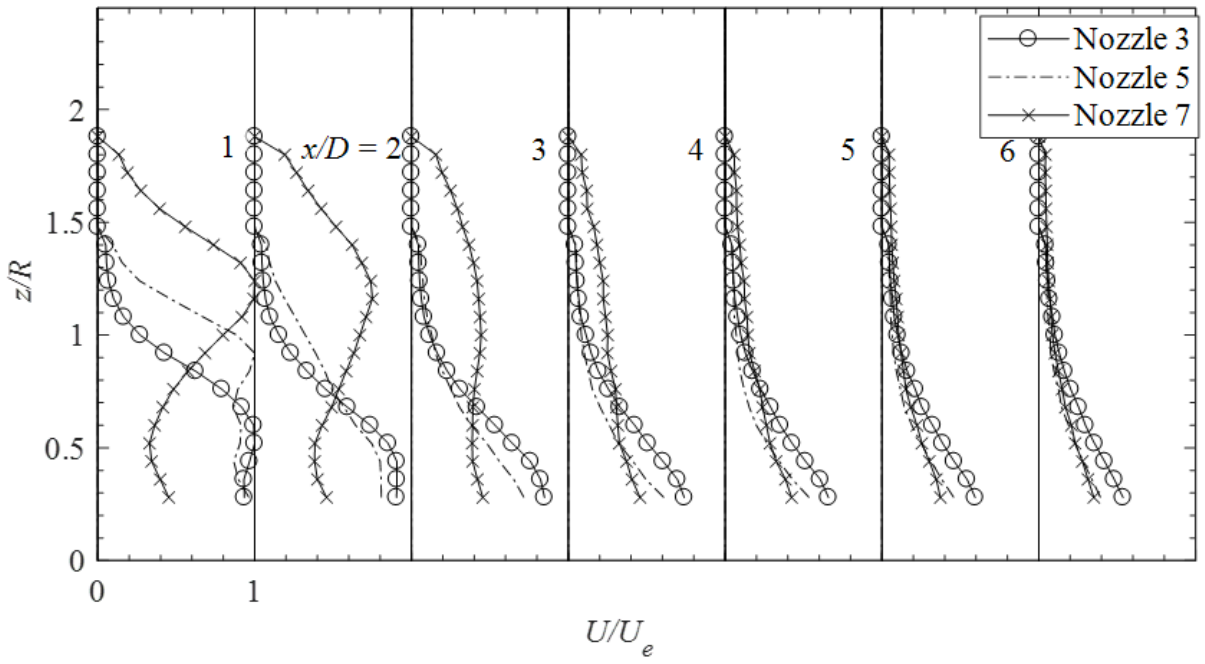

Fig 3.6.1: Axial mean velocity profile (*U*) at seven stations along the jet axis; Nozzles 3, 5 and 7 with impingement wall at d = 2", U_e = 40 *m/s* & θ = 67.5°.

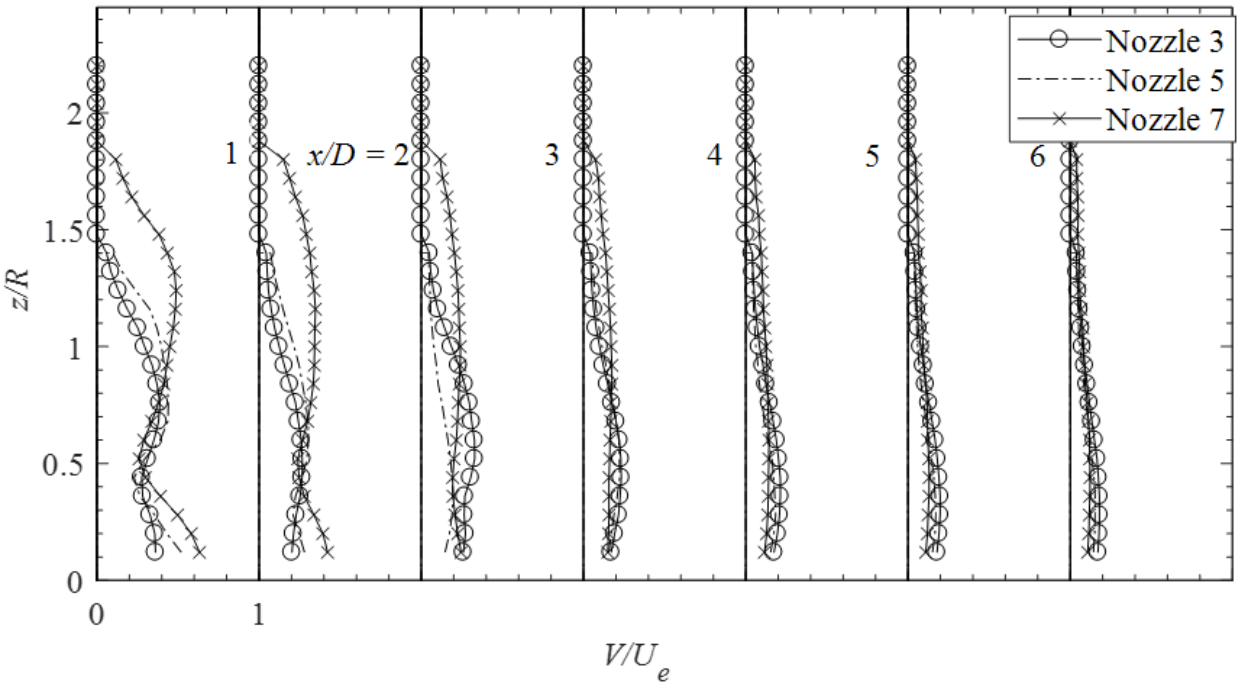

Fig 3.6.2: Azimuthal velocity profile (*V*) at seven stations along the jet axis; Nozzles 3, 5 and 7 with impingement wall at d = 2", U_e = 40 *m/s* & θ = 67.5°.

quickest decay, falling below the other profiles in peak and mean speed at station 4*D*. Nozzle 5 is the next quickest to decay in the later stations. Overall, while there are some differences between the rates at which each azimuthal jet stream profile dissipates each of them show the same general trend. In the azimuthal direction the swirl of the vortex does not seem to have the effects that the impingement wall has on the axial jet stream.

The next comparison that will be made is for the three swirling nozzles when the impingement angle is at 45°, see Fig 3.6.3 and Fig 3.6.4 for the axial and azimuthal plots respectively. In the axial direction, at station 0*D* each of the nozzles have very different shapes. Nozzle 3 has a peak at 0.6*R* and reduces as it approaches the surface. Nozzle 5 has a peak at 0.75*R* but also has another peak at 1.25*R* with a smaller amplitude. While Nozzle 7 has a peak at 1.4*R* and another small peak near the impingement surface. To generalize, the major peak of the jet stream profile moves away from the wall's surface as the swirl number increases. As the flow moves downstream the velocity of each nozzle decreases slowly and the major peak of the profile moves towards the impingement surface. The shift in both amplitude and peak location appear to be similar in scale for each of the nozzles. The general trend shows that in the axial direction the effect of the impingement wall increases as the swirl number decreases when the wall is angles at 45°. This is the opposite effect that was observed when the wall was angles at 67.5°.

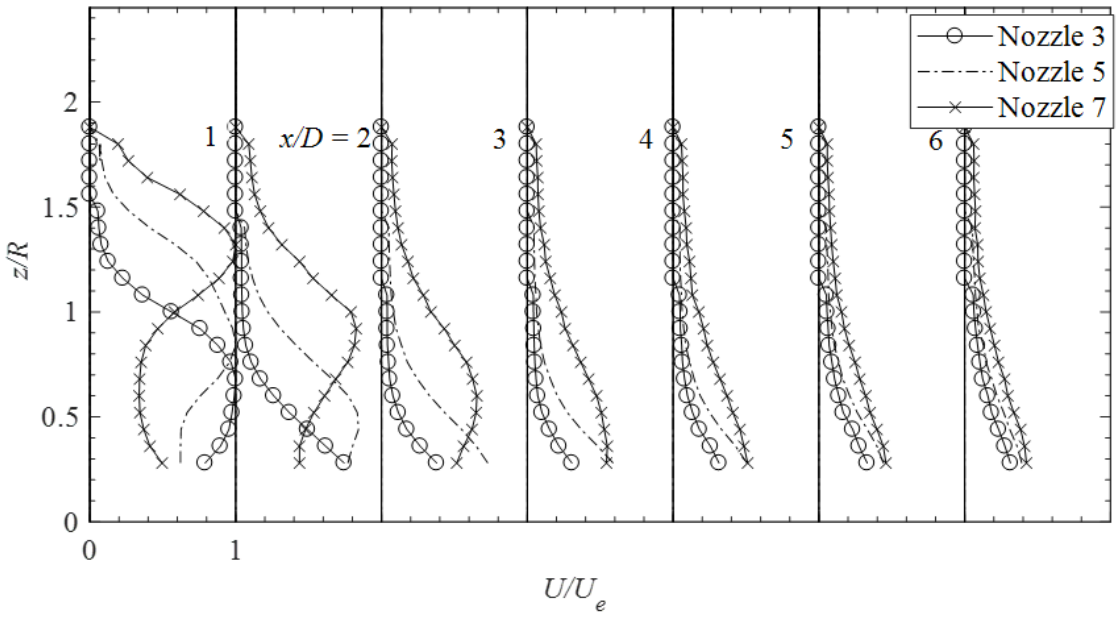

Fig 3.6.3: Axial mean velocity profile (*U*) at seven stations along the jet axis; Nozzles 3, 5 and 7 with impingement wall at *d* = 2", U_e = 40 *m/s* & θ = 45°.

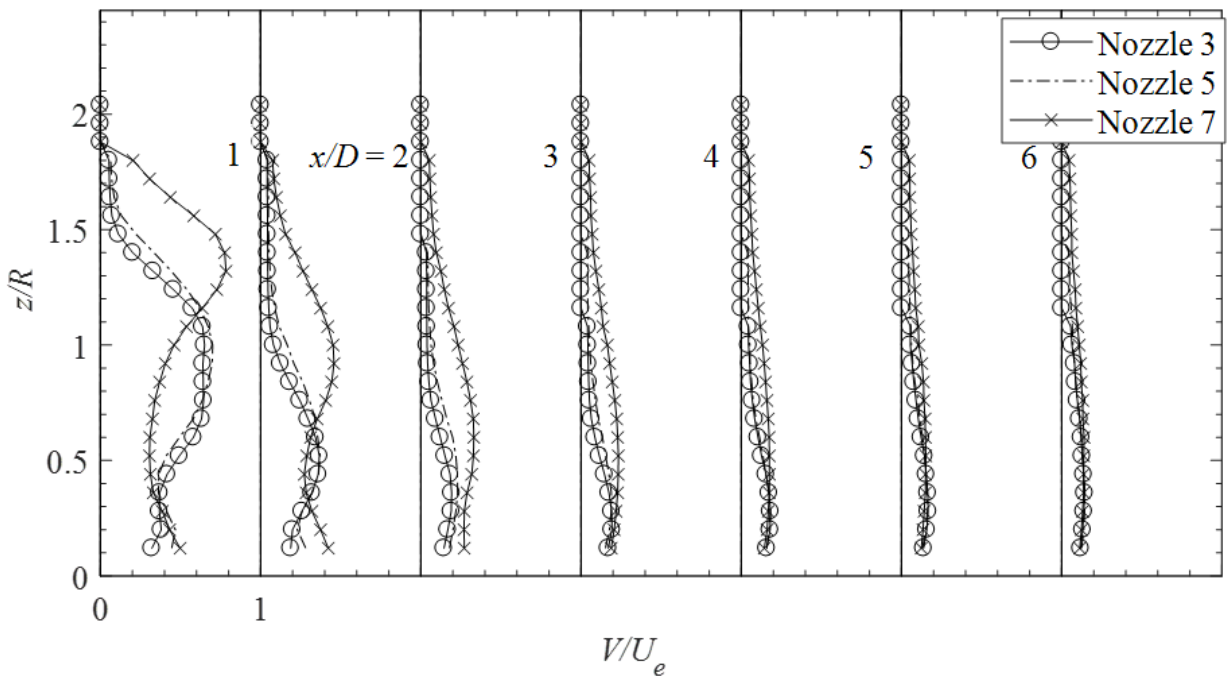

Fig 3.6.4: Azimuthal velocity profile (*V*) at seven stations along the jet axis; Nozzles 3, 5 and 7 with impingement wall at d = 2", U_e = 40 *m/s* & θ = 45°.

In the azimuthal direction the profile, at 0*D,* the Nozzle 3 and 5 are tracking closely with a wide peak from 0.6*R* to 1.2*R* and a decaying in strength on both sides. While the Nozzle 7 profile has a narrower peak and higher at 1.4*R* with a velocity at 80% axial exit speed. At station 1*D* all three profiles dampen in speed and their peaks shift towards the impingement surface. Nozzle 3 and 5 tracks closely at all stations measured. As the flow progress forward, they continue to slow at each station and the peak broadens out until there is no discernable peak at station 4*D*. At station 5*D*, the profiles align and do not have a velocity higher than 10% of the axial exit velocity. Nozzle 7 maintains a relatively high mean velocity until the jet stream reaches station 4*D*, two stations further than the other two vortex flows. While this does not lend for a general trend to be made it can be said that vortex flows that are near a swirl number of 0.71 show less dissipation effects from an impingement wall at 45° then vortex flows below said swirl number. It is also observed that vortex flows at or below 0.59 swirl number can effectively demission in the azimuthal direction with the use of a 45° impingement wall. Overall, this wall setup is very effective for the Nozzle 3 jet stream in both the azimuthal and axial directions, effective for Nozzle 5 in the axial direction and not effective for the Nozzle 7 vortex flow in either orientation of flow.

The final set of jet stream profiles that will be compared is the three nozzles where the flow is impinged by a wall angle at 22.5° from vertical, see Fig 3.6.5 and Fig 3.6.6 for the axial and azimuthal figures respectively. For the axial flow at station 0*D*, Nozzle 3 and 5 again have very similar profiles, a broad peak spanning from 1*R* to 1.5*R* at its maximum speed and slowing down on either end. The Nozzle 7 profile at 0*D* is quite different having a sharp peak at 1.75*R*, much further away from the center of the peak for the other nozzles. As the flow progress to the next station, 1*D*, the profile for all there jet streams shift significantly. Nozzle 3 and 5 track closely for all stations measured, at 1*D* the peak is much narrower, reduced to 40% the exit speed and sits close to the impingement surface. The profile for Nozzle 7 also shifts its peak toward the wall to 0.75*R* and the amplitude of the peak has reduced to 40%, while slightly spreading out in shape. The Nozzle 3 and 5 peak reduces at each remaining station, slowing to 20% of the initial peak at station 6*D* and showing no measurable flow past 1*R*. Nozzle 7's jet stream is slower to dissipate but the peak continues to move toward the impingement wall and the flow slows as well, aligning with the other nozzles at stations 5*D* and 6*D*. While Nozzle 7 does react slower than the other nozzles to the impingement surface interaction, all three jet stream profiles are sufficiently decayed. This suggests that the impingement wall set at 22.5° is effective at stopping all vortex flows tested in the axial direction.

In the azimuthal direction, the three 0*D* profiles are interesting, Nozzle 3 and 7 take a shape similar to that of the axial direction described above with the exception being that the peaks are further out, 1.5*R* and 1.9*R* respectively. The Nozzle 5 profile however looks more like a combination of Nozzle 3 and 7 where there are two peaks one at the start of the Nozzle 3 peak, 1.25*R*, and one at the peak of Nozzle 7 at 1.9*R*. While Nozzle 5 has this profile difference from the axial direction, at station 1*D* it tracks closely with Nozzle 3 and has the same general trend as the azimuthal direction. Nozzle 7 also shows the same typical profile transforms as the axial directions as its axial direction, measuring below 20% across the whole profile at station 2*D* for all three jet streams. The impingement wall positioned at 22.5° from vertical is very effective at dissipating the azimuthal flow generated by all three nozzles tested. Overall, the 22.5° configuration appears to be the most influential for all the vortex jet stream flows with swirl numbers ranging from 0.31 to 0.71.

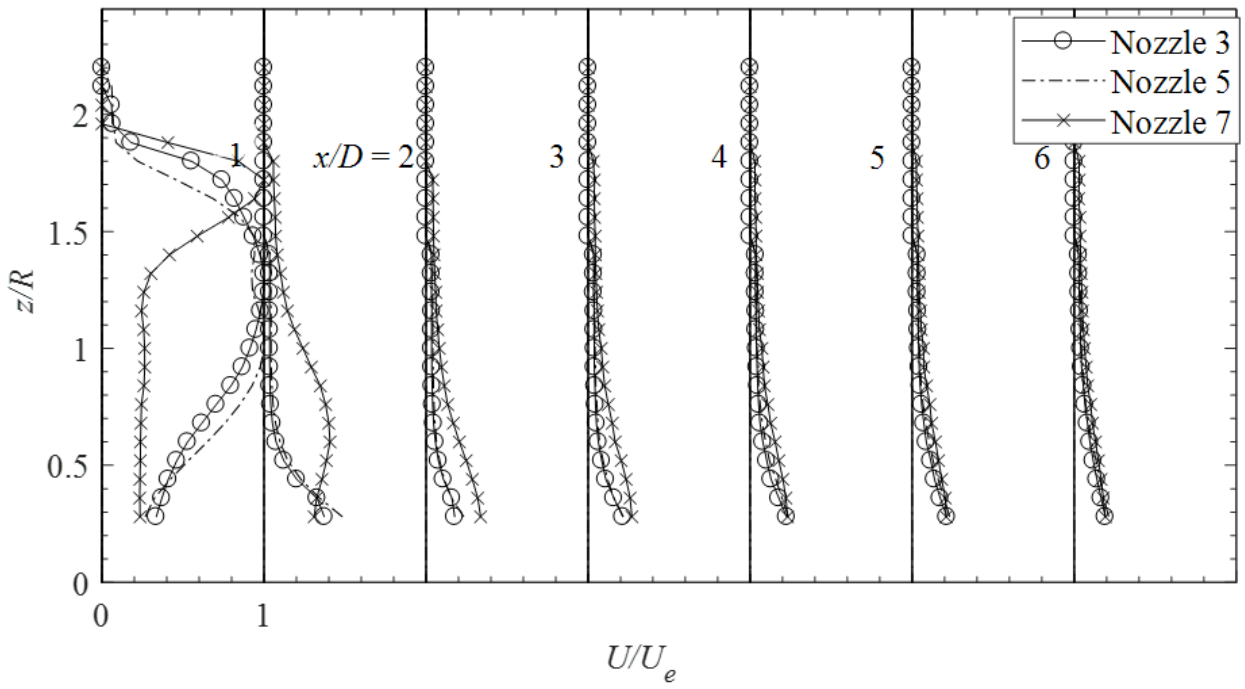

Fig 3.6.5: Axial mean velocity profile (*U*) at seven stations along the jet axis; Nozzles 3, 5 and 7 with impingement wall at d = 2", U_e = 40 *m/s* & θ = 22.5°.

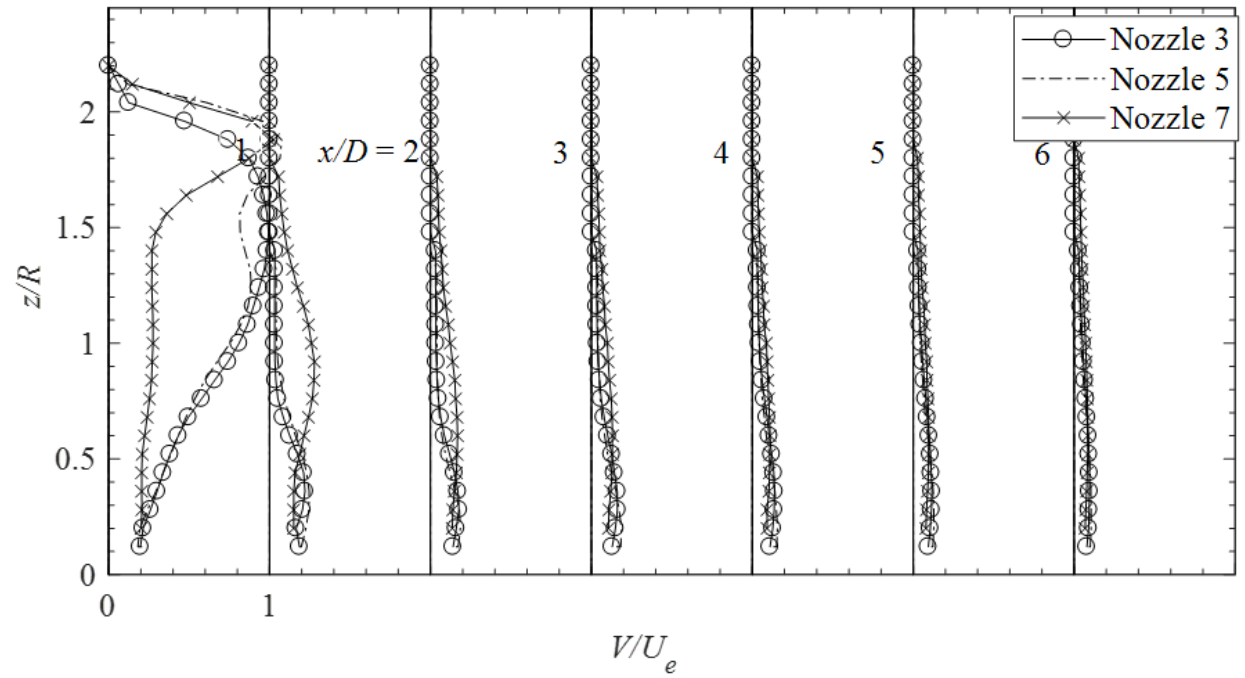

Fig 3.6.6: Azimuthal velocity profile (*V*) at seven stations along the jet axis; Nozzles 3, 5 and 7 with impingement wall at d = 2", U_e = 40 *m/s* & θ = 22.5°.

4. Flow Visualization Results

4.1 Nozzle Characterization through Flow Visualization

The data presented in Section 3 has been able to give a great deal of insight into how the different nozzles, speeds, and impingement angles transform the flow of the jet stream. However, the information provided from these hot wire anemometer measurements does not completely characterize the flow. In order to get a different perspective of the jet stream, flow visualization was utilized. This will allow for the overall transformation to be observed. The technique that was used to observe the jet stream was Schlieren imaging described in detail in Section 2.3.

Like the nozzle characterization that was performed with the hot wire measurements the four different nozzle's flow will be analyzed visually. Since it has been determined that the exit velocity does not play a role in the jet stream profile all the images presented in this section will be at a tripped nozzle exit velocity of 30m/s. This speed was chosen primarily because the images at the lower speed were clearer because the ratio between the nitrogen seeding was highest at this velocity. To start each of the flows will be presented without any impingement surface. This will act as a baseline for each of the jet streams, showing how the flow progresses without any interference.

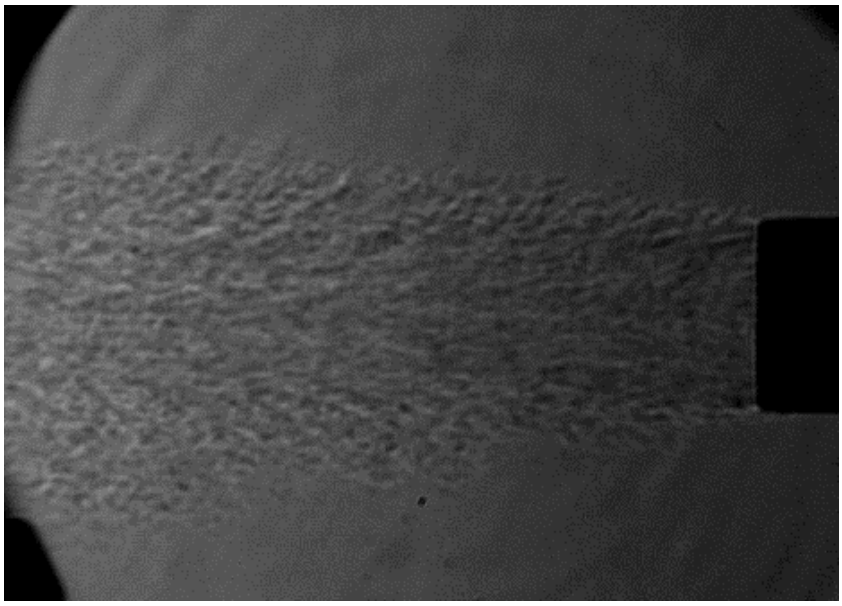

Fig 4.1.1: Schlieren image of tripped nozzle jet stream flow at U_e = 30m/s seeded with CO_2.

The first setup to be presented is the tripped nozzle jet stream flow, see Fig 4.1.1. Based on the image, the flow appears to be uniform at the exit. The center of the jet stream maintains a dense structure while the outer edges of the flow spread in the azimuthal direction. These observations follow suit with the hot wire measurements which indicates that the flow spreads out and slow down at the exterior of the profile while maintaining a relatively constant peak velocity. The image and video taken from for this setup do not show any significant azimuthal movement or vortex flow. The image for the tripped nozzle also resembles that of the Schlieren images taken from S. C. Crow & F. H. Champagne (1971) [6]. This is yet another data point to suggest that the setup used for those experiments should yield the same results as the setup used for their paper [6].

The vortex swirling jet streams will now be examined without any impingement interaction, see Fig 4.1.2 for the Nozzle 3 image. While the flow seems quite uniform at the exit, the shape of the flow quickly changes. The jet stream expands and appears to have a denser cross section on the outer edges then in the middle of the flow at about 2*D* from the exit. Unlike the shape of the tripped nozzle the edge of the stream is not quite as sharp and uniform. The high-speed video taken for this setup also shows that there is a significantly more azimuthal flow interaction than in the tripped flow. It is also worth noting that flow seems to expand to about 3 diameters at the edge of the mirror which is approximately 6*D* from the exit of the nozzle and the flow density has decreased quite a bit.

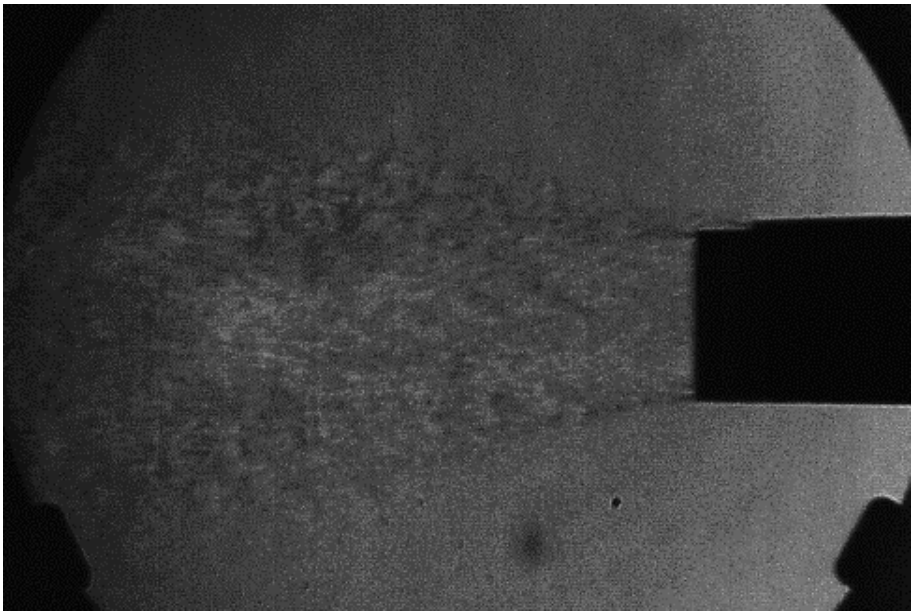

Fig 4.1.2: Schlieren image of Nozzle 3 jet stream flow at U_e = 30m/s seeded with CO_2.

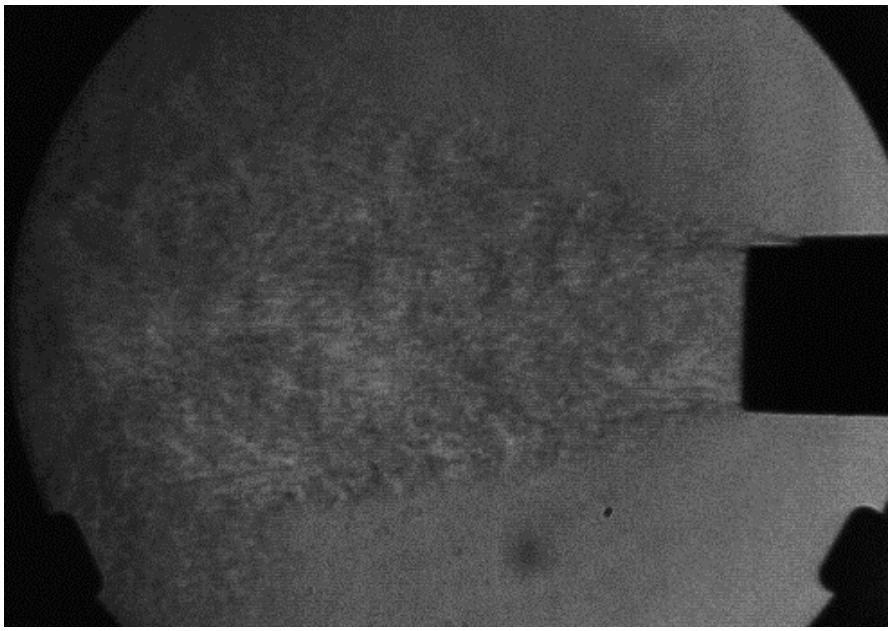

Fig 4.1.3: Schlieren image of Nozzle 5 jet stream flow at U_e = 30m/s seeded with CO_2.

The next jet stream that will be examined is the unimpeded flow from Nozzle 5, see Fig 4.1.3. The overall shape of the profile is very similar to the Nozzle 3's flow but it expands much quicker. The jet stream grows half of a diameter in width for every diameter it moves from the nozzle exit. This growth along with the video captured indicates that this nozzle is generating more azimuthal speed than that of Nozzle 3. The flow near the edge of the mirror is about one and half the width of the Nozzle 3 flow and appears to have less density as well. This dispersion suggests that this nozzle, while generating more swirl, also slows down quicker because the jet stream is not concentrated like the previous two flows.

The final image that was be presented in this section is the Nozzle 7 flow with no interference, see Fig 4.1.4. While the general shape of the profile is consistent with the other two vortex generating nozzles the type of flow is different. With the Nozzle 3 and 5 the axial jet stream is much greater than the azimuthal where it is clear the flow is moving right to left with only a component moving out of plane. For the Nozzle 7 image however the azimuthal and axial components of the flow are much closers in magnitude. This is showing up in Fig 4.1.4 with the irregular profile seen on the edges of the jet stream. This flow expanders outward as quickly as it is moving forward. Overall, the Nozzle 7 has the greatest expansion and swirl with Nozzle 5 being the next and Nozzle 3 being the less effected by the vortex geometry. All these findings align with the results of the hot wire results.

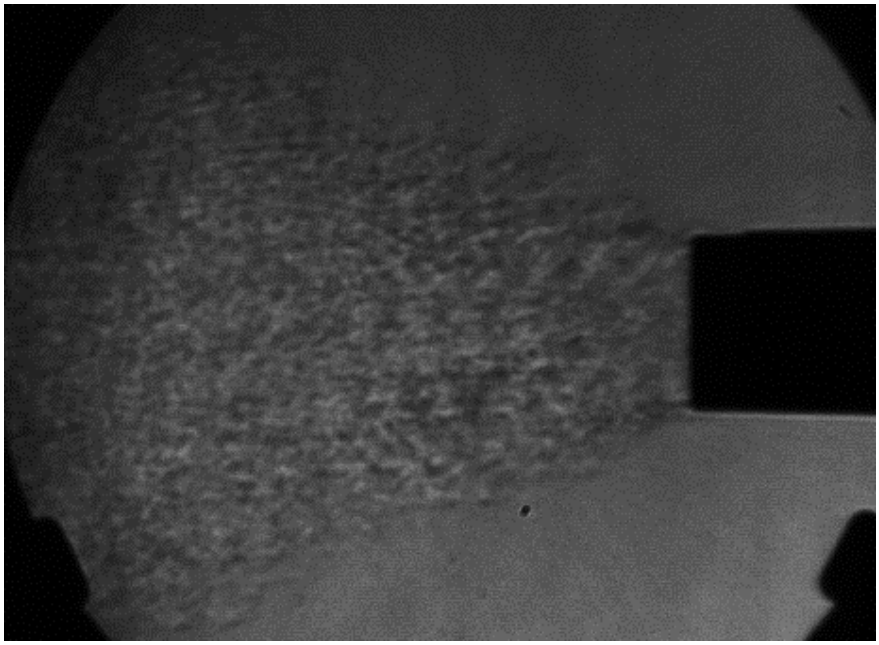

Fig 4.1.4: Schlieren image of Nozzle 7 jet stream flow at U_e = 30m/s seeded with CO_2.

4.2 Flow Visualization of Tripped Jet on Impingement Surface

To finish the package, the tripped nozzle Schlieren imaging and high-speed videos were taken. Although this is not new material it can be used to validate other studies that have already been performed. The one advantage that imaging has over the discrete measurement with the impingement wall setup is that area underneath the nozzle can be analyzed. Because of the setup restrictions only the profile above the nozzle could be measured.

The first setup presented in this section is the tripped nozzle with the impingement wall angle at θ = 22.5° from vertical, see Fig 4.2.1. The flow from the nozzle exit to the wall appear to be the same as the unimpeded jet stream. Once the jet stream impacts the wall the velocity of the flow slows down and spreads out drastically above the nozzle. Below the centerline a vortex forms at the acute angle where the main jet stream is recirculating the flow that deflects off the wall. The rest of the jet stream is pushed out across the bottom part of the wall much like the flow over the exit centerline. There is some azimuthal flow created by the interaction with the wall but slows down as it moves across the surface. Overall, the oncome flow appears to flatten out in all directions on the impingement surface reducing the speed and concentration of the flow quickly.

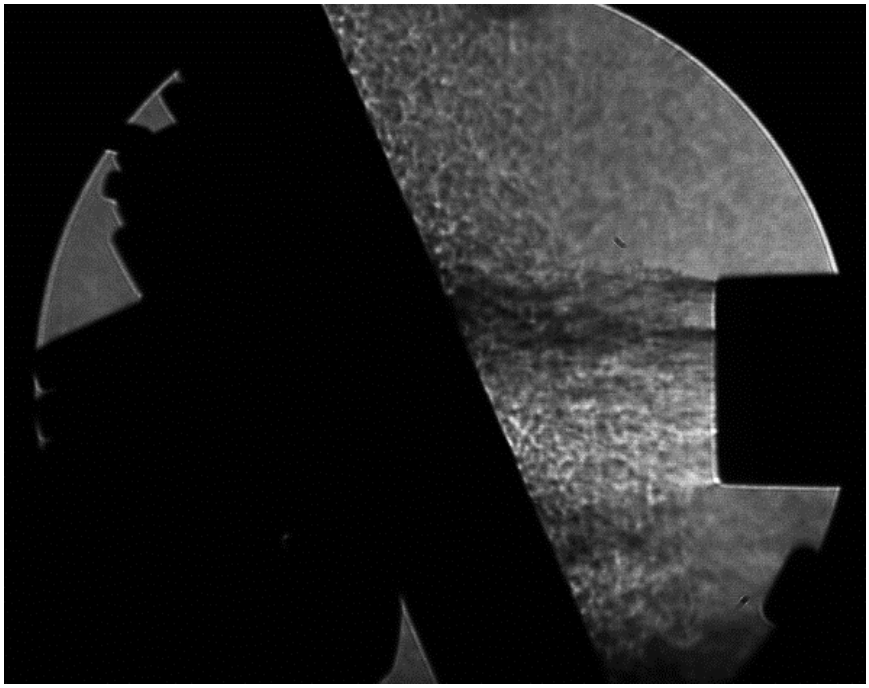

Fig 4.2.1: Schlieren image of tripped nozzle jet stream flow at U_e = 30m/s and impingement wall at θ = 22.5° seeded with CO_2.

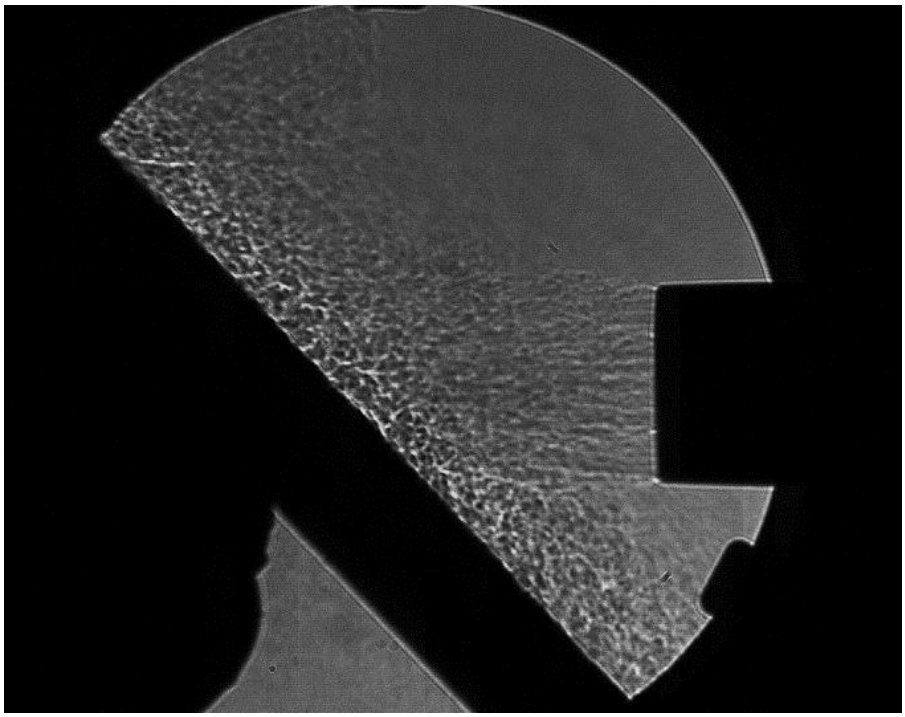

Fig 4.2.2: Schlieren image of tripped nozzle jet stream flow at U_e = 30m/s and impingement wall at θ = 45° seeded with CO_2.

The next setup to be examined is the tripped nozzle with the impingement wall angled at 45° relative to vertical, seen in Fig 4.2.2. Like the previous configuration the flow interaction with the wall causes the flow to slow and expand across the surface. At the 45° angle however, the flow's rate of decent is about half of that of Fig 4.2.1. The jet stream still spreads in all directions and has a vortex that is generated below the centerline of the nozzle. The vortex is much smaller in size and rotates about twice as fast as the previous setup. There is still an azimuthal component created when the flow interacts with the impingement wall and appears to be slightly great as well. Overall, the wall is effective at slowing the flow and dissipating it, but it takes a larger distance for this to occur than the 22.5° configuration.

The final setup that will be examined in this section is the tripped nozzle with the impingement wall angles at 67.5°, see Fig 4.2.3. The flow interaction with the wall is quite different than the other two configurations. While the flow profile above the nozzle centerline remains similar to the 45° setup, there is virtually no flow below the centerline. All the jet stream flow moves up and out along the surface of the wall. This change in flow direction creates less of an effect on the jet stream, the slowing of the flow is a factor of 2 less than the previous setup. While this setup does slow the flow, it takes a much longer time for the velocity to reduce compared to the other configurations.

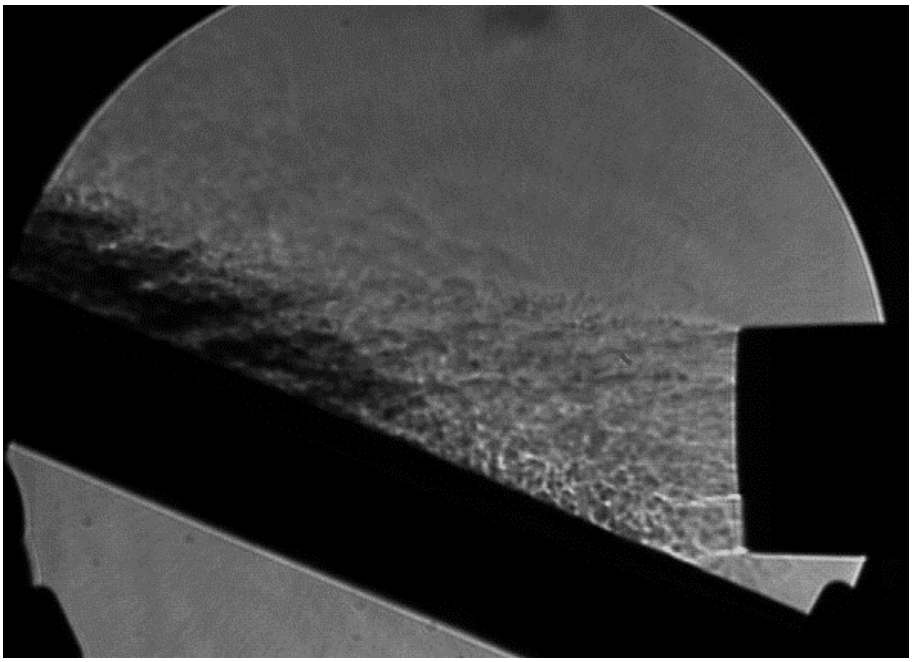

Fig 4.2.3: Schlieren image of tripped nozzle jet stream flow at U_e = 30m/s and impingement wall at θ = 67.5° seeded with CO_2.

4.3 Flow Visualization of Swirling Jet Nozzles on Impingement Wall

This will be the final section of the flow visualization portion of the results section for this paper. The Schlieren images for each of the swirling nozzles will be presented at the different impingement wall angles. Like the tripped nozzle configuration, all the images were taken was the blower setup such that the tripped exit of the nozzle speed would be 30m/s. Also, the flow was seeded with CO_2 to better define the shape of the stream. The nozzles will be analyzed in order of their swirl number from least to greatest swirl.

The first configuration shown below is the Nozzle 3 jet stream interacting with the impingement wall which is set two inches downstream of the nozzle's centerline, seen in Fig 4.3.1. The wall is angles at 22.5° from vertical. The jet stream, upon hitting the wall, quickly redirects, spreading out along the surface in all directions. In the Z_S axis most of the flow moves upward while some of the flow does move below the centerline of the nozzle. A small, slow moving vortex does form at the acute angle created between the nozzle and the lower portion of the impingement wall, but it is much less than that seen for the tripped nozzle. Both the azimuthal and axial components of the flow slow quickly and appear to approach zero as it reaches the edges of the mirror's diameter of 8 inches.

Fig 4.3.1: Schlieren image of Nozzle 3 jet stream flow at U_e = 30m/s and impingement wall at θ = 22.5° seeded with CO_2.

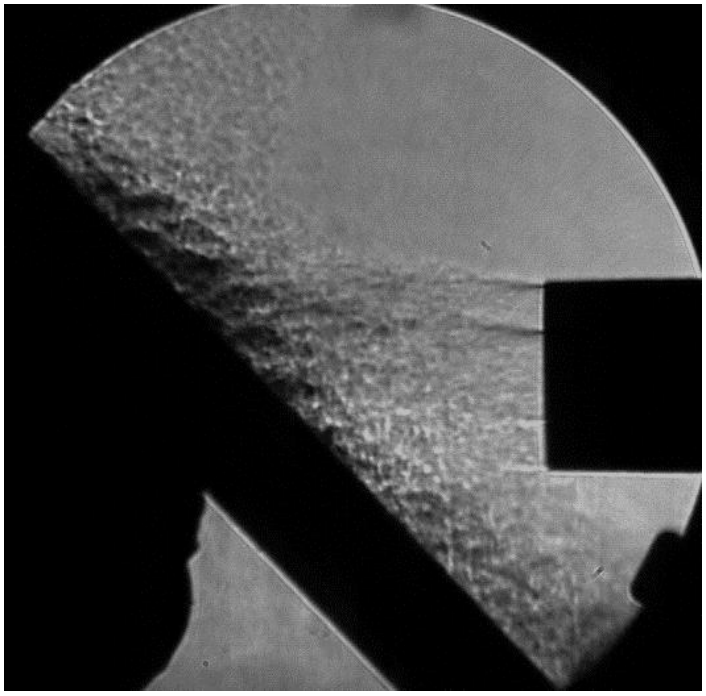

Fig 4.3.2: Schlieren image of Nozzle 3 jet stream flow at U_e = 30m/s and impingement wall at θ = 45° seeded with CO_2.

The next configuration shown is the nozzle 3 jet stream with the impingement wall set to 45° from vertical, see Fig 4.3.2. Like the first configuration, the flow slows quickly after hitting the wall. The jet stream redirects and follows the surface where again much of the flow moves upwards. Some of the flow moves below the centerline of the nozzle but it is a smaller percentage than in the 22.5° setup. There is still a vortex present, but it is smaller and faster moving. The axial and azimuthal flow have the same general trends of the first configuration, but it takes about a factor of two further downstream for the flow to reach the same velocity. This indicates that the impingement wall is dissipating the flow as expected but not as efficiently as the 22.5° wall.

The final setup for the nozzle 3 is with the impingement wall angled at 67.5°, seen in Fig 4.3.3. The jet stream interacts with the wall much like the tripped nozzle flow did with this wall configuration. All the stream moves upward along the surface of the wall. Its flow does appear to be slowing but the rate of deceleration is a factor of four slower than the 45° setup. The flow is still moving at least half of the exit speed in the axial direction when it reaches the edge of the mirror. There is no vortex present below the nozzle. When comparing the images from the tripped nozzle to Nozzle 3 they look identical. It could be said that a vortex flow with a swirl number equal or less than 0.31S behaves like a normal tripped jet stream when a wall is present.

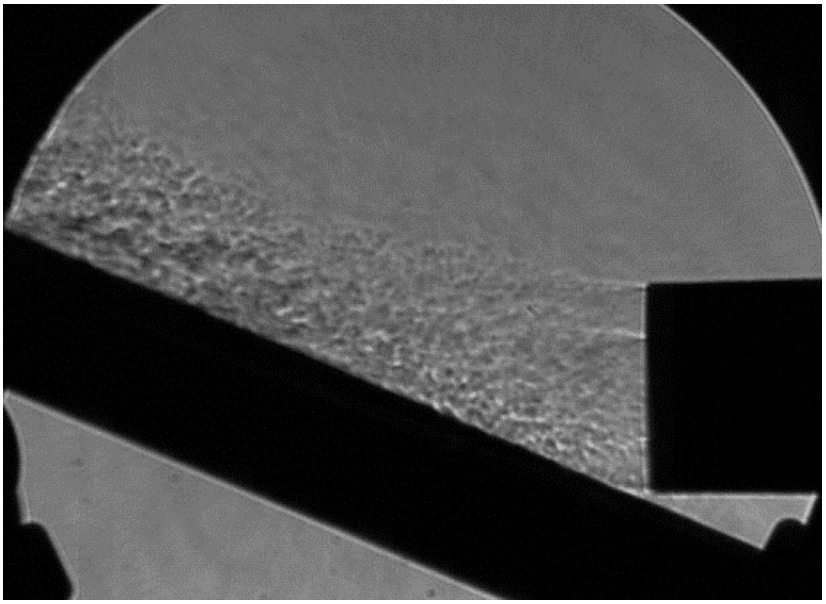

Fig 4.3.3: Schlieren image of Nozzle 3 jet stream flow at U_e = 30m/s and impingement wall at θ = 67.5° seeded with CO_2.

The following set of images that will be examined are for the Nozzle 5 impingement wall configurations with the first being for the wall at 22.5°, seen in Fig 4.3.4. Most of the flow moves upward in the axial direction after hitting the impingement wall. This is consistent with the other two nozzles seen at this same wall angle. However, the percentage split of the flow is closer to 60% upward and 40% downward where the other two nozzles has a split around 70% and 30% respectively. Also, the vortex is not seen in the lower half of the flow. The higher concentration of azimuthal flow appears to make the jet stream dissipate more evenly on the surface of the wall then previously seen. The jet stream does slow quickly, basically stopping before the flow reaches the edge of the mirror.

The second image presented for the Nozzle 5 set is the impingement wall set to 45° from vertical, see Fig 4.3.5. In this configuration the flow does not behavior like the previous nozzles. The deceleration rate of the flow is a fourth of that of the 22.5°. This means that the impingement wall is having much less of an effect on the jet stream. The flow is still moving at half the exit speed as is reaches the edge of the mirror. The jet stream does have a small vortex below the centerline of the nozzle, but it is much slower than the other nozzle's vortex. In the azimuthal direction however, the flow does seem to slow at the same rate as the original wall angle. Overall, the wall at 45° is not very effective at slowing the vortex flow at 0.59*S*.

Fig 4.3.4: Schlieren image of Nozzle 5 jet stream flow at U_e = 30m/s and impingement wall at θ = 22.5° seeded with CO_2.

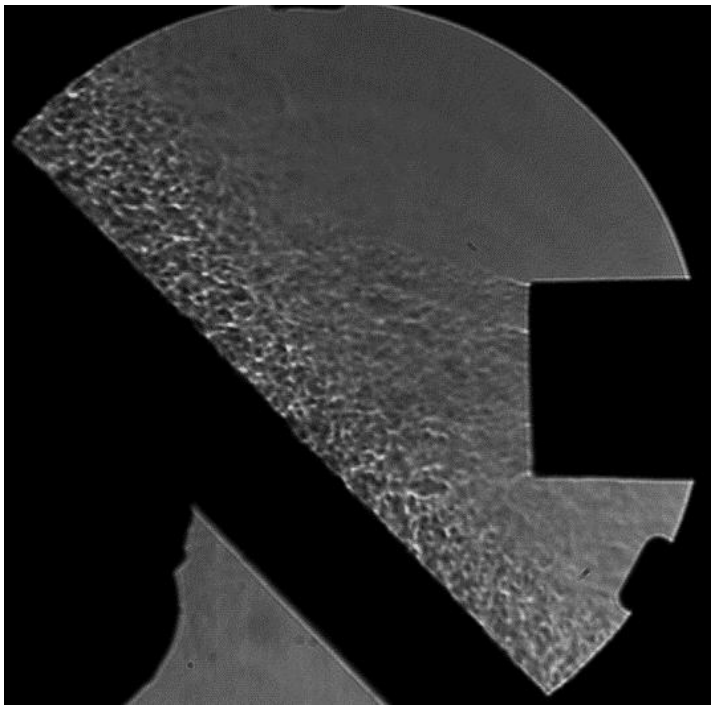

Fig 4.3.5: Schlieren image of Nozzle 5 jet stream flow at U_e = 30m/s and impingement wall at θ = 45° seeded with CO_2.

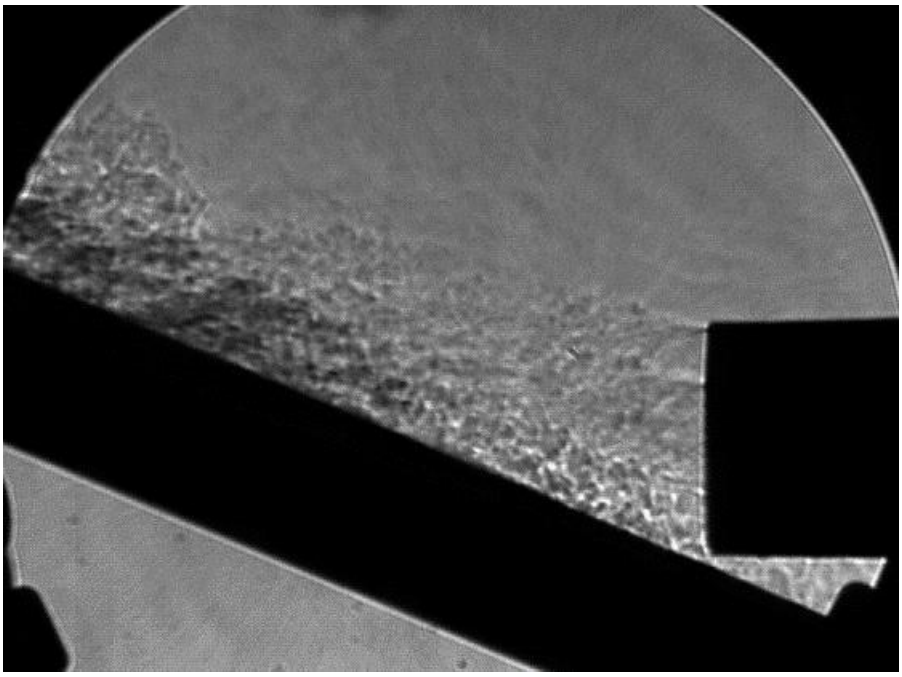

Fig 4.3.6: Schlieren image of Nozzle 5 jet stream flow at U_e = 30m/s and impingement wall at θ = 67.5° seeded with CO_2.

The final image for the Nozzle 5 set shown is for the configuration with the impingement wall set to 67.5°, Fig 4.3.6. When the jet stream hits the wall it redirects, moving along its surface. All the flow moves up the impingement wall following suit with the other nozzles. In the azimuthal direction the deceleration rate of the flow is basically identical to that of the 45° configuration. This also holds to for the axial component of the flow. Again, there is no longer a vortex below the nozzle because the angle is so small that the flow does not move in that direction. When comparing the three different directions only the 22.5° angled impingement wall is effective at slowing the jet stream in both velocity components when the swirl number is around 0.59.

The last set of images will be for the Nozzle 7 configuration with the impingement wall at the three different theta angles. Like the other two nozzles the 22.5° wall angle from vertical will be examined first, see Fig 4.3.7. After the flow contacts the wall it slows significantly as is spreads in all directions. The jet stream slows to a stop before exiting the range of the mirror. Like the Nozzle 5 setup the jet stream is more evenly split between the upward and downward directions. There is also no vortex in the lower half of the wall comparable to the Nozzle 5 configuration. Overall, the image shows that the wall at 22.5° is slowing the jet stream flow efficiently in both the azimuthal and axial directions.

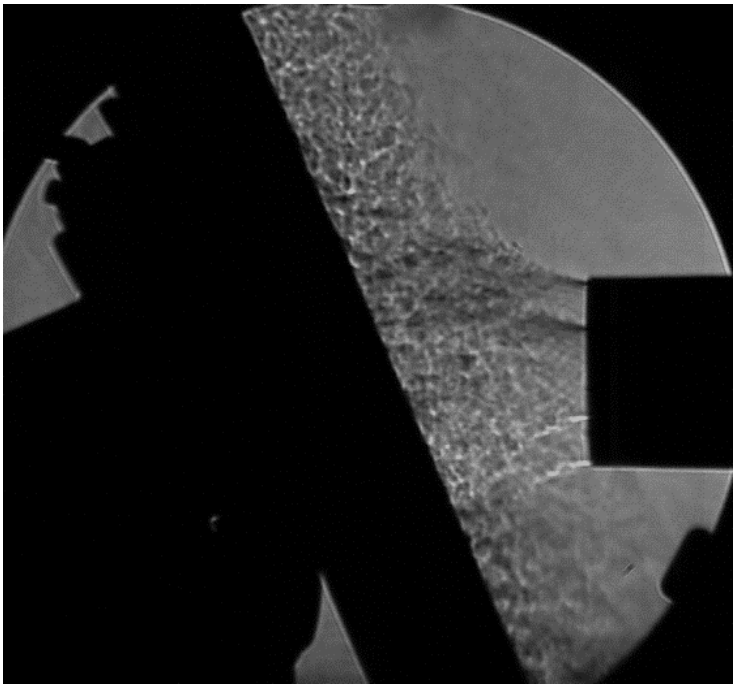

Fig 4.3.7: Schlieren image of Nozzle 7 jet stream flow at U_e = 30m/s and impingement wall at θ = 22.5° seeded with CO_2.

The next Nozzle 7 configuration to be analyzed is the impingement wall angled at 45°, see Fig 4.3.8. This setup has some interesting differences from the other nozzles. The flow's deceleration rate is much slower than the 22.5° configuration, at about a fourth. The flow is still moving at about half the velocity as the exit speed as it passes the edge of the mirror. This is twice as fast as any other 45° setup shown for the other nozzles. This could be due to the location of the peak velocity of the jet stream at the nozzle exit. The peak is much further out at about 1R as it exits the nozzle. This means that the peak has further to travel before it reaches the impingement wall before impact. The deceleration is then delayed further downstream because there has been less time to interact with the surface of the wall. Also, in the azimuthal direction there appears to be a vortex that has formed below this axial peak velocity. This could explain the dip in the azimuthal direction profile seen in section 3.4. Finally looking below the centerline of the nozzle, a vortex in the axial direction has formed, similar to nozzle 3 and 5. The vortex is slow moving and wide as it recirculates from the incoming flow of the nozzle. Because of the peak velocity location for the Nozzle 7 jet stream, it is evident that the impingement wall has a limited effect of the on the jet stream.

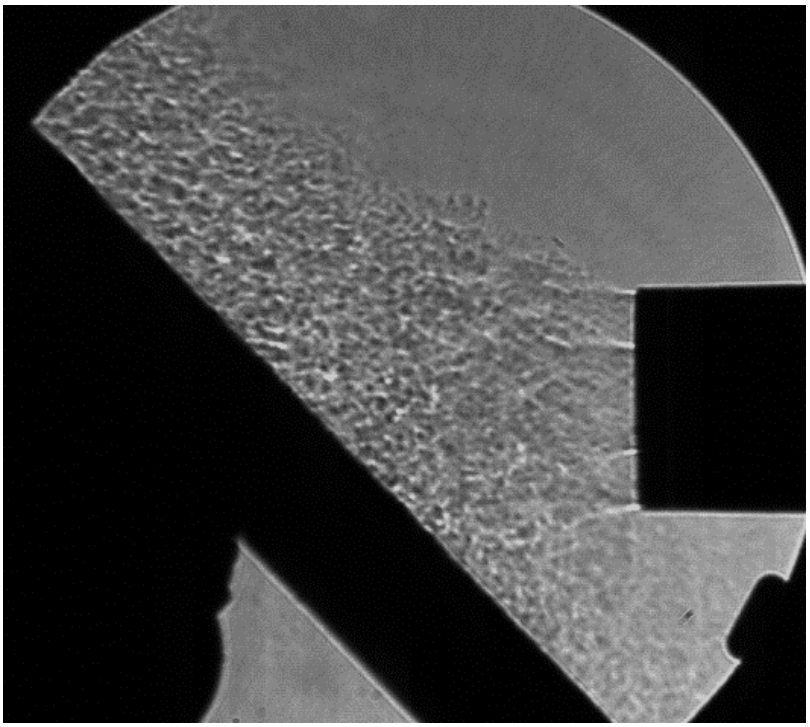

Fig 4.3.8: Schlieren image of Nozzle 7 jet stream flow at U_e = 30m/s and impingement wall at θ = 45° seeded with CO_2.

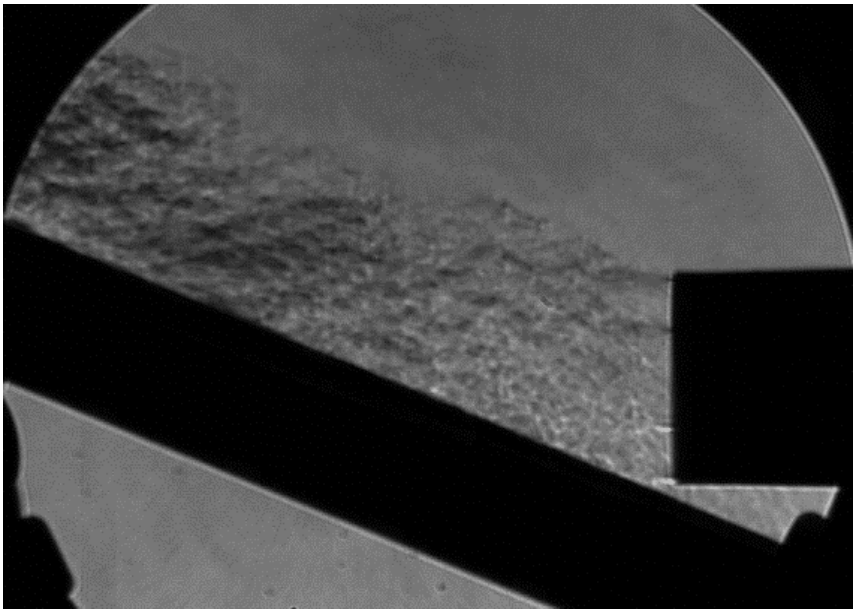

Fig 4.3.9: Schlieren image of Nozzle 7 jet stream flow at U_e = 30m/s and impingement wall at θ = 67.5° seeded with CO_2.

The final image that will be presented is for the Nozzle 7 setup is with the impingement wall angled at 67.5° from vertical, Fig 4.3.9. Interestingly the jet stream does not continue having higher than average speeds for this configuration. While the initial flow follows suit with the other setups the flow slows quicker than all other configurations. It could be that the wall is at such as shallow angle that there is little interaction with the surface of the wall. It is worth noting however that the deceleration rate is still half as fast as the 22.5° setup. In the azimuthal direction the vortex above the centerline of the nozzle exit still exists as about the same strength as the previous configuration. But the vortex below the nozzle has disappears like the other 67.5° images. While the jet stream does slow quicker than the 45° setup, it is not enough to consider it effective in dissipating the flow. Overall, it has been observed that when the vortex flow had a swirl number near 0.71*S*, the impingement wall needed to be at least 22.5° from vertical to be effective in both directions of flow.

5. Conclusion

5.1 Results Discussion

For this research effort there have been four major goals that where accomplished, verify the jet stream setup, develop vortex nozzles, validate the tripped nozzle and characterize the vortex flow on an impingement surface. To confirm that the blower jet stream setup and measurement technique were accurate the results from the unimpeded tripped nozzle was compared to the data collected from S. C. Crow & F. H. Champagne (1971) [6]. This was performed at different Reynolds number to ensure that from 6.2×10^4 to 1.24×10^5 *Re* the axial profile did not change. This was successfully performed and the results validating the experiment setup are shown in Fig 3.1.2. Along with discrete measurements taken from the hot wire anemometer, Schlieren images for the tripped nozzle were also taken and align with the images from S. C. Crow & F. H. Champagne (1971) [6]. With the combine information collected from both types of data collect it shows that this blower jet stream system creates a comparable jet stream to that of previous configurations used for research.

Now that the test setup has been checked to other existing setups, the experiment could move on to the development of the vortex nozzles. To induce this vortex form from the blower setup

turbine like blades were 3D printed into nozzles with different pitch rates to convert the normal jet stream into a vortex jet stream. From the unimpeded characterization that was performed it is evident that these blades were successful in generated the intended swirl flow. As the pitch of the nozzle blades increase so does the swirl number respectively. While the trend is not perfectly linear the swirl number on average increases by 0.1 for every inch of pitch added to the nozzle blades. This gives the three-inch pitch nozzle a 0.31 swirl number, the five-inch pitch a 0.59S and the seven-inch pitched blades a 0.71S. The swirl number represent the percentage of mean azimuthal velocity to axial velocity. Along with the hot wire measurements Schlieren images were taken of each unimpeded swirling nozzles to better understand their general jet stream profile. From these images it was noted that as the swirl number increased so did the obtuse angle created from the exit of the nozzle. With these three different nozzles there is enough difference between the vortex shapes to be useful for the next sets of the experiment.

The third goal of this research was to create a baseline for the impingement experiment. To accomplish this the tripped nozzle was used with the impingement wall at the three different angles of theta and the three different speeds of exit velocity. This gives a full matrix of the test setups using a nozzle that has been studied in previous experiments. From this data set, it was shown that just like the unimpeded jet stream flow the change in velocity, within the Reynolds numbers used in section 3.1, did not significantly change the profile of the jet stream. As for the impingement angle, it was observed that as the impingement wall got closer to vertical the dissipation of the jet stream became greater. Based on the comparison made in Fig 3.3.7 it was determine that the wall needed to be 45° or less to be effective at slowing the jet stream down. The Schlieren images taken also verify the hot wire data collected and show how the flow was being stop. For the lower angles of theta, vortexes were created on both sides of the wall which circulate from the nozzle's oncoming flow and the rebound from the wall aiding in slowing the flow from moving upstream along the surface of the wall. While the larger angles of theta do not have these features, but rather follow the surface upward reducing the interaction with the wall as much as possible. This set of data enables the next task to be tied back to as the tripped nozzle and will act as a starting point for that data.

The final goal of this research project was to characterize how different vortex flows interacted with an angled impingement wall. For this experiment all three swirling nozzles were tested with the impingement wall set at their peak velocity which was roughly 2D from the exit plane of the

nozzle. The wall was set to the same three angles of theta, 22.5°, 45° and 67.5° as the previous tripped experiment and the same three blower speeds, 30m/s, 40m/s and 50m/s related to the tripped nozzle exit it speed. This gave each of the nozzles a slightly different axial peak exit speed but the overall Reynolds number of the flow stayed the same. The first comparison made from the hot wire data was the difference in velocities for each of the wall configurations and nozzles. Except for a few minor outliers the overwhelming consensus showed that there was no difference in the azimuthal and axial jet stream profiles from a change in velocity. This of course only applies to the 30m/s to 50m/s range that was used for this experiment. There is no way to tell if there is changes to the profile from velocities outside of the range used. Because of this discovery it was determine that the rest of the data presented in the paper only used the 40m/s data to reduce the number of plots and images shown since they would be redundant. Also, the Schlieren image were most clear at the lower speed of 30m/s because the concentration of CO_2 was great than the other two speeds.

The next comparison made was how the impingement wall angle affected each of the nozzles. While there were two different sets of plots made to make clearer comparison between nozzle pitch and impingement angle, they tell the same story. The effect the impingement wall has on the vortex flow reduces as the swirl number increases. For the nozzle with a pitch of 3 the wall could be at 45° or less to be efficient at dissipating the oncoming jet stream. The nozzle with a pitch of 5 however needed to be less than 45° and finally the nozzle with pitch of 7 needed to be 22.5° or less to effectively slow the flow. The Schlieren images back up with data collected by the hot wire probe and revealed other effects that the impingement had on the vortex flow. The 3-inch pitch nozzle acted very similar to the tripped nozzle, suggesting that a flow with a swirl less than or equal to 0.31 it could be considered a normal turbulent flow. While the 7-inch pitch nozzle had a vortex created in the azimuthal direction above the centerline of the nozzle when the impingement wall was at 45° or less. This phenomenon was not seen in any other conditions and could be caused by the large azimuthal component as well as the peak velocity location in the azimuthal direction. Overall vortex flow has shown to be at a minimum the same, if not more difficult, to impede than normal turbulent flow depending on the swirl number of the jet stream.

5.2 Future Work

While the data from the hot wire anemometer and Schlieren images have revealed a great deal about how the vortex flow interacts with the impingement wall it is by no means fully defined. Other techniques could be implemented to see two different other aspects of the flow. First there was an oil field configuration that was used in C. D. DONALDSON and R. S. SNEDEKER (1970), were they coated the impingement surface with used engine oil [2]. The jet stream was then blocked by a diverter until the blower motor reached steady-state flow. The diverter was then removed for a short duration, allowing the jet stream to interact with the oil field on the surface of the wall. This technique could allow for a better understanding of how the vortex flow interact with the surface of the wall showing stable and unstable flow patterns. This was one of the major limitations of the hot wire probe, which was not able to measure the flow rate near the surface.

The other experiments that could be performed is testing with the same nozzles at higher Reynolds numbers. There are a few points of interest for this type of study. One would be if the profiles diverge from research shown in this study. This could define the upper limit of the constant profile. The other point of interest would be if the azimuthal vortex seen from the nozzle with a pitch of 7 inches, where the wall was 45° or less, changes. It would be worth studying if the vortex moves positions at higher angles of the impingement wall or at lower swirl numbers. This would require a different visualization technique because the CO_2 seeded would most likely not be effective at these higher Reynolds numbers.

References

[1] Cherry, B. E., Constantino, M. M., "The Burble Effect: Superstructure and Flight Deck Effects on Carrier Air Wake", United States Naval Academy, Annapolis, MD, 21412, 2010.

[2] Donaldson, C. D., Snedeker, R. S., "A study of free jet impingement. Part 1. Mean properties of free and impinging jets", Journal of Fluid Mechanics, 45, pp281319 doi: 10.1017/50022112071000053, 1970.

[3] Proctor, R F. H., Han, J., "Numerical Study of Wake Vortex Interaction with the Ground Using the Terminal Area Simulation System", 37th Aerospace Sciences Meeting & Exhibit, Reno, NV January 11-14, 1999.

[4] Lamar, J. E., "Modifying Ship Air-Wake Vortices for Aircraft Operations", NASA Tech Briefs, March 2004, pp15, doi: 20110016658, 2004.

[5] Mendez, M. A., Buchlin, J. M., "Quantitative flow visualization of confinement-driven instabilities of an impinging slot jet", 11th international symposium on particle image velocimetry - PIV15 Santa Barbara, California, September 14-16, 2015.

[6] Crow, S. C., Champagne, F. H., "Orderly structure in jet turbulence", Journal of Fluid Mechanics, vol. 48, pp 547-591, doi: 10.1017/S0022112071001745, 1971.

[7] Chigier, N. A., Chervinsky, A., "Experimental investigation of swirling vortex motion in jets", J. Appl. Mech. 34, 443-451, 1967.

[8] Reynolds, A., "On the dynamics of turbulent vortical flow". Z. Angew. Mat. Phys. 12, 149-158, 1961.

[9] Gupta, A. K., Lilley, D.G., Syred, N., “Swirl Flows”, ABACUS Press, Cambridge, 1985.

[10] Buresti, G., Talamelli, A., Patagna, P., “Experimental characterization of the velocity field of a coaxial jet configuration”, Exp. Thermal Fluid Sci 0, 135-146, 1994.

[11] Bruun, H. H., “Hot-Wire Anemometry: Principles and Signal Analysis”, Oxford University Press Inc., New York, USA, 1995.

[12] Örlü, R., Alfredsson, P. H., “A study of swirling turbulent pipe and jet flows”, Physics of Fluids, Volume 19, Issue 3, doi: 10.1063/1.2710287, 2007.

[13] Polsky, S., “NAVAIR Airwake Modeling & More!”, HPC User Group Forum, AIR 4.3.2.1, April 2008.

[14] Huang, R. F., Tasi, F. C., “Flow field characteristics of swirling double concentric jets”, Experimental Thermal and Fluid Science 25, 151-161, 2001.

[15] Rusak, Z., Zhang, Y., Lee, H., Wang, S., “Swirling flow states in finite-length diverging or contacting circular pipes”, Journal of Fluid Mechanics, vol. 819, pp 678-712, doi: 10.1017/jfm.2017.179, 2017.